THE TRANSIENT BEHAVIOUR OF THE CO-AXIAL NON-SYNCHRONOUS ROTATING ASSEMBLY OF A DECANTING CENTRIFUGE

A thesis submitted in partial fulfilment of the requirements
for the Degree of

Doctorate of Philosophy (PhD)

in the Department of Mechanical Engineering

of the College of Engineering

by

BRIAN DONOHUE

BE (hons). University of Canterbury, NZ 1974

MSc. Cranfield College of Technology, UK 1984

University of Canterbury

New Zealand

2013

Table of Contents

Preface iv
Acknowledgements v
Abstract vi
Glossary vii
Nomenclature x
Chapter 1 Introduction 1
1.1 Background and context 1
1.2 Aims and objectives 3
1.3 Scope 6
1.4 Novelty and contribution of the work 8
Chapter 2 Literature review 9
2.1 Background to rotor dynamics 10
Chapter 3 Problem formulation 21
3.1 The bowl 23
3.2 The conveyor (auger screw) 25
3.2.1 Stiffness and asymmetry 27
3.2.2 Natural frequency 30
3.3 The bearings 32
3.3.1 The main bearing housings 36
3.3.2 The bearing loads 36
3.3.3 Bearing stiffness 41
3.4 Noise and vibration 45
Chapter 4 Routes to a solution 48
4.1 Rotor dynamics modelling 49
4.2 FE Models 57
4.3 Centrifuge Rotating Assembly 58

Chapter 5 Modifications to the test machine 63
5.1 Design Procedure 66
5.1.1 Main Bearings 67
5.1.2 Calculate the dimensionless quantities 70
5.1.3 Calculate the oil flow 71
5.1.4 Heat balance 73
5.2 Seals 78
Chapter 6 Testing 80
6.1 Sound level 80
6.2 Vibration 82
6.3 Shaft motion 87
Chapter 7 Conclusions and recommendations 89
7.1 Summary 89
7.2 Effect of the feed 90
7.3 Machining errors 90
7.4 Assembly errors 91
7.6 Final remarks and recommendations 92
7.6.1 Recommendations 93
References 95
Appendix A The working principle of the decanting centrifuge 99
Appendix B The Polymer Concrete Base 106
Appendix C Rotating Assembly Unbalance 117
Appendix D Fortran Program for calculation of the bearing characteristics 127
Appendix E Rotor dynamics in ANSYS 134
Appendix F Drawings 144

Preface

This project came about because of an unusual vibration characteristic that occasionally appeared in both new and overhauled decanting centrifuges from different manufacturers – i.e. a generic problem. The author conducted vibration measurements and analyses on various machines but that failed to identify a cause. There were manufacturing and delivery pressures that prevented extended review of any one particular machine and one had to wait on the next randomly occurring problematic machine in order to carry out further trials. It was possible that the problem may have resulted from multiple inputs and without a fixed machine to use as a reference the possibility of not finding the solution became evident. Thus this current study was proposed for which a reference machine was supplied. This study was part of a larger project funded in part by the manufacturer and in part by the New Zealand Government through the Ministry of Research, Science and Technology. This larger project enabled not only the present study to be completed but also gave the opportunity to visit several areas where new technology might be applied in order to secure performance enhancements.

The problem that the current project relates to is characterized by the presence of a high second order vibration component. That is, the machine has a vibration at a frequency equal to twice the rotational speed. The decanter is a twin spool machine, one rotor inside another, where the rotating elements spin at different speeds. However, the speed differential is generally less than 1 Hz, and may be as low as 0.1Hz, and is dependent upon the products being separated. There are always components at the rotational frequencies of the bowl and conveyor (the rotating elements) due to residual unbalances in the two assemblies. The difference in the two states of residual unbalance is characterized by a very low audible beat frequency as the unbalance forces come in and out of phase due to the speed differential. In bad running machines, the high second order component is at considerably higher magnitude than that of the first order and puts the machine outside the vibration specification's upper limit.

Acknowledgements

As with works of this ilk there are many people who have made contributions and given their support over the course of my study, some of whom may not have been obvious at the time. I take this opportunity to thank all those people and also to make special mention of key mentors who have provided inspiration, goals, and constructive direction along the way. Firstly, Mr. George Cox of Rydens Grammar School (Hersham, Surrey, UK), who first inspired me to enter the field of mechanical engineering through his excellent teaching. Since then, my academic career has been sporadically filled with decade long spans of government laboratory and industry employment and this current work should have directly followed on from my Masters work in 1984 but unfortunately prevailing circumstances prevented that. Emeritus Prof. Harry McCallion, here at Canterbury, has consistently been supportive of my many approaches for his help on a number of research programs over the years and this current work proved to be no exception. I was inspired by his undergraduate course in vibration (and suspect that I could have done better!) and went on to choose this as a career focus. The present work stems from a desire to revisit old territory, learn new techniques, and solve a long standing industry problem that was shelved due to commitments and the solution for which I needed to acquire new skills.

I thank my supervisory team of Dr John Pearse and Dr Stefanie Gutschmidt, whose efforts kept me focused - despite occasional (desperate!) cravings to divert into other avenues of interest.

I thank all the post graduate students of the Acoustics Research Group who have accepted an old guy in their midst for the duration of this study and I hope the intellectual exchanges have been two way!

I also thank my industry sponsor, Kevin Bell, from Bellmor Engineering Ltd, who supported this project from its inception and who provided material, financial, and workshop support. Without his belief in the value of my assertions this project would not have been possible. I am also thankful for financial support from the New Zealand Foundation for Research, Science and Technology, who sponsored a larger project of which this present work forms part.

Abstract

This study identifies the cause of unstable vibrations that sporadically occur in decanting centrifuges as being caused by a combination of internal bearing clearance, conveyor unbalance and low bearing loads. These centrifuges are different from other rotating equipment common in industry (pumps, fans, compressors, electric motors) in that they are dual rotor systems – one rotor inside the other. Unbalance in either rotor can produce severe vibration of the whole machine when the running speed is close to a mode of vibration – that is, running at or near a critical speed. The external rotor, called the *bowl*, is subjected to an internal pressure generated by the centrifugal force of the product being separated. The internal rotor is supported from the bowl and is in the form of an auger screw. The main supporting bearings are subjected to forces from both the bowl and the auger - the liquid end bearing also supports the gearbox. Being able to predict critical speeds through numerical or computational analysis is a necessary step in the design process or for troubleshooting vibration problems. As part of the study, the main rolling element bearings were replaced by oil-film journal bearings to assess the viability of their use. Journal bearings are simpler, of lower cost and generate less noise than their rolling element counterparts. However, instability in running above the first critical speed can result due to oil film forces and internal hysteresis of the rotor assembly. The auger is asymmetric so instability in running is possible at around half the first critical speed.

This study was undertaken to understand the dynamics of decanting type centrifuges and develop a methodology for identifying their critical speeds and cause of unstable vibration. In the longer term this will assist in the generation of new designs that are quieter, use less energy and have better separation efficiencies.

Glossary

Beach: The dry portion of the conical above the surface of the pond.

Bowl: The rotating body of the centrifuge that withstands the pressure developed by the process fluid under centrifugal loading. Also known as the clarification section.

Chaos/chaotic vibrations: these motions have no rules that may be used for prediction of rotor displacement and are an extension of unstable vibration resulting from bifurcation.

Clearance (c): the radial space between the journal and bearing surfaces, taken as the difference in their diameters.

Conical: That part of the bowl that reduces in diameter approaching the solids discharge end of the bowl. Also known as the drainage or beach section.

Conveyor: a rotating helical auger screw within the rotating bowl that transports solids along the bowl to discharge ports in the conical section. The conveyor rotates at a slightly different speed to that of the bowl.

Critical speed: is that speed at which resonance occurs in the rotor bearing system. Rigid rotors are said to operate below the first critical speed where flexible rotors operate above the first and sometimes above higher order critical.

Decanter centrifuge: an industrial machine used for the continuous separation by centrifugal sedimentation of two or more phases of a process fluid.

Eccentricity (e): the distance between the bearing's centre and the rotating journal centre. Its maximum value is equal to c, the clearance.

Film thickness (h): varies with angular position but generally refers to the point where there is minimum clearance between the journal and the bearing. It is equal to the clearance minus the eccentricity.

Flight(s): refers to the helical blade(s) of the feed-screw or auger. They are also called *flite(s).*

Harmonic vibrations: are those that occur with the same frequency as the rotor's rotational frequency, i.e. $\omega = \boldsymbol{\Omega}$.

Journal: that part of the rotating shaft that runs inside the bearing. It is subject to wear and is often a replaceable sleeve that has an interference fit on the shaft. The surface finish is important and the surface texture is often specified to a recognized standard, for example

Pond: The pool of liquid above the sedimented solids. The surface level of the pond is closest to the axis of rotation and set by adjustable weirs in the liquid end hub.

Viscosity of the lubricant film, whilst technically a measure of its resistance to shear, is usually taken as a measure of its ability to flow. Lubricating oils are generally graded according to their dynamic viscosity, in poise or centi-poise (cP), which is the *kinematic viscosity* multiplied by the density.

Rigid rotor: A shaft system that runs below its first critical speed – generally at or below a frequency ratio of 0.707

Separation margin: A specified speed margin for operating rigid rotors at or close to their first natural frequency (critical speed). The separation margin is related to the amplification factor (generally response displacement /excitation displacement).

Superharmonic vibration: occurs at frequencies that are larger than the rotational frequency by an integer multiple, e.g. 2x, 3x, 4x etc.

Subsynchronous vibration: has a frequency that is less than the rotational frequency of the rotor and is usually an irrational fraction of rotor speed dependent upon restoring force and damping in bearings.

*Supersynchronous vibratio*n: has a frequency that is larger than the rotational frequency of the rotor and is a non-integer multiple of that frequency, e.g. 1.5x, 2.5x etc.

Time-marching: A numerical procedure to solve a system of differential equations in time steps moving forward from a specified initial position.

Whirling: This is the angular orbital motion of the deflected rotor about its neutral axis and may be either forward (same sense as the shaft rotation) or

backward. A special case of Subsynchronous whirl induced by dry rubbing (or for non-loaded rotors in journal bearings) is called *whip*.

Nomenclature

$C = R-r$	Radial clearance
C_b	Assembled clearance
C_p	Machined clearance
$C_{ij} = C_p\omega C_{ij}/W$	Dimensionless damping coefficient
D	Bearing diameter
F	Oil film force
H	Heat generated in the film per second
$K_{ij} = C_p k_{ij}/W$	Dimensionless spring coefficient
L	Bearing length
M	Rotor mass
N	Rotational speed (rpm)
$Q_c = q_c/(R\omega C_p L)$	Dimensionless circumferential oil flow
$Q_f = q_f/(R\omega C_p L)$	Dimensionless forced oil flow
$Q_s = q_s/(R\omega C_p L)$	Dimensionless side flow of oil at ends of the bearing
$R = D/2$	Bearing radius
$Re = C_p U/\upsilon$	Reynolds number
$S = \mu NLD(R/C_p)^2/W$	Sommerfeld number
T	Temperature (°C)
T_o	Torque (Nm)
T_T, T_S	Tight and slack side drive belt tensions
U	Unbalance
V	Journal surface velocity
W	Bearing load
c_{ij}	Damping coefficient of the oil film ($i, j = x, y$)
d	Journal diameter
e	Journal eccentricity
f	Oil film force

f_J	Frictional force on the journal
$h = C + e\cos\theta$	Oil film thickness
h_{min}	Minimum oil film thickness
k_{ij}	Spring coefficient of the oil film ($i, j = x, y$)
m	unbalance mass
$m_p = 1 - C_b/C_p$	Preload factor
p	Oil film pressure
p_f	Oil feed pressure
$p_m = W/(LD)$	Mean bearing pressure
$r = d/2$	Radius of the journal
r_e	Effective pitch radius of belt drive
t	Time (s)
x, y, z	General coordinate directions (z is axis of rotation)
u, v, w	shaft deflections in generalized coordinate directions, x, y, z
$\varepsilon = e/C_b$	Journal eccentricity ratio
θ	Circumferential angle (deg)
μ	Absolute or dynamic viscosity of the lubricant, (Pa.s)
v	kinematic viscosity of the lubricant, (m^2/s)
ρ	Density of the lubricant (kg/m^3)
ϕ	Attitude angle (deg)
$\varphi = C_p/R$	Clearance ratio
$\Omega = 2\pi N$	Angular velocity of the journal (rad/s)
ω_c	frequency of a critical speed (Hz)
ω_n	natural frequency (Hz)

Chapter 1 Introduction

1.1 Background and context

This work investigates the dynamics of a concentric dual rotor system where the inner rotor is an asymmetric screw conveyor that spins at a slightly different speed to the outer bowl rotor (that is symmetric). This rotating assembly forms the basis of the decanting centrifuge as shown in Figure 1.1. The centrifuge is an industrial size machine used for the continuous separation of multi-phase mixtures by centrifugal action – referred to as sedimentation.

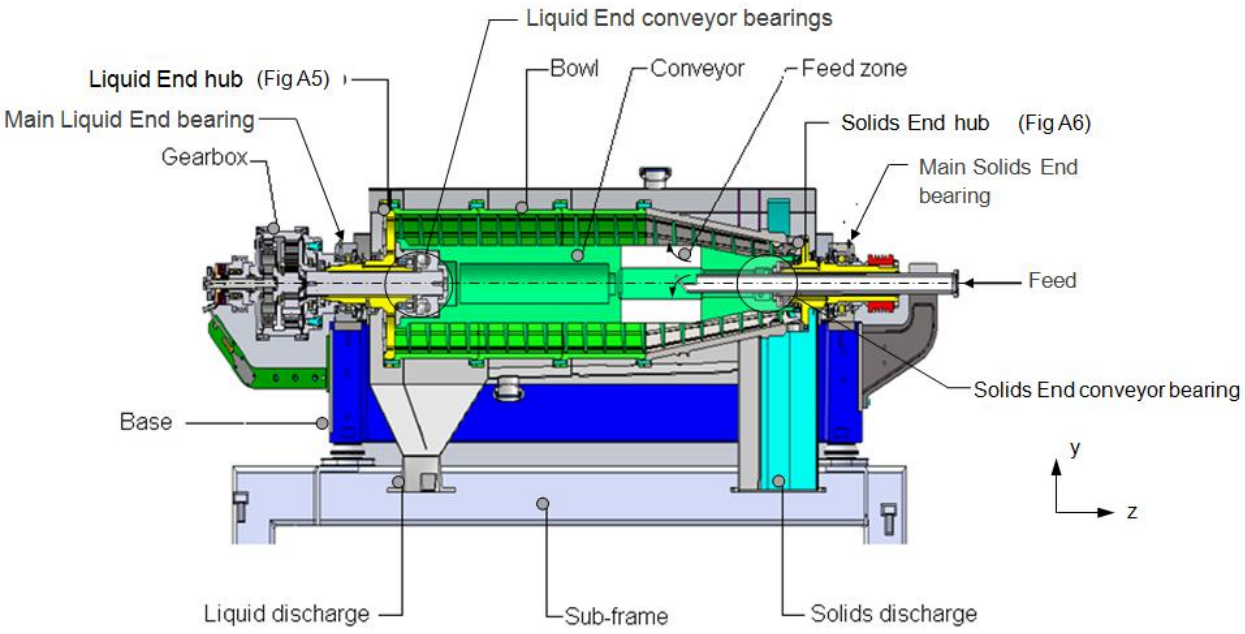

Figure 1.1 Cross-section of a typical solid bowl decanter centrifuge

The present study is concerned with the investigation of the physical dynamics that control vibration of one or both rotors of the centrifuge and developed as a result of troubleshooting different models of used and new machines that exhibited high levels of vibration. Occasionally, a machine would exhibit a high audible beat with an associated high level of vibration well above the acceptance limit for the machine. Linear finite element analysis (FEA), traditional condition

monitoring, and diagnostic techniques had failed to identify a cause of those vibrations, but intuition led to a short term remedy that resulted in reduced levels of vibration [1]. The mechanics behind the excitation was not understood so that it was not possible to properly assess a new design and avoid expensive post manufacturing modifications and design changes. Vibration in machinery can be externally forced or be self excited, i.e. no external stimulus is required, and vibration from both sources may be present under some operating conditions. This present study determined that the main vibration was caused by the radial clearance in a rolling element bearing, the low loading of the bearings, machine run-out and the asymmetry of the conveyor, which together provided a route to nonlinear vibrations.

Rotor dynamics is an established applied mechanics discipline for studying the dynamics of rotating systems and there exists a very extensive collection of published work that pertains to the study of rotating systems. Rao [2] presents an historical perspective review of the field and introduces the methods for modeling and mathematical treatment. Most published work is specific to the individual authors' problem area and cannot be readily applied to other examples without extensive modification to both the theory and solution software. The major differences are in considering the rotor as a rigid or flexible shaft, with mounting in rigid (rolling element) or flexible bearings (fluid film), and in the manner of connectivity of the assembly to the ground. The analyses also vary in their mathematical treatment whether considering linear or non-linear effects, and in the various integration schemes for studying time varying response. Many of the studies are concerned with lateral response to unbalance and use linearized equations of motion to obtain solutions. Historically this limitation was imposed by computational power and the incomplete understanding of the physical dynamics of the problem. Moreover, many studies focused on discrete parts of the whole installed system, ignoring coupling effects, damping, mass and stiffness of foundations and supports. Often simple models are used to represent real systems in attempts to qualify the effects of various features.

For this current study, the non-linear effects of clearance in the rolling element bearings, coupled with low bearing loads and excitation from torque and unbalance, led to the problematic vibrations experienced. This combined forced

and self excited vibration problem in centrifuges has not been previously published.

In the general field of rotor dynamics, the study of dual and multi-rotor systems is less well covered than the mono rotor type - but there are a few references on recent work. Co-axial dual rotor systems that have been studied [2], [3], [4], include simplifying assumptions or exclusions that, whilst making the models non-realistic, are valuable for gaining insights into the contributions of relative changes in parameters such as stiffness, damping, unbalance, and speed. For example, Bonello's and Hai's [5] treatment of the dual rotors of an aircraft engine ignores the load torque and aerodynamic effects of the bladed discs. Their study is focused on lateral bending and does not consider the coupling effects of torsion or torque and uses linear characteristics in the supporting bearings. Lalanne and Ferraris [3] introduced a simple dual rotor model with rigid bearings to demonstrate analytical procedures – but excluded cross coupling effects as the bearing stiffnesses are assumed to be linear and symmetric. Other work focuses on studying the non-linear effects of squeeze film dampers – a method of isolating one rotor from the other. Kamenicky [6], and Hai and Bonello [7], did not include all expected loads for the models they used, overlooking some important effects such as asymmetric whirl and non-linear jumps.

Traditional analyses of decanter centrifuge rotors assume simply supported shafts that although linked can be treated as separate entities. This study shows that whilst the rotors can be classed as rigid, the response of the auger conveyor is dependent upon its mounting to the hubs of the outer rotor, the bowl assembly, and the degree of residual unbalance. Published work on the non-linear aspects of rolling element bearings, such as[8], [9], formed the basis for forming the hypothesis on the motion of the conveyor in response to unbalance.

1.2 Aims and objectives

This study is aimed at solving a generic problem that has a number of possible contributing causes. Some of these were eliminated in the process of refining the research focus, so that only the stability of the rotating assembly was of specific interest and of which remained a problem after the initial investigatory work was completed.

The bowl is a large cylindrical element with high stiffness so that the intuitive assumption is that the first natural frequency in bending would be much higher than the run speed frequency of 3250 rpm (54.2 Hz). This proved to be the case by FEA (finite element analysis) and by testing, so that even allowing for the spin softening effect of asymmetry [10], the first critical speed would be expected to be significantly higher than the disturbing vibration components present. Figure 1.2 shows two types of motion present in the decanter's vibration. In the high resolution plot the fundamental frequencies of the bowl and conveyor are evident – separated by 1Hz. There are associated sidebands at the fundamental and also for the second harmonic that indicate vibration of the conveyor due to bearing clearance – having eliminated the possibility of loose fits. At the outset it was not clear why there are more sidebands at the second harmonic. However, the study later showed that the horizontal bearing stiffness can approach zero, leading to an unstable running condition as the conveyor's stiffness also has a twice per rev change due to asymmetry. The low resolution plot shows that there are many harmonics of the fundamental frequency of rotation that could be the result of bearing clearance or misalignment. Rubs produce similar spectra but generally with additional half order components and the time based waveform contains truncation that enables elimination or confirmation of this as a cause. In the cases shown in Figure 1.2 the second order component has a higher magnitude than that of the fundamental (53.2Hz). Two objectives of the research are to identify why some machines exhibit the spectra of Figure 1.2 whilst other ostensibly identical machines do not and to discover what the mechanism of generation is.

The principal objectives of the study is to develop realistic numerical and analytical models of the decanter to study the mechanics of the centrifuge's rotating assembly and use them to determine if clearances in the rolling element bearings affect stability of running and to what extent they affect the values of the critical speeds?

The second objective is to design, manufacture and install fluid film bearings to substitute for the rolling element bearings and demonstrate stable running, observing the effect on noise and vibration emissions.

The goal is to test the hypothesis that *currently unpredictable (or unstable) vibrations in the decanter centrifuge result from a loss of horizontal stiffness that*

causes a twice per revolution excitation of the vibrations of the conveyor and is caused by a combination of low loading, unbalance and radial clearance in the conveyor 's rolling element bearings.

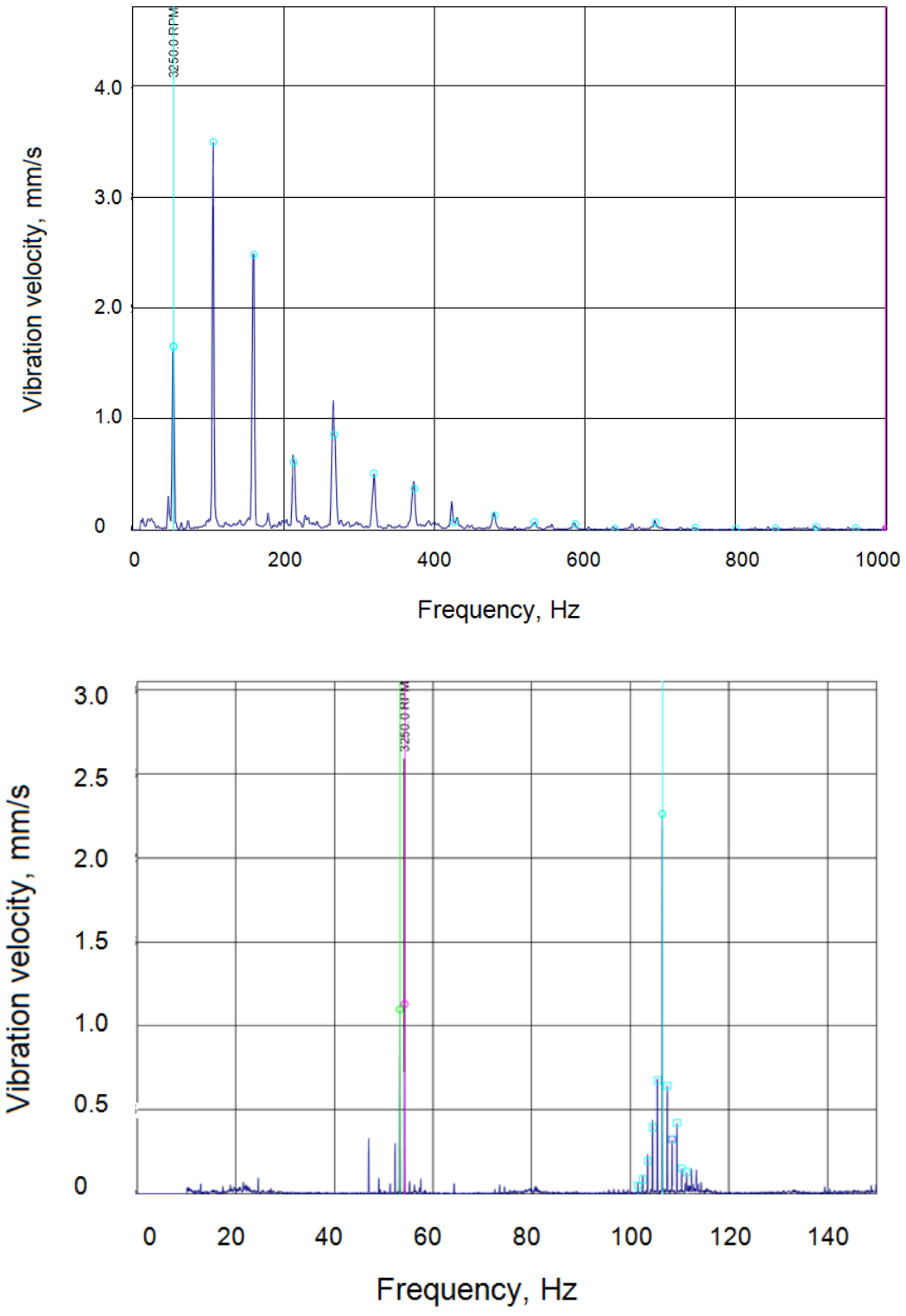

Figure 1.2 Typical fault vibration spectra of a decanter centrifuge: top – low resolution; bottom – high resolution

1.3 Scope

The focus of this study is solely on the mechanical engineering and applied mechanics aspects of the rotor dynamic vibrations in the bowl and conveyor, their mechanisms of generation and mitigation.

There is a generic problem that has not been addressed in the published literature and this study identifies the source of the problem and identifies the solution.

Hydrodynamic bearings for the main rotor support are designed, manufactured, installed and tested. This follows preliminary work on solving a base resonance problem by designing and fabricating a polymer concrete base (Appendix B).

The work does not include investigations into any aspects of centrifugation technology, i.e. that technology required to match product and centrifuge to separate process fluids for a given output. There are many text books on the subject of the vibration of machines but often a practical view is required in order to understand the mechanics involved - what makes shafts vibrate, how do they vibrate, and what controls their displacements? In Chapter 2, the specifics of rotor dynamics technology is presented along with a review of the most relevant published papers.

In Chapter 3 the problem is formulated through identifying the components and applied loads, and developing the equations of motion. The problem is a non-linear one and is solved using the finite element method as presented in Chapter 4. Chapter 5 details the modifications that were made to the test machine and the results are presented in Chapter 6. Chapter 7 contains the conclusions and recommendations.

Figure 1.3 shows the decanter centrifuge that was used for the present work. Industry designs are generic and the outcomes of the study are applicable to all centrifuge systems of this grouping.

Figure 1.3 View of a decanter centrifuge machine – cover open
(courtesy of *Bellmor Engineering Ltd., Christchurch, New Zealand*)

Decanters are principally used to separate process fluids into solids and liquid phases, but occasionally the liquid phase can be discharged as two sub-phases of slightly differing densities. The primary separation is of suspended solids that have a higher specific gravity than the liquid phase [11]. The use of the centrifuge is designed to speed up the natural gravity settling of particles in liquids by several hundred times so that very short separation times are achieved. The solids phase, the highest density particles, collect at the bowl wall under the action of centrifugal force and are removed by the scraping action of a screw conveyor – see Appendix A. The bowl wall/solids interface pressure is not inconsiderable, resulting from some 2000 to 3000 times the acceleration due to gravity. The residence time of product in the bowl is determined by the relative speed difference between the conveyor and bowl and the length of the liquid pool. Appendix A gives basic detail of the working of the decanter centrifuge.

The decanting centrifuge appears as a deceptively simple machine yet there are six basic parameters that can be changed to control the input and output that are interactively linked with the dynamic response. These parameters are:

- feed rate
- bowl speed
- pond depth
- differential speed
- constituents and temperature of the feed

Typically, operators know a lot about the machines they control and the product being processed. However, operational decisions are based on the material outputs rather than, or being inclusive of, power consumption, wear, or levels of noise and vibration. Variations in material throughput are reflected in the drive torques for bowl and conveyor [11] and whilst the present study does not include for these variations, parallel doctoral work by *Bell* [12] is being carried out at the University of Canterbury into energy use and optimization.

1.4 Novelty and contribution of the work

The research contained in this dissertation contributes to the specific field of centrifuge dynamics and to the general rotor dynamics field through:

- Identifying the effects of conveyor bearing clearance on the vibration of a decanter centrifuge rotating assembly
- Identifying the effects of lightly loaded conveyor bearing in the presence of high residual unbalance of the conveyor
- Quantifying the effects of mitigation of the gravity load by the residual imbalance of the conveyor
- Development of a method that can be applied in-situ for the dynamic balance correction of the conveyor (inner rotor) of a decanter centrifuges.

Chapter 2 Literature review

As with all vibrating mechanical systems, the theory of rotor dynamics shows that the resonant frequencies of rotors (their critical speeds) for a given system are determined by stiffness and damping [8] – as it is generally not realistic to change the mass. Stiffness is provided by structural properties as well as from the spring like characteristics of fluid films (in bearings and processed materials). However, unlike linear mechanical systems where the stiffness is constant with frequency of vibration, in rotor systems the stiffness varies with rotational speed. Damping is provided internally by friction (within materials and at features such as joints) and externally by the effects of lubricant in bearings and by fluid effects from the medium in which the rotor is spinning. Both stiffness and damping apply non-linear forces to the rotor that are most often linearized for simplified analyses.

Non-linear treatment of bearings has been demonstrated by application to rigid rotors [[13] - [14]], flexible rotors [5],[15], [16], or the simple Jeffcott/Laval rotor [17], but their focus is on the development of analytical methods or new finite element formulations rather than prediction of real world rotor systems. Non-linear analysis of rotor systems must be used where the assumption of small perturbations about an equilibrium point is no longer valid, and is the only method from which a solution or close approximation can be found.

In addition to the non-linear characteristics of the bearings, for the decanting centrifuge, the conveyor's asymmetry means that the controlling parameters change with time when the response is viewed from a stationary reference frame and therefore it is beneficial to derive the equations of motion in a rotating frame. In this way the controlling parameters remain constant [18].

2.1 Background to rotor dynamics

It is difficult to immediately study a dual rotor system without some background in the single rotor case. The greater part of published work is concerned with the single rotor and in methods of analysis to understand the various aspects of controlling parameters such as the mass, damping and stiffness.

The study of rotating systems has extended from Rankine's first paper in 1869 [19]. On-going research in this field is driven by the development of new technologies in materials, bearings, and lubricants that allow the operation of lighter and higher speed rotors. In addition, advancements in numerical methods and developments in software allow more and more precise analysis of models that closely approximate real systems.

Apart from the shaft on its own, the simplest form of a rotor is the disc and shaft as shown in Figure 2.1. When the disc is positioned at the centre of the shaft it is commonly referred to as the Laval, Jeffcott or Föppl rotor [2]. The earliest form of rotor model considered the rotor as a fixed mass on a spring – a single degree of freedom system, where the spring stiffness was the stiffness of the shaft. Later, the shaft was modeled as a continuous system with the rotor supported on identical springs in one plane only, without any damping component, and with the disc centralized on the shaft.

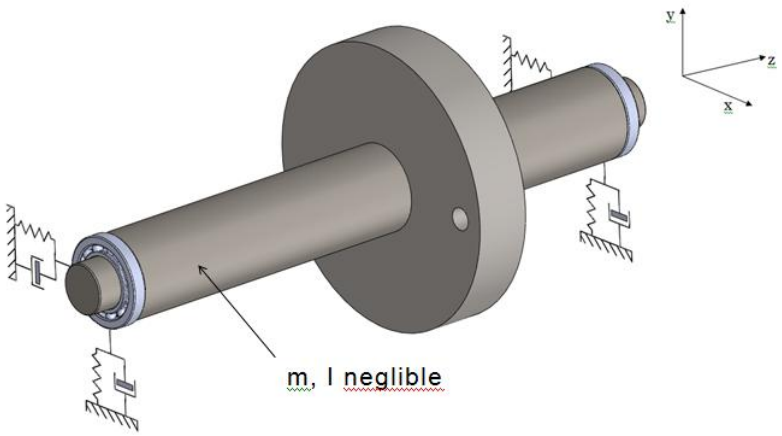

Figure 2.1 The asymmetric Jeffcott rotor[1]

[1] Note the *z* axis is the axis of rotation throughout this study

As understanding of the mechanics developed so did the mathematical models and allowed for an offset disc and springs with different properties in two planes. Offsetting the disc showed the Coriolis effect of the torque produced when the disc wobbles during whirl – this is also referred to as the gyroscopic effect; the treatment is determined by the frame of reference used for the analysis. Rigid body modes in rocking and translation were studied as outcomes of the dissimilar spring properties. Later studies on fluid bearings showed that the motions in the two orthogonal planes can couple through the forces developed in the bearings and interpretation of mode shapes became a 3D art. For example, the simple planar rocking displacement motion develops into a conical whirling motion as shown in Figure 2.2.

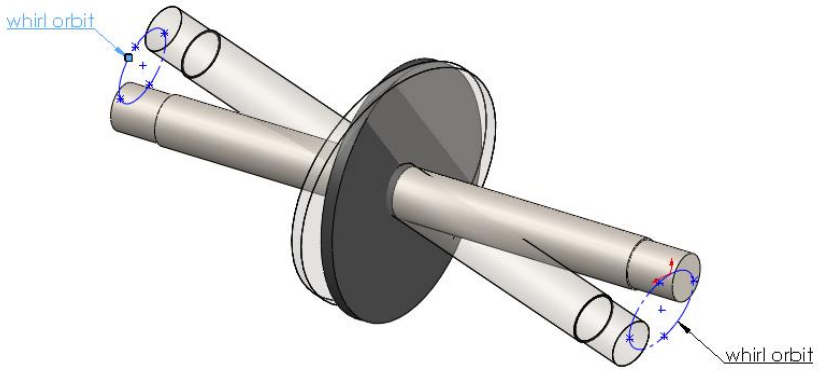

Figure 2.2 Conical rocking mode of vibration

The major expansion in the study of rotating systems occurred after the Second World War (1939-1945). In the early studies the primary aim was to be able to predict the lowest critical speed – that natural frequency for which the rotating assembly resonates. The study of torsional vibration (particularly of crankshafts) was simplified by Holtzer (1921) and Jeffcott's theory (1919) for lateral vibration needed to be improved upon to answer questions about unbalance response and supercritical running speeds.

The Campbell diagram, which today is a valuable tool in visualizing the position of critical speeds relative to a rotor's exciting frequencies, was developed in 1924. As the designed speed of running rose above the first critical speed then problems of instability and self-excited vibrations arose and attracted much attention from researchers.

Foundation work on fluid film bearings was carried out by Newkirk in the 1920's that showed the existence of oil whip and oil whirl. Complex motions arising from bearing asymmetry began to be investigated in the 1930's [20], and continued through to the late 1960's. That decade also saw the emergence of more general equations of motion for continuous shaft systems that included the effects of rotary inertia, shear deformation and gyroscopic torque [21]. The properties of bearings are very complex and much work has been done to determine whether they are able to be scaled from experimentally determined characteristics. In 1984 Harris [22] published a historical perspective and theory of rolling element bearings and in1989 Someya [23] published data and theory for a range of fluid film bearing types. There is now an extensive list of publications on the theoretical and experimental treatment of bearings to determine their operating characteristics – particularly stiffness. A review of some 180 plus published works on fluid film bearings has been by presented by Tiwari et al [24].

A detailed history of the development of rotor dynamics as a specialist subject can be found by referring to texts such as Childs [8], and Rao [2].

It is the effects of motion of the rotating shaft that differentiates its response from that of static beams of the same geometry. Effects such as whirling, fluid instability (from bearings and fluid or aerodynamic loading), friction rubs, and asymmetry all make for confusion in modal interpretation. The simplest view of whirling for a simply supported shaft is as a skipping (or jump) rope where the rope is the axis or rotation of the shaft and the volume that it sweeps is defined by the whirl orbits – see Figure 2.3.

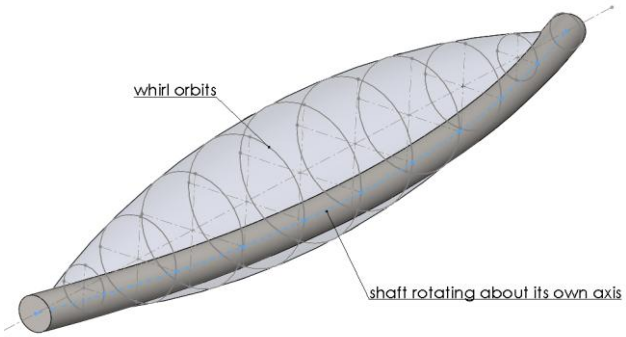

Figure 2.3 Sketch of a whirling shaft

The whirl motion results from unbalanced internal and external forces including hysteresis damping, unbalanced mass, fluid film forces in the bearings and friction. The shaft is rotating about its own geometric axis as well as whirling and so visualizing the motion of a point on the rotor can become quite complicated. Further complication arises when damping or asymmetry are included, since backward whirling is possible – that is, the direction of whirl is in the opposite direction to the rotation of the shaft as shown in Figure 2.4.

These two types of whirl are important to recognize as the stress states for the rotor are different. In the top diagram of Figure 2.4, the stressed outer fibres of the shaft remain in the same state as the shaft rotates and whirls – since the two motions are synchronous. In the lower diagram, where whirl is in the opposite direction to shaft rotation it is seen that the shaft undergoes reversal of stress – a condition that could lead to fatigue. Reverse or backward whirl is not common but systems must be checked for possible occurrence.

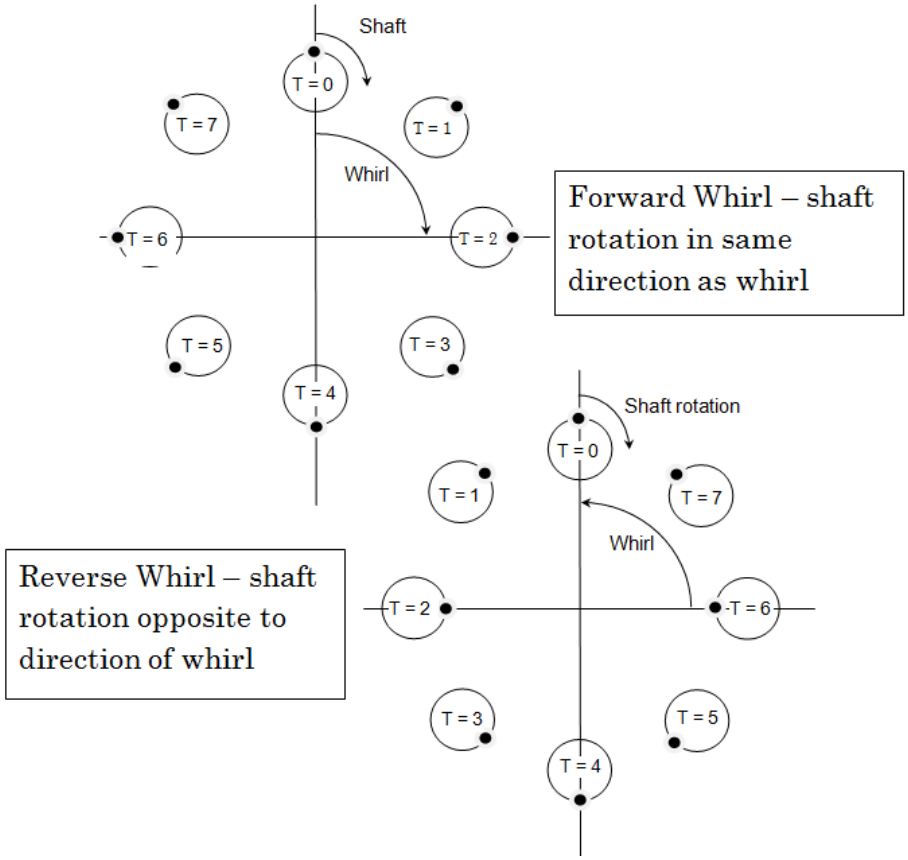

Figure 2.4 End views of the whirling rotor

In addition, the speed of the whirl may or may not be synchronous. Synchronous whirl is associated with mass unbalance – the most common source of vibration in machinery [25]. In Figure 2.5, at any point in time the x and y coordinates of the unbalance mass are changing, due to shaft rotation, so that the forces (as seen by the springs) become harmonic functions given by:

$$F_x(t) = mR\omega^2 COS(\Omega t);\;\; F_y(t) = mR\omega^2 SIN(\Omega t)$$

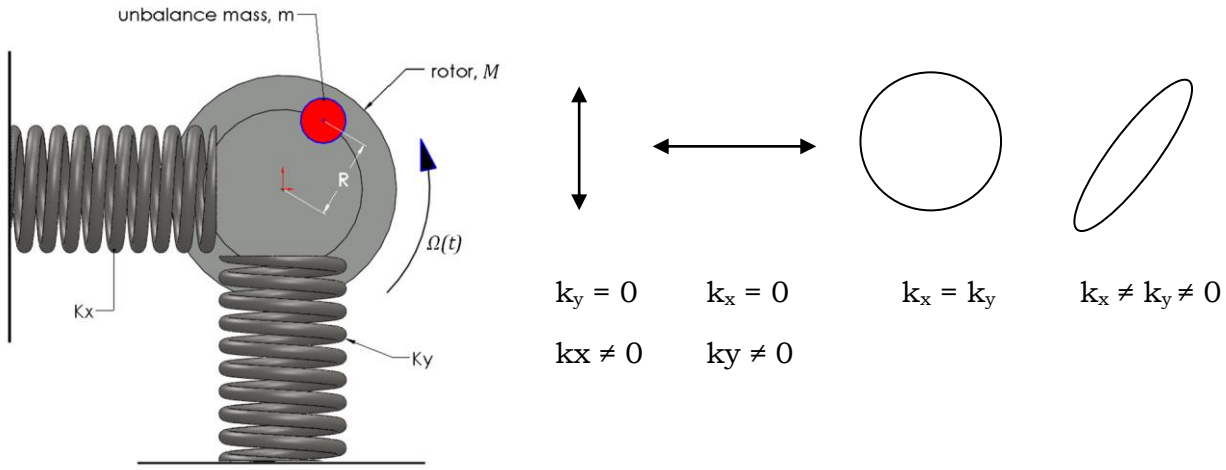

Figure 2.5 Simple rotor model – disc on two springs. The locus of the centre of the shaft is described by the whirl orbits whose shape changes for different spring stiffnesses – as shown at the right

Letting the displacements of the springs in the x and y directions be u_x and u_y, then the force balances in x, y directions can be written as:

$$-k_x u_x = (M-m)\ddot{u}_x + m\frac{d^2}{dt^2}(u_x + R cos\Omega t) \quad \text{and}$$

$$-k_y u_y - Mg = (M-m)\ddot{u}_y + m\frac{d^2}{dt^2}\left(u_y + R sin\Omega t\right),$$

where M is the rotor mass, m is the unbalance mass at radius R.

The equations of motion are written in the form:

$$M\ddot{x} + k_x x = m\omega^2 R\cos(\Omega t) \quad \text{and} \quad M\ddot{y} + k_y y = -Mg + m\omega^2 R sin(\Omega t)$$

Where the stationary shaft will have modal frequencies that correspond to the equivalent beam it appears obvious that these frequencies will be affected by the boundary conditions i.e. the way in which the shaft is supported. A rigid shaft

on flexible (soft) mounts will vibrate in a translatory or rocking manner without deformation of the rotor – Figure 2.6.

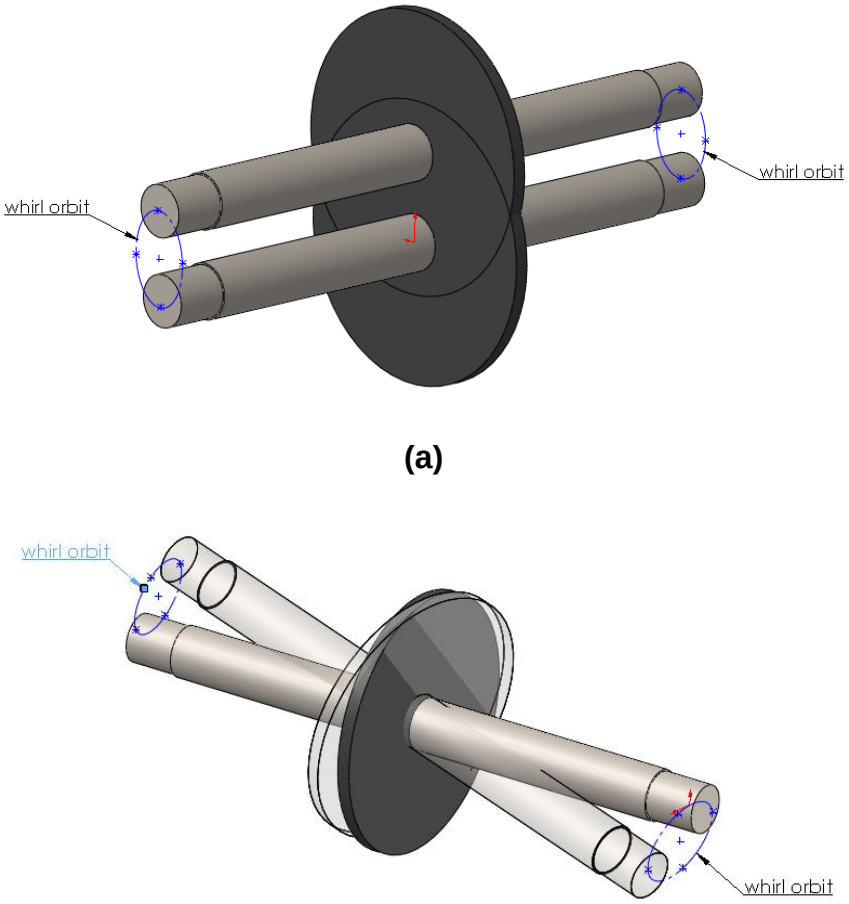

Figure 2.6 Modes of vibration of rigid shaft on soft mounts: (a) translation, (b) rocking or conical

The modal frequencies vary under the influence of the support stiffness so that only at the very stiff (rigid) values do the values of frequency calculated using simple methods and models, match those for the simply supported beam case. Ruddy [26] and Ruddy and Summers-Smith [27] include typical charts, called critical speed maps, that show the effects of changing support stiffness on modal frequency and mode shapes – see Figure 2.7. The rotor response falls roughly into three ranges: the lower range is predominantly controlled by the support stiffness so that displacements are rigid body modes; the middle range is

transitional between rigid and flexible modes, where the upper range is controlled by rotor flexibility with rigid boundary conditions.

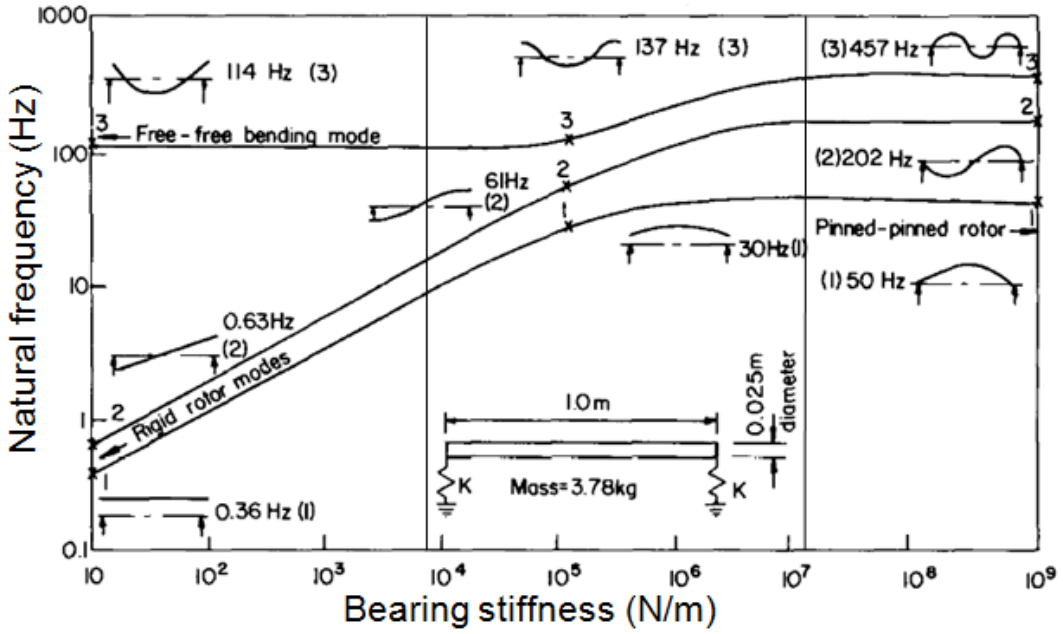

Figure 2.7 Critical speed map showing effect of bearing (support) stiffness on modal frequencies and mode shapes (taken from [27], Ruddy & Summers-Smith).

Kim and Lee [28] include critical speed maps for the decanter centrifuge auger, bowl assembly and the combined rotating assembly. Their paper is the only published work on the dual rotor decanting centrifuges that was found during an extensive literature search. They go on to establish a range of possible bearing stiffness, taken from Harris [22], to show that the lowest bending modes of vibration lie above the maximum design run speed. Kim and Lee also made the assumption for their model, that all the bearings have the same stiffness. In the practical sense this is clearly not the case as, using their own reference from Harris, the stiffness varies as the number and diameter of the rolling elements. The bearings at each end of the bowl and of the conveyor are of different diameters and are of both ball and roller types. Intrinsically roller type bearings are stiffer than the ball type as the former has a line contact under the load path compared with the point contact for the latter type.

Harris gives the stiffness as:

$$k_{b=}\frac{ZD^{\frac{1}{2}}cos^{\frac{5}{2}}(\alpha)\delta_r^{\frac{1}{2}}}{4.77E-6}$$

where,

Z = the number of rolling elements per row

D = the diameter of the ball or roller element`

α = the contact angle, and

δ = the radial deflection (deformation),

showing the non-linearities introduced by the rolling element diameter and the deflection under load.

Many papers have been published showing models with symmetric supports in order to simplify the mathematical treatment. However, in practice it is far from the norm to have symmetrically disposed and identical bearings as the two supports of a rotor. From Figure 2.7, it is clear that unless there is fairly accurate data on the bearing/support stiffness then the rotor response will not be accurately predicted. For the case of the decanter, there are basically two rigid rotors - one inside the other. The rotors are classified as rigid as the run speed is (normally) well below the calculated first natural frequency in bending. However, whilst the rotors are rigid, the bearings are not. The bearings that support each rotor are not identical, not only being different in size but also being a ball bearing at one end and a cylindrical roller bearing at the other. Thus the analysis by Kim and Lee [28] is rather simplistic and does not reflect a typical centrifuge rotating assembly.

For most rotating systems, including decanter centrifuges, the fundamental mode is the one that falls closest to the running speed. There are several simple methods used for the calculation of the lowest critical speed, two of which are: Dunkerley's method and Rayleigh's method.

2.1.1 Dunkerley's method

This method, published by Dunkerley in 1894, is used to calculate the fundamental critical speed of a shaft carrying one or a number of rotors. The rotating system is reduced to sub-systems each of which is a single rotor on a massless shaft. The individual critical speeds for each subsystem are calculated and the overall rotor response is [29]:

$$\frac{1}{\omega^2} = \frac{1}{\omega_1^2} + \frac{1}{\omega_2^2} + \frac{1}{\omega_3^2} + \cdots$$

2.1.2 Rayleighs method

Rayleigh's method (1945) is an energy based method for a conservative system where the maximum kinetic energy equals the maximum potential energy undergoing free vibration. Assuming a profile defined by the deflections y, then

the potential energy is given by: $U_{max} = \frac{1}{2}\int \frac{M^2}{EI} dx$ and

the kinetic energy by $T_{max} = \frac{1}{2}\int \dot{y}\, dm = \frac{1}{2}\omega^2 \int y^2\, dm$

The natural frequency is given by:

$$\omega^2 = \frac{\int EI\left(\frac{d^2y}{dx^2}\right)^2}{\int y^2 dm}.$$

Using these simple methods the lower mode frequencies can be quite accurately calculated [30]. The Rayleigh-Ritz or extended Dunkerley method [29] can be used to calculate the higher modes. However, these methodologies are limited to simply supported beams – the model assumed for a large range of rotating equipment that operates below the first critical speed and at the upper range of stiffness shown in Figure 2.7.

For a simply supported beam, say the conveyor/auger, assuming a massless shaft with the auger mass being positioned at centre span, where: m = 243 kg; L = 1.20m; E = 209E9 N/m$^{2;}$ and I = 6.58E-5 m^4, then Dunkerley's method gives,

$$f = \frac{1}{2\pi}\left(\frac{g}{\delta}\right)^{0.5}$$

where δ is the maximum deflection, (at mid span), then:

$$f = 257 \text{ Hz}$$

Considering the shaft as weightless with a central load (stiffness = $48EI/L^3$) gives:

$$f = 200 \text{ Hz}$$

The stiffness used for the UDL case yields a result that is roughly 3% lower than the first mode found using COSMOS (250 Hz) – see Figure 2.8.

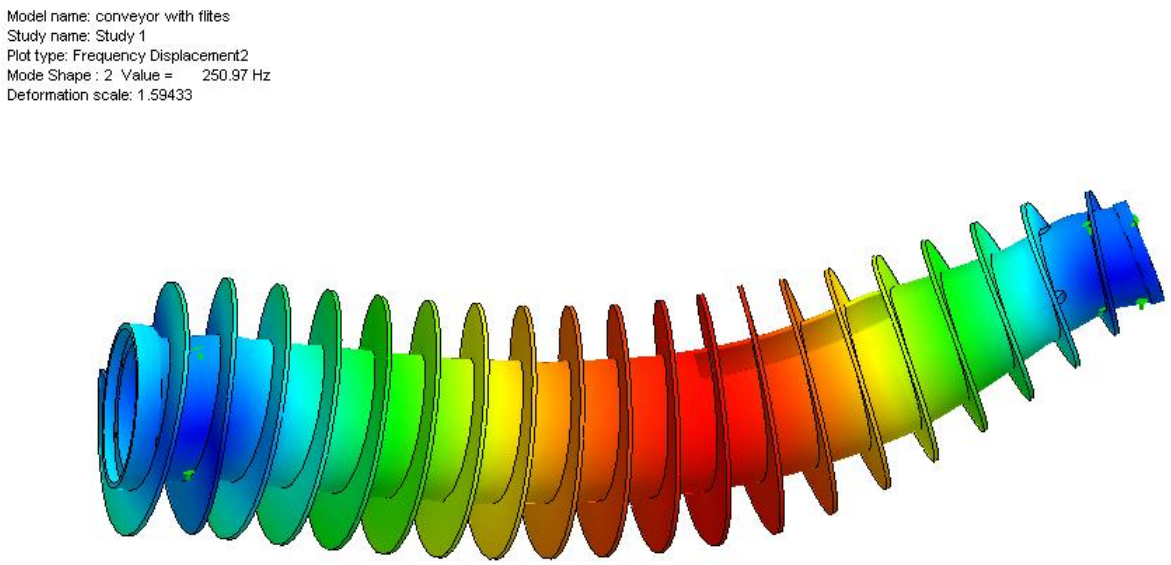

Figure 2.8 1st bend mode, slot vertical, of the conveyor by FEA.

However, whilst these simple methods are useful as a reality check they do not allow for the flexibility in the supports. The simple methods show a first critical speed that is more than four times the normal run speed and almost four times the maximum design run speed, giving the impression that the rotor design is more than satisfactory. The FEA analysis would support this view if the effects of support flexibility were ignored. This is discussed further in Chapter 3.

It is clear that the numerical model needs to include for support flexibility and that there should be good estimates of that flexibility if accurate predictions are to be made.

Only the dynamics of simple rotors are amenable to solution by exact analytical methods but real rotor systems are complex and methods using approximations must be used. The popular methods using discretized elements of the rotating system are the transfer matrix method and the finite element method. The finite

element method is now generally the most popular method as major software packages interface with CAD for importing solid models. Solid Works and ANSYS Workbench were used for this present study.

Chapter 3 Problem formulation

From the physical dynamics point of view, the centrifuge's rotating assembly has two main components - the bowl assembly and the conveyor, who's individual and joint responses determine the state of vibration of the machine under operating conditions. The bearings are the components that make the greatest contribution to the rotor responses however, as they determine the boundary conditions of restraint. Analysis of the rotating system must therefore include the dynamic performance of the bearings. Figure 3.1 shows the key elements addressed in this thesis and whose motions will later be examined in detail.

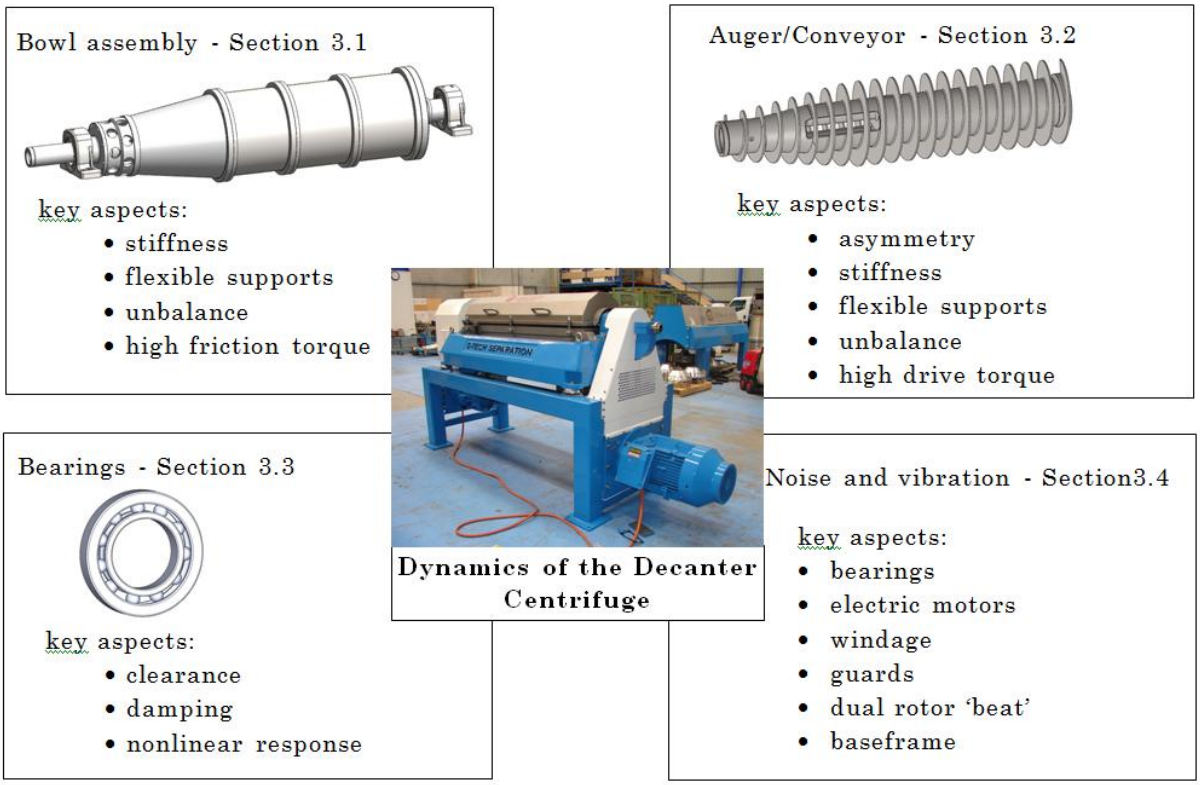

Figure 3.1 Components of the investigation that are to be addressed in order to determine the dynamic response of the rotating assembly

In machines of proven design, vibration can usually be traced to defects in assembly, unfavorable tolerance build-ups, state of balance, and sometimes errors made to the installation itself. Condition monitoring uses measurement and analysis tools to diagnose problems and identify a solution or solutions [25]. Increasingly, new designs are subject to modeling and numerical analysis using finite element (FEA) or similar methods in order to be confident that manufacture can proceed. However, in both design and diagnostics the analysis of the problem is constrained by the information available at the time and the knowledge of the engineer/diagnostician. For this present study many trials were conducted to test for, or eliminate, the following most common sources of vibration. These trials were in the unloaded state and included:

- Ensuring correct alignment of the main bearings
- Checking tightening torque of all bolts, flatness and integrity of the mounting surfaces of the bearing housings and base (for soft foot or looseness)
- Measuring run-out of the bowl, correcting or closing fits by TIG welding
- Checking all bearing fits
- Changing out machined parts, i.e. assembly in substitute parts
- Applying pre-load to the thrust bearing
- Checking the balance of the conveyor and the bowl assembly (see Appendix C)
- Checking the vibration response of the base – see Appendix B

Following these trials, the audible beat and vibration problems remained but production demands meant that the machine associated with the trials had to be released. It was some time before another troublesome machine was identified during production testing and yet the symptoms were the same. Simple calculation of the first critical speeds for the bowl assembly and for the conveyor showed them to lie above 350 Hz, which is more than 6 times the operating speed – see Figure 3.2. An elastic bending problem was therefore not anticipated as the two rotors could be treated as rigid. The occasion of a rogue machine arising within a batch was taken to be an indication that more than one factor was involved, related to the way in which the rotors are supported, asymmetry of the conveyor rotor, bearing stiffness and manufacturing limits and fits.

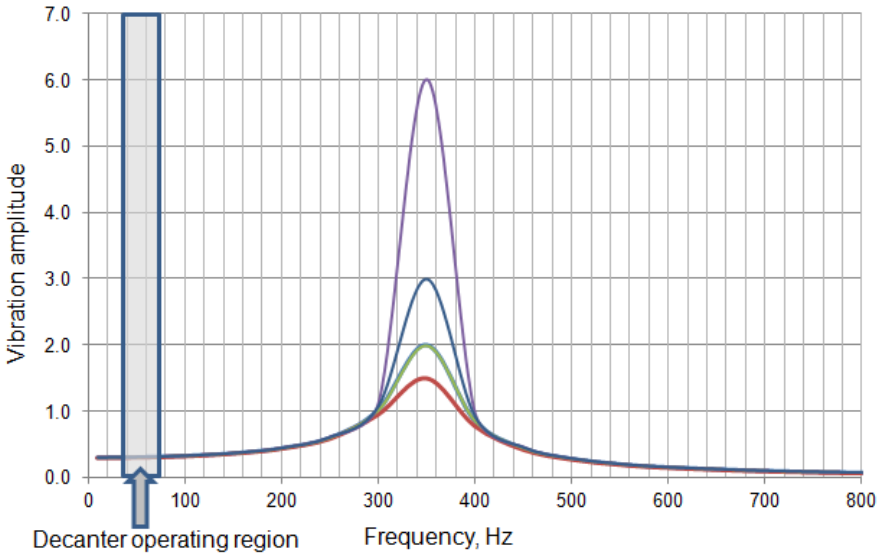

Figure 3.2 Typical frequency response curve where $\omega = \omega_n$=350 Hz, showing the decanter centrifuge's normal operating speed range

The major components of the rotating assembly were modeled using the finite element method to confirm the assumption that they are rigid bodies. Solid models were prepared in Solid Works and exported to ANSYS Workbench.

3.1 The bowl

The bowl assembly may consist of one, two or three bowl sections together with a conical section - as shown in Figure 3.3. The capacity of the centrifuge machine is determined by the number of bowl sections used – a longer bowl leads to longer residence times. The bowl is rotationally symmetric and very stiff, being designed for the radial dimension to produce a desired accelerated gravity force rather than for strength. For the test decanter for example, the typical bending stress is less than 1 MPa, the hoop stress less than 20 MPa and the longitudinal stress less than 10 MPa. It is subjected to internal pressure, axial loading, centrifugal and torsional loading.

The assembly is supported on rolling element bearings – deep groove ball type at the solids end and cylindrical roller type at the liquid end. Both bearing sets are assembled in cast stainless steel plummer blocks.

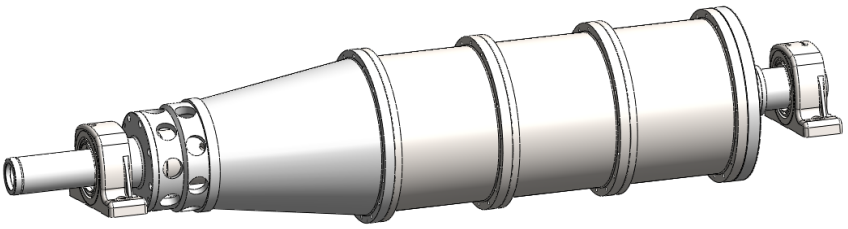

Figure 3.3 The bowl assembly

The sectional moments of inertia vary along the length with discontinuities at the flanges. A step change in inertia occurs at the liquid end hub, with a more gradual change occurring at the solids end – see Figure 3.4.

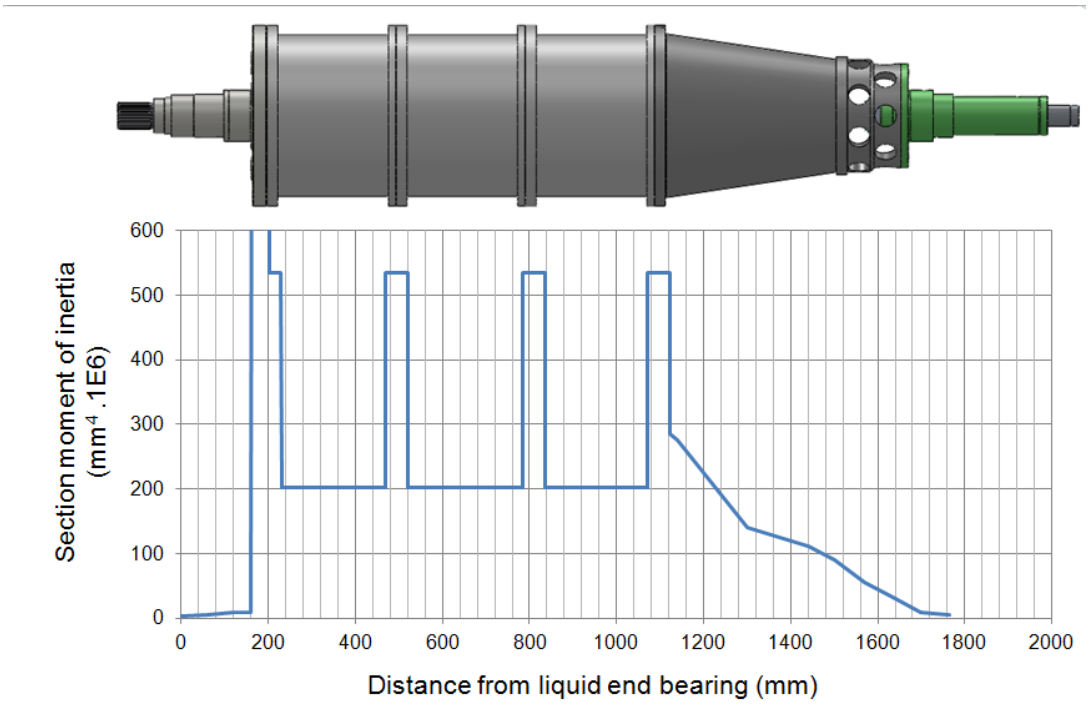

Figure 3.4 Variation of section inertia along the length of the bowl

Using the simple Dunkerley formula [29] gives the first lateral natural frequency as 310 Hz. By way of a comparison, finite element analyses using COSMOS and ANSYS both give 375 Hz for models with infinitely stiff supports – Figure 3.5.

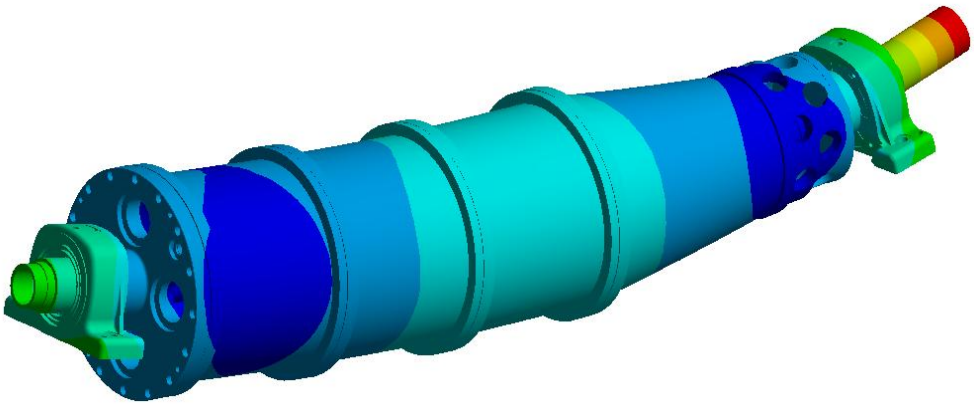

Figure 3.5 The 1st bending mode (375Hz) of the bowl assembly by FEA

The analysis confirmed that the bowl's first bending mode frequency is many times the normal run speed frequency so that neither the first (1 x rpm) or second component of vibration could be attributed to the bending mode.

3.2 The conveyor (auger screw)

A detailed knowledge of the conveyor and its supports is required in order to define its dynamic characteristics. The conveyor is mounted on rolling element bearings on journals at the liquid end hub and solids end hub. In normal operation the conveyor is subject to torsional and axial loading. However, there could be small transverse loads if the feed material is non-uniform, or if there were uneven fluid forces developed at the feed section and at the solids discharge ports. Some degree of transverse loading may arise from fluid forces caused by the radial acceleration of feed material that occurs at the periphery of the conveyor feed slot. The driving torque is applied at the liquid discharge end where there is radial "location" of the conveyor using a deep groove ball bearing. There is greater flexibility in the support at the solids discharge end, where the conveyor is supported on a needle roller bearing that has a larger radial internal clearance.

The conveyor (Figure 3.6) is a weldment consisting of fabricated or cast hub parts and helical flighting. For the machine in this study, the body is made from three parts that are castings, pre-machined to provide fits for assembly, that are then final machined after welding on the flights and stress relieving. Invariably the flights are normal to the hub surface but some manufacturers have used positive or negative rakes, especially in the dry beach area of the conical

discharge section. The body incorporates a slot whereby the feed material issues in a radial direction – this results in two principle axes of stiffness (leading to asymmetry). The feed material is fed through a stationery feed pipe that is coaxial with the conveyor body and supported off the decanter base.

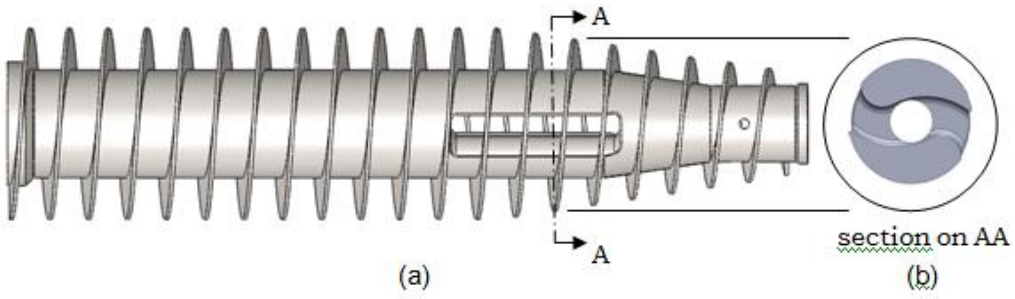

Figure 3.6 Model of the conveyor with (b) a section through the feed slot

The purpose of the conveyor is to transport the process solids to the conical section and then out to the solids discharge porting. At some axial position along the conical the process solids are transported out of the liquid surface (called the beach area see Figure A.7) and further axial motion dries the solids and introduces some compression of the bulk (or cake). The throughput of the decanter is determined by the relative rotational speeds of the bowl and conveyor. When both components are rotating at the same speed then there is no transport of solids. The maximum speed that the conveyor can rotate at is determined by the torque available to overcome the friction and the direct force required to push the process solids along the bowl. It should be remembered that the solids are under pressure developed by centrifugal action and that therefore the apparent density of the product is many orders of magnitude higher than normal – typically in the range 2000 to 3000 times.

The weight of the conveyor in this study is 252 kg (with flights) – the main body weight is 193 kg. The study of the dynamic response of the conveyor is important, even for the normal operating speed range, as the radial clearance in the bowl is of the order of 1.5mm. The dynamic deflection under unbalance and thrust loads must be less than the radial clearance in order to avoid abrasion, wear, and possible instability through rubbing.

3.2.1 Stiffness and asymmetry

The conveyor is rotationally asymmetric due to the feed slot – as shown in Figure A.4 (b) and Figure 3.7 below. In Figures 3.8 and 3.9, the variation of section inertia is shown with distance along the hub, for the two principal axes. When the slot is horizontal, the central portion of the conveyor has a fairly uniform second moment of area but there are step changes within 200 mm of each support bearing position. The section inertia is halved at the slot when it is vertical and the effect is obvious in Figure 3.8. As a result of the variation in stiffness then a range of speeds exists where shaft motion is expected to be unstable [30]. In addition the asymmetry is significant and leads to a twice rpm vibration frequency [19].

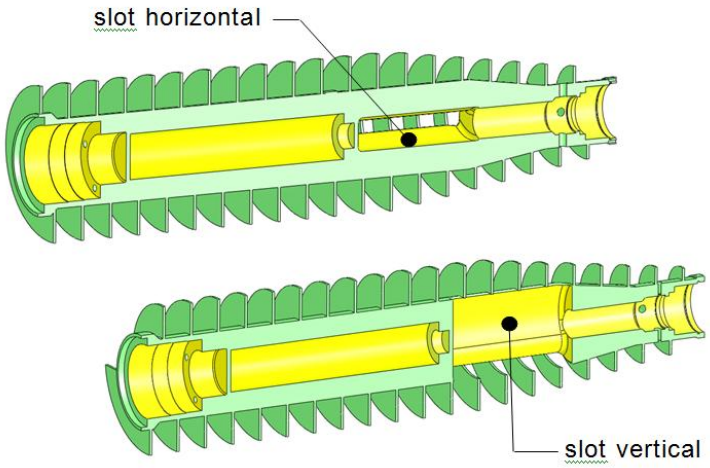

Figure 3.7 Mutually perpendicular sections through the conveyor showing asymmetry as a consequence of the feed slot

Because of the asymmetry, under the action of its own weight and even with very low levels of residual imbalance, the conveyor shaft motion has forced components of vibration that will have a resonance at approximately half the mean of the two critical speeds [30]. It is referred to as the *secondary critical speed* and is caused entirely by the gravity load and parametric excitation. This frequency and any of its harmonics must not coincide with the run speed or the natural frequencies of any components in contact with the machine (e.g. guards, base frame).

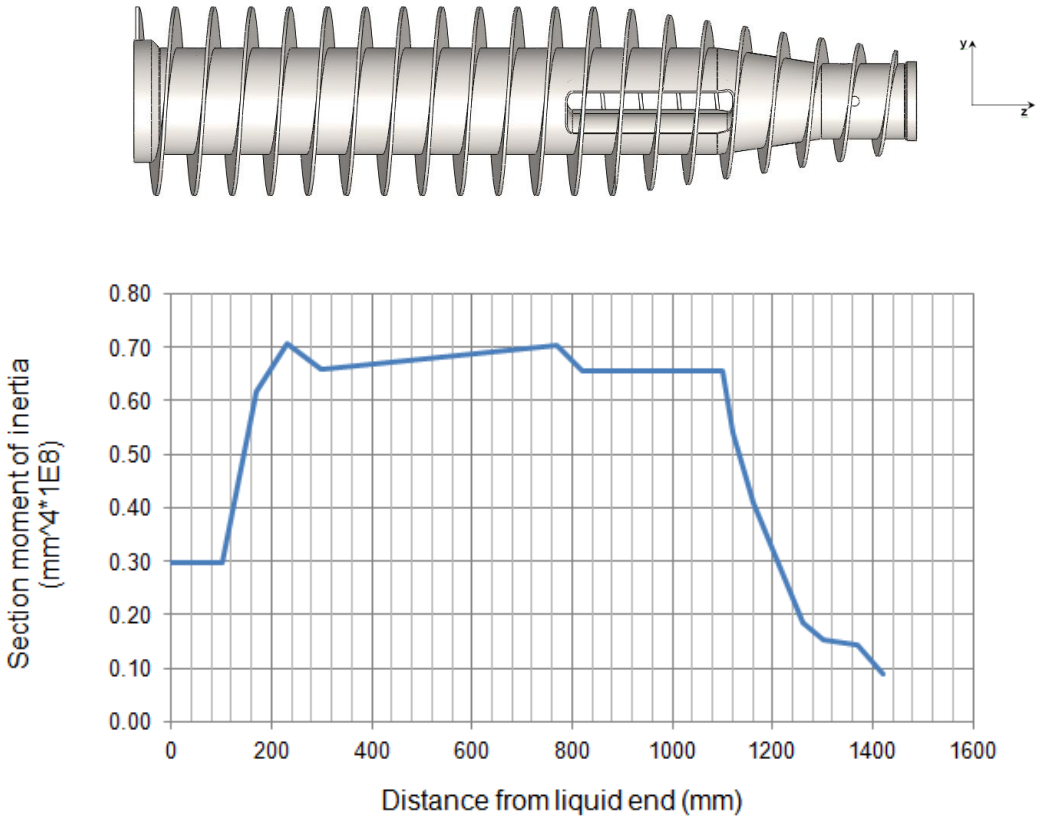

Figure 3.8 Variation of section inertia along length of the conveyor for the feed slot oriented in the xz plane

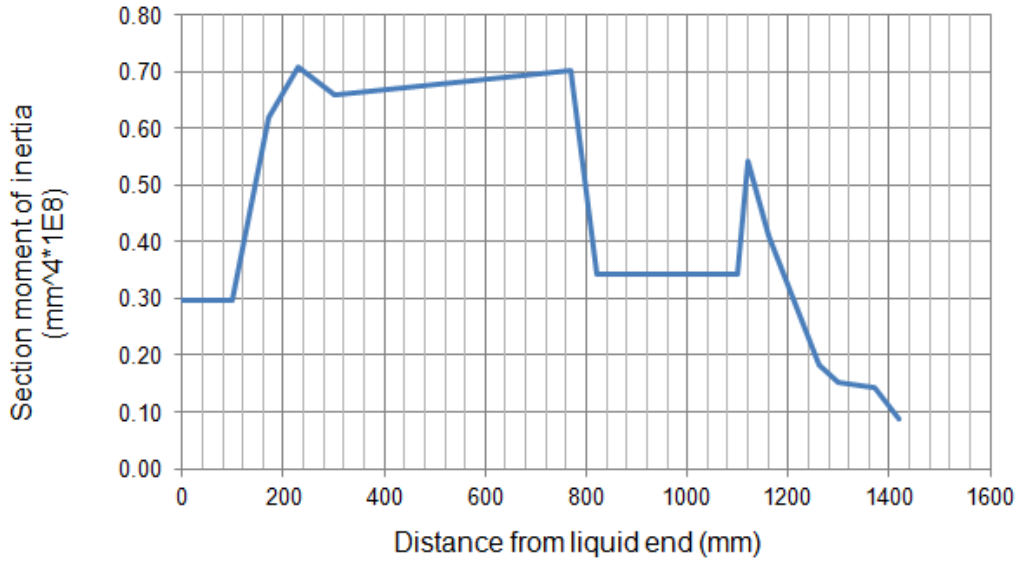

Figure 3.9 Variation of section inertia along length of the conveyor for the feed slot oriented in the yz plane

Residual imbalance of the conveyor would be almost indistinguishable from bowl imbalance unless balancing instrumentation with a resolution better than 1 Hz was available. It is therefore important to gain an understanding of the vibration modes of the conveyor and the effect that asymmetry has on its dynamic response as it may not be clear what frequency in a vibration spectrum is associated with which rotating component.

The conveyor's first bend modal frequencies, for infinitely stiff supports ("rigid" in ANSYS), were found using ANSYS to be 356 Hz (slot oriented in the xzplane) and 359 Hz (slot oriented in the yz plane) – Figure 3.10. The flights were omitted in order to shorten the solution time.

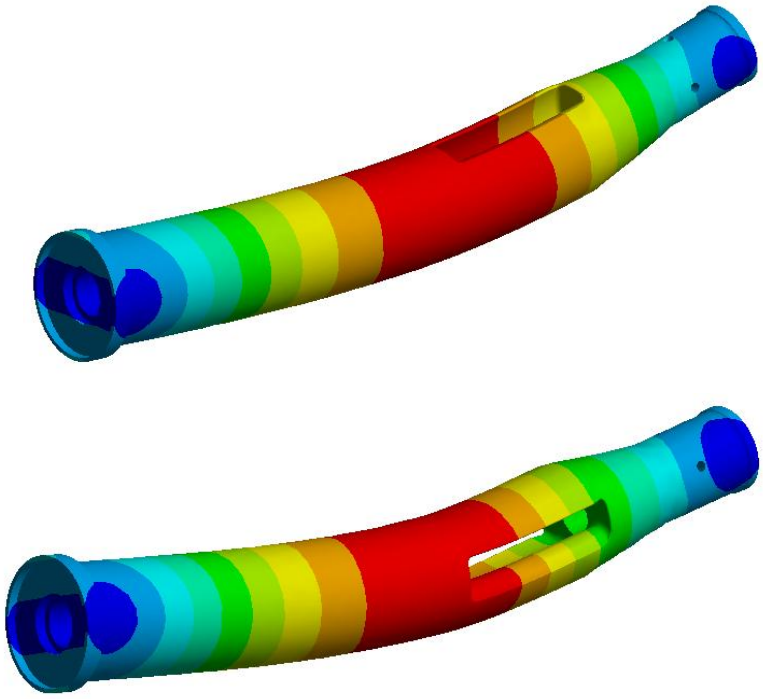

Figure 3.10 Conveyor 1st lateral vibration modes by FEA (rigid supports): top xz plane – 356Hz, bottom yz plane – 359 Hz

This result was surprising given the significant difference between the section inertias at the feed slot, although no rotational effects are included at this stage.

Laboratory load testing was carried out to assess the contribution made by the flights to conveyor stiffness and asymmetry. Figure 3.11 shows the conveyor body set up for testing without the flights, feed slot vertical. The test was

repeated for the feed slot in the horizontal position and then tested again once the flights had been welded on. Comparisons were made with the displacements obtained from a finite element study using the ANSYS software suite. This was done in order to show whether the flights could be omitted from the model without significantly affecting the solutions and whether modeling shapes of this type gives realistic solutions.

Figure 3.11 Conveyor body set up in a Baldwin Universal Test Machine for load deflection testing using DTI's.

3.2.2 Natural frequency

The value of the inherent or structural damping can be found from the free-free impact response plot shown in Figure 3.12. The *logarithmic decrement* applicable in single degree of freedom systems can be utilized by filtering the response to obtain the damping contributions at each of the modes. The logarithmic decrement is the natural logarithm of the ratio of the amplitudes of two successive peaks in the decay curve. That is:

$$\delta = ln\frac{a_1}{a_2} \qquad \ldots\ldots (3.1)$$

and

$$\delta = \frac{2\pi\zeta}{\sqrt{(1-\zeta^2)}} \qquad \ldots\ldots (3.2)$$

where ζ is the damping factor (= C/C_c). When ζ is small then $(1-\zeta^2)$ approximates to 1.0 and so,

$$\delta \cong 2\pi\zeta \qquad \ldots\ldots (3.3)$$

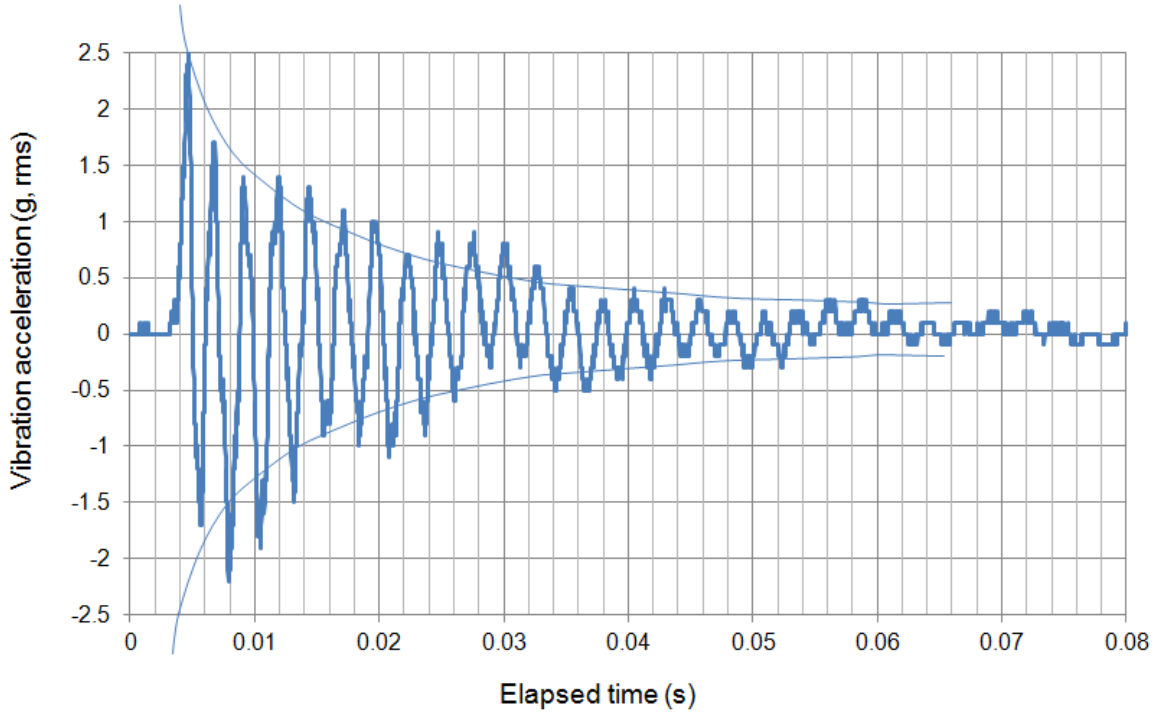

Figure 3.12 Impact response for freely suspended conveyor

From Figure 3.12, the logarithmic decrement δ is approximately 0.100 and so the damping factor is approximately 0.016 – relatively high for a steel structure. This is indicative of the degree of damping that can result through frictional forces at joints in welded structures. In a symmetric rotor, inherent damping does not contribute to control of the rotor's vibration since the deflected profile (in whirling) does not change shape. However, for the asymmetric case, horizontal and under gravity load, the mode shape may change twice per revolution between the two first bending mode natural frequencies (critical speeds) and so inherent damping would play a larger role. For the case studied here however, the rotors operate well below the first bending critical speeds and so the inherent damping is only of passing interest. The biggest contribution to the control of vibration amplitude comes from damping generated by motion within the clearance space in fluid film bearings but there is little or no damping provided by rolling element type bearings.

In summary, analysis of the conveyor has shown that its first bending mode frequency is of a similar value to that of the bowl and many times higher than the run speed frequency. The bending mode does not contribute to the first (1x rpm) and second harmonic components of vibration. Testing showed that the

fights do not contribute to flexural rigidity but their mass must be included in order to study the dynamic response. A free response test showed that the conveyor is well damped – resulting from the body consisting of multiple jointed parts welded together.

3.3 The bearings

The fundamental objective in the use of bearings is to minimize friction whilst allowing one part that supports a load to rotate inside another stationary part that provides structural support. The actual design and selection of the bearing requires engineering knowledge that can be dangerously under applied if influencing factors are not well understood. For example, modern computer codes for structural analysis often model bearings as rigid or with some form of linear flexibility. However, non-linear forcing is present in both rolling element and journal bearings due to clearance, compliance and damping, which may lead to unstable operation with unexpected vibration at speeds other than those critical speeds predicted by linear analysis, [9], [31]. Without accurate knowledge of the bearing's characteristics the results can be misleading.

Essentially the conveyor is a simply supported beam rotating inside the bowl and supported on rolling element bearings. The bearing at the solids end hub (Figure 3.13) is a needle roller type for the centrifuge type considered here. At the liquid end hub there are two bearings to support the radial and thrust loads; a deep groove ball bearing reacts the radial loading and a four point contact bearing, or an angular contact bearing, reacts the thrust. Figure 3.13 shows the assembly details at the hubs.

In Figure 3.13(a) it can be seen that the thrust bearing appears to be relatively large compared with the radially loaded roller bearing. This is because the thrust load can be high as the auger is transporting solids that are under pressure. The thrust is determined by the density of the product and the coefficients of friction at the bowl wall and surfaces of the flights. Higher friction forces occur at the dry beach zone. Typically, for this size of decanter centrifuge, the thrust can be between 1 and 12 tonnes - but the load could be higher if the discharge blocks up and the clutch fails! The axial load contributes to stiffness of the conveyor and varies according to the product application.

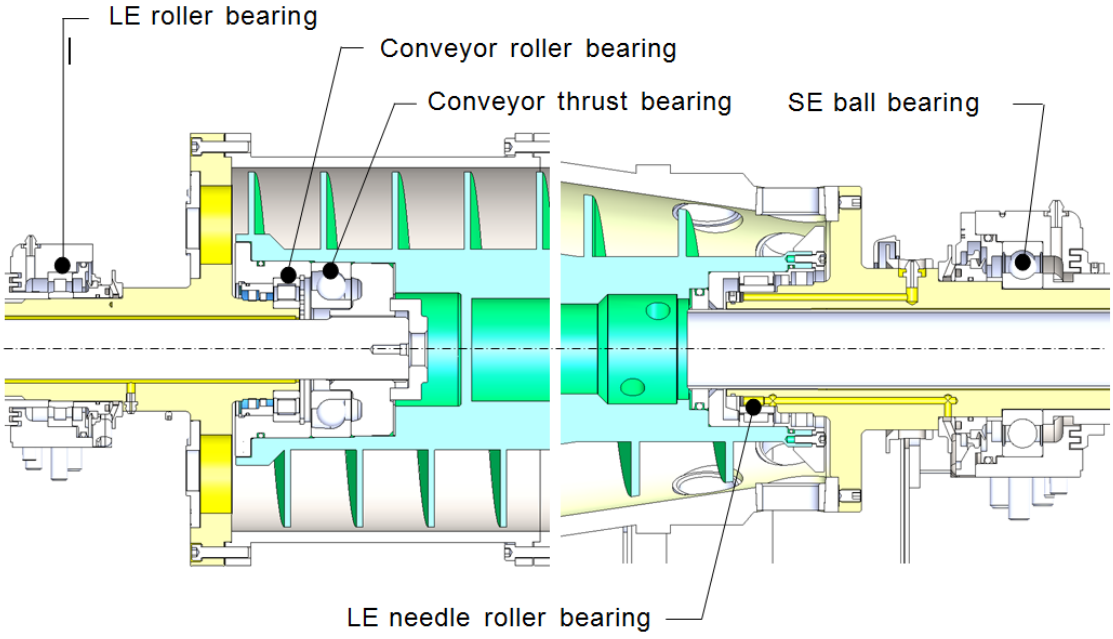

Figure 3.13 Bearing arrangements at the (a) liquid and (b) solids hubs

The supports for the bowl assembly and conveyor are problematic in that they are rolling element bearings that are oversized by necessity – to accommodate the feed tube at one end and the drive shaft at the other, and are lightly loaded as a result. The rolling element bearings have clearances to facilitate assembly and this affects their stiffness, leading to substantially lower critical speeds than those for rigid supports. The bearing clearances also result in asymmetry where gravity pre-loads the bearings in the vertical direction so that the vertical and horizontal bearing stiffnesses are different from each other. This is analogous to the stiffness characteristics of fluid film bearings [32] which are discussed later as an alternative to rolling element type. However, as far as the author is aware (with five years in the industry) decanter centrifuges use rolling element bearings exclusively.

In order to have some confidence in the prediction of rotor motion the contributions of the following influencing factors should be assessed:

- the effects of low values of loading
- the effect of internal clearance
- the effect of the number of rolling elements, and
- the effect of the diameter of the rolling element (ball or roller)

The simplest of rotor analyses assume rigid bearings – usually as simple supports allowing rotations but no translations. This assumption overestimates the stiffness and results in calculated critical speeds that are higher than are evident in reality. Rolling element bearings have clearance to facilitate assembly of the rolling elements (balls, rollers, etc) and to control the temperature at which the bearing runs. They are manufactured to international standards and each size has tolerance grades of clearance that can be specified when purchasing. For example, the decanter being studied for this project has a solids end plummer block bearing of type NU1020 C3 with a 100mm bore with a diametral clearance of 150 to 220 microns. Similarly, the liquid end plummer block bearing is a type 6218 C3 of 90 mm bore, with a diametral clearance of 60 to 116 microns. Manufacturer's clearance tables give the radial clearance, but for applications where the centrifuge is mounted horizontally it is loaded by gravity and therefore the clearance is zero at the load zone and is equal to twice the radial clearance at the top of the bearing. This leads to significant stiffness asymmetry and in the presence of unbalance will promote whirling. Although damping in rolling element bearings is not negligible, it is low and may not be sufficient to control whirl amplitudes at or near resonance [22, 32].

A further complication is added by considering the possible asymmetric flexibility introduced by elasticity (compliance) of the bearing housing(s).

The bearings for the decanter centrifuge have been sized to be geometrically large enough to allow the hubs to be hollow to accommodate the gearbox drive shaft to the conveyor at the liquid end and the feed tube at the solids end. The conveyor mass is not high (around 245kg) so there exists a possibility that the bearings could be lightly loaded and skidding may occur.

Bearing manufacturers recommend a minimum load be applied in order to avoid skidding and its damaging effects. The following expressions for estimating the minimum load for single row roller and ball bearings and needle roller bearings are:

$$F_{rm} = k_r \left(6 + \frac{4n}{n_r}\right)\left(\frac{d_m}{100}\right)^2 \quad \text{and} \quad F_{rm} = 0.02C \qquad \ldots\ldots (3.4)$$

where:

F_{rm} = minimum radial load (kN)

k_r = minimum load factor (from product data)

n = rotational speed (rpm)

n_r = reference speed (rpm) (from manufacturer's product data)

d_m = mean diameter of the bearing (mm)

= 0.5(d + D)

C = the basic dynamic load rating

(i) For the conveyor's liquid end bearing (type NU216EM):

d = 80mm, D = 140mm, n = 60 rpm, n_r = 5300 rpm, k_r = 0.16

Then F_{rm} = 1.17kN or an equivalent mass of 119kg

(ii) For the conveyor's solids end needle roller bearing (typeNKI85/26):

C = 73700N and therefore

F_{rm} = 1.47kN or a minimum equivalent mass loading of 150kg.

The conveyor mass is 243 kg and is distributed almost equally on its bearings, being 123kg at the solids end (SE), and 120 kg at the liquid end (LE) - Figure 3.15. Thus it can be seen that the load on the liquid end bearing marginally meets the minimum recommended by the manufacturer, and the solids end needle roller is below the minimum. On start up, when the grease in the bearings is more viscid, the minimum loads need to be higher [*SKF product guides*] and so vibration and possible noise problems are expected – especially at the solids end. This is indeed the case in practice and the solids end always exhibits the higher vibration levels and skidding of the rolling elements – evidenced by audible squealing. Adding more grease stops the squeal.

In the presence of unbalance, the light loading combined with internal clearance in the bearing at the solids end will promote whirling – this is examined in Chapter 4.

3.3.1 The main bearing housings

Physical testing has not been carried out on the plummer block housing but the author conducted a FEA study using ANSYS to determine what degree of asymmetry the housing exhibits under load – refer Figure 3.14.

The study showed that the housing is approximately five times stiffer for loading in the horizontal plane than for loading in the vertical plane. However, under the action of typical imbalance loading, the housing is expected to deform by less than 1 micron, which is substantially lower than the clearance in the bearing (<1%).

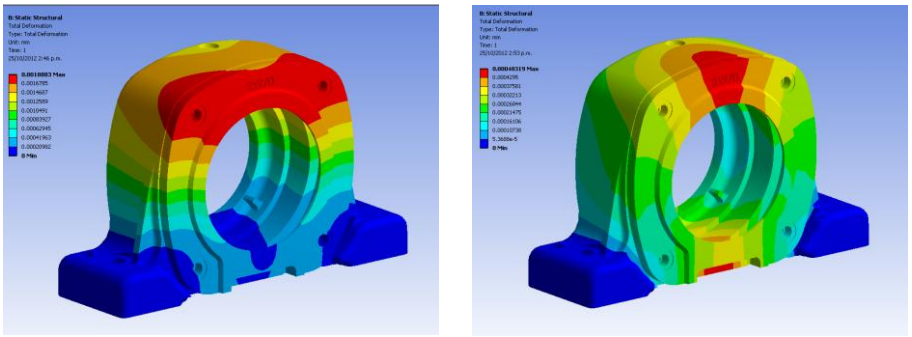

(a) (b)

Figure 3.14 FEA plots of displacement for (a) horizontal loading and (b) vertical loading

3.3.2 The bearing loads

The bearings are statically loaded with fractions of the deadweights of the rotors – as distributed about their centres of gravity as shown in Figure 3.15. In addition, the solids end bearing is loaded by the main drive belt tension and the liquid end bearing by the weight of the gearbox and its drive belt tension. Dynamically they also each have components of radial loading from the residual unbalances of the conveyor and bowl assembly. Figure 3.16 shows the locus of the resultant load vector from the bowl unbalance interaction with the deadweight load with rotation for two unbalance cases: (a) for a 20 g weight and (b) for a 55 g weight at the bowl radius. For case (b), the unbalance force is sufficiently high as to offset the dead weight of the bowl and the bearing momentarily carries no load.

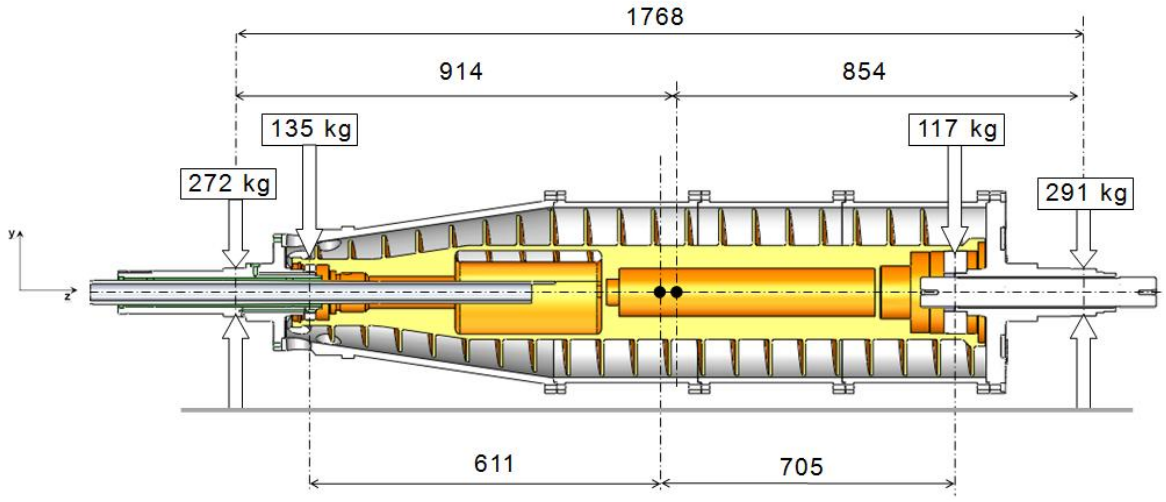

Figure 3.15 Weight distributions and position of mass centres (●). The loads at main bearings are for bowl and conveyor combined

The unbalances could result from mass/density variations in castings but is more typically due to run out on machined spigots or bearing surfaces. In case (b), where we introduced an unbalance of 9625 g.mm, then the mass centre of the liquid end of the conveyor needs to be displaced by 0.082 mm to obtain an unbalanced force that periodically nulls that weight at a run speed of 3250 rpm. This required run-out approximates to the actual production machining tolerance of ± 0.01 mm together with the typical bearing clearance for the solids end bearing. For a rotational speed of 3250 rpm, this displacement generates a vibration velocity of 20 mm/s rms, or 28 mm/s peak – which is well outside the acceptance specification for ISO1940 Grade G6.3! Whilst the balancing process can correct to better than this level it is to be noted that even when machined all over, components are likely to be unbalanced due to the machining tolerance, tolerance build-up on assembly and bearing clearances. The spin axis of the conveyor is dependent upon the concentricity of the two journals relative to the main bearing journals at each hub.

Balance correction is made to the bowl following machine assembly but this does not correct for any imbalance of the conveyor that is introduced as a result of the concentricity run outs of the journals. Whilst there is a wide range of publications on rotor balancing there is very little on the dual rotor case and only a few papers on dual rotors with very little speed difference [33]. This is a

separate problem but does highlight the possibility of there being significant periodic force from imbalance of the conveyor.

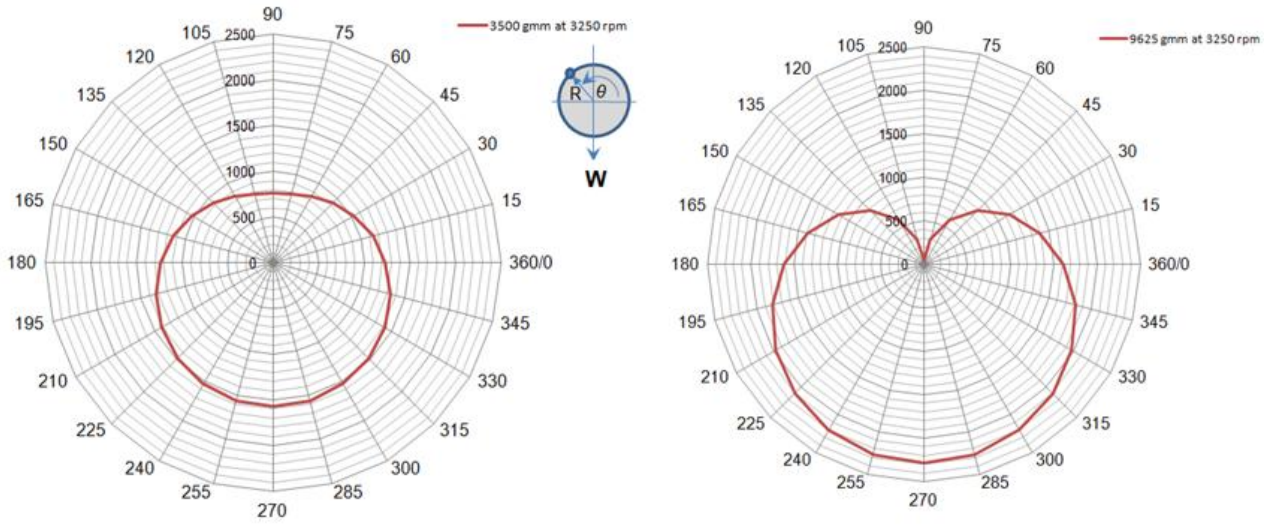

(a) (b)

Figure 3.16 Two cases of unbalance force and the effect on bearing load at 3250 rpm
(a) 20 g at 175 mm radius (3500 g.mm),
(b) 55 g at 175 mm radius (9625 g.mm)

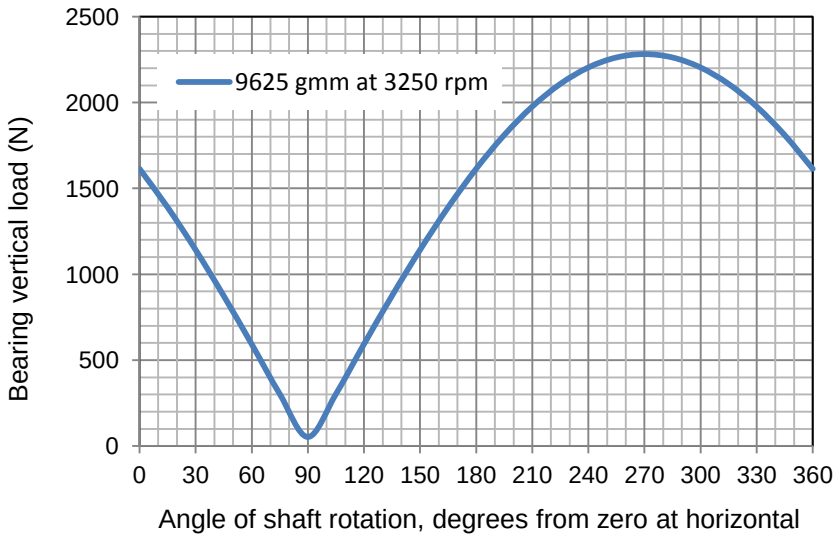

Figure 3.17 Force variation with shaft rotation due to self weight and unbalance - Cartesian version of Figure 3.16(b)

The situation becomes further complicated when the residual unbalance of the conveyor is added to that of the bowl. Since the conveyor rotates at a different

speed the two unbalances slowly come in and out of phase. If the conveyor unbalance component is sufficiently high then it will periodically cancel out the bowl unbalance as shown in Figure 3.16(b) and Figure 3.17. The beat phenomenon that occurs because of the differential in speed between the two rotors is shown in Figure 3.18. For the two chosen values of rotating unbalance shown in Figure 3.18, the total unbalance force periodically vanishes with a period equal to the period of the differential speed – in this case for 1Hz.

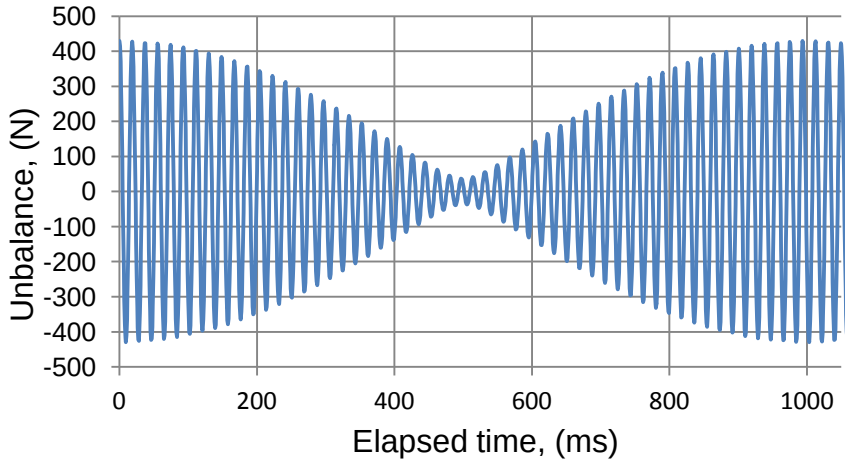

Figure 3.18 Time varying effect of the combined conveyor and bowl unbalances (case of unbalances of: bowl – 1750 g.mm and conveyor – 2000 g.mm)

For the bearing loads, the gravity load is augmented by the periodically varying unbalance loading so that together the main bearing load is as shown in Figure 3.19.

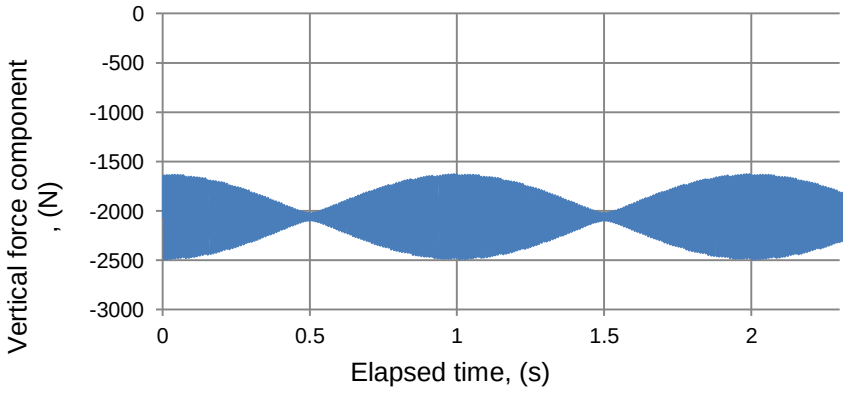

Figure 3.19 Variation in vertical force at the main bearing due to unbalance and deadweight

The force variation occurs at the frequency of the differential speed ($\boldsymbol{\Omega}_{\text{bowl}} - \boldsymbol{\Omega}_{\text{conveyor}}$), and for some unbalance combinations the gravity load may be mitigated.

The unbalance forces appearing at the bearings (F_b), can be determined from the time varying displacement *x(t)* as:

$$F_b = m\ddot{x}(t) \qquad \ldots\ldots (3.6)$$

where $x(t) = (A\sin(\Omega_b t + \vartheta) + B\sin(\Omega_c t + \alpha))$ $\ldots\ldots$ (3.7)

m = mass loading at the bearing

A = displacement amplitude due to bowl unbalance

B = displacement due to conveyor unbalance

$\boldsymbol{\Omega}_{\text{b}}$, $\boldsymbol{\Omega}_{\text{c}}$ = rotational angular frequencies of bowl and conveyor resp., usually $\boldsymbol{\Omega}_{\text{c}} > \boldsymbol{\Omega}_{\text{b}}$

ϑ, α = relative phase angles, from a reference on the bearing, for bowl and conveyor respectively.

The amplitudes A and B are dependent upon the unbalances at the liquid and solids ends and on the influence coefficients between them. In addition, the phase angles of the unbalances at the liquid and solids ends of the machine will invariably not be the same - see Figure 3.20. They are coincident once every $2\pi/(\boldsymbol{\Omega}_{\text{bowl}} - \boldsymbol{\Omega}_{\text{conveyor}})$ second, e.g. a period of 60 seconds for a speed differential of 1rpm (2π rad/s).

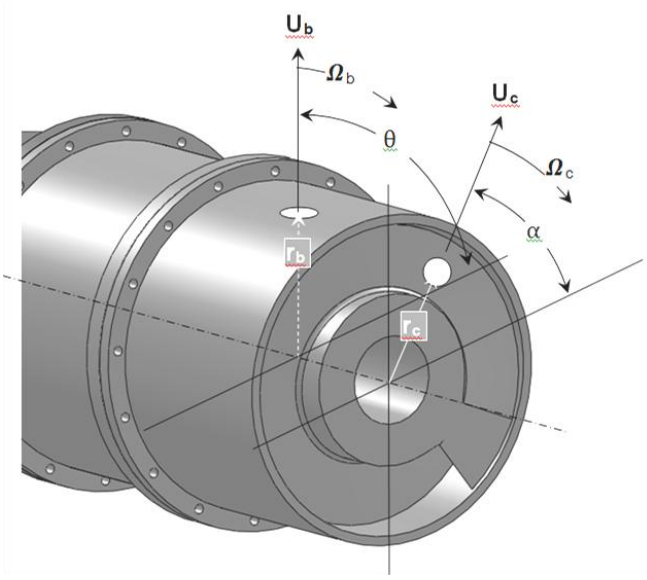

Figure 3.20 Unbalances in conveyor and bowl

The close proximity of the two speeds of rotation makes balancing difficult and most often it is incorrectly carried out. Access to the conveyor of an assembled machine is extremely limited – being basically through any of the discharge ports, making attachment of correction weights after assembly very difficult. This means that even in the best achievable balance state there will still be residual unbalance to act as a source of excitation.

3.3.3 Bearing stiffness

The stiffness of a rolling element bearing varies around its periphery as a consequence of the number of rolling elements that are loaded, the materials of the elements and raceways, the clearance and geometry of the bearing, and the direction and magnitude of the applied load [22]. Both inner and outer raceways and the elements themselves are considered to deform locally under load and if mounted in flexible housings then their deformations must also be considered. Clearances in mechanical systems generate strongly non-linear responses that can be non-periodic or even chaotic in some conditions [34]. The clearance in bearings is also referred to as the *deadband* although Childs [8] also uses that term for the clearance provided in the housing for fitting the bearing. In Childs' later paper [35] he sets out to show mathematically that ellipticity in the *deadband* clearance generates a twice rotational speed component. However, in his concluding comments he notes that the magnitude predicted does not match observed data so that whilst elliptical clearance can produce a second order vibration, the levels are substantially lower than that for the first order. The observed second order vibration component in the decanter centrifuge is almost always greater than that of the first order. However, whilst subsequent testing by Childs revealed structural modes with resonance in close proximity with the second order frequency, testing showed that this is not the case for the centrifuge. It should be noted that Childs' analysis for the elliptical clearance case followed Yamamoto's early work [36] featuring a vertical shaft in order to remove the gravity load. Gyroscopic and cross coupling effects were also removed as the shaft had a central disc and both support bearings had the same properties – an unrealistic proposition.

For the horizontal rotor, there is no clearance at the bottom arc of the bearing; the inner ring loads the rolling element which in turn loads the outer ring and

support housing – the clearance is a maximum at the top arc of the bearing as shown in Figure 3.21.

The inner ring, rolling element and outer ring all deform locally under the action of the load *W*. The rolling elements are spaced apart by an integral cage, to prevent bunching and maintain separation, and precess around the bearing at a rate referred to as the "ball (or roller) pass frequency – or BPF". The load imparted to each element depends upon its location within the bearing, the number and diameter of the elements, and the internal clearance. Maximum loading occurs when an element is directly under the load vector as shown in the left drawing in Figure 3.21.

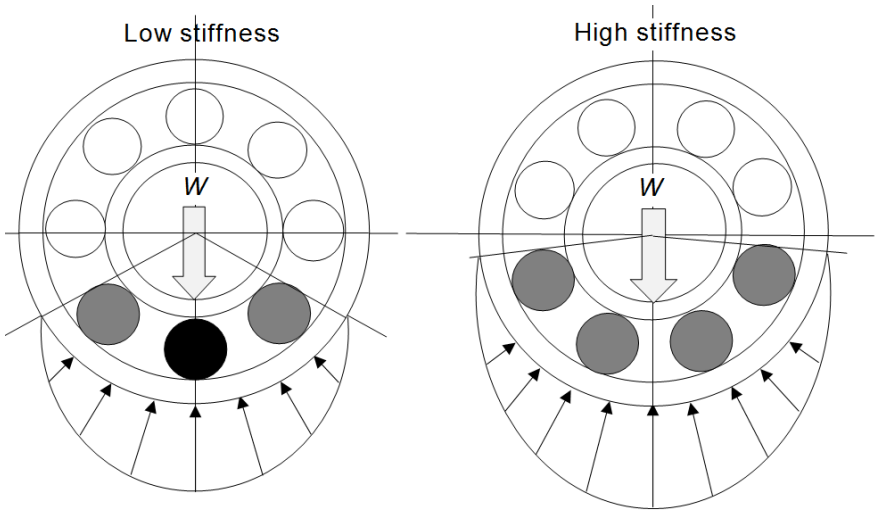

Figure 3.21 Two load cases showing the effect of the number of rolling elements on the loading zone

In Figure 3.21 it can be seen that the load zone changes shape with rotation of the cage as the load is shared by a varying number of elements. Clearly there is a stiffness variation determined by the number of rolling elements and since rotor response is sensitive to bearing stiffness then accurate data must be used. Consequently, for realistic studies a single value stiffness values cannot be used.

Yi Guo [37] presents research by the National Renewable Energy Laboratory (NREL) that shows serious differences between various established theoretical models (those of Harris, Gargiulo, Jones, and While). The variations ranged from 41% to 118% and represent a serious challenge to established rotor dynamics codes that are based on theoretical values for bearing stiffness. Three

proprietary programs showed variations from +10% to -66% for radial stiffness k_x of a cylindrical roller bearing and from -12% to +74% for k_y. The variations were smaller for a ball bearing but still of significant difference (max -22%). NREL carried out FEA studies for ball and roller bearings with the results being supported by experiment, in order to study the contributors to the variations. They further showed what modification had to be made in order for established theory to match experiment. The expected variation in stiffness, resulting from the change in load zones as depicted in Figure 3.22, appears to be the root of the differences in proprietary software since they use averaged values. Figure 3.22 shows a figure extracted from Guo's results, where the low stiffness values are for 4-element load sharing and the high stiffness value peaks are for 5-element load sharing.

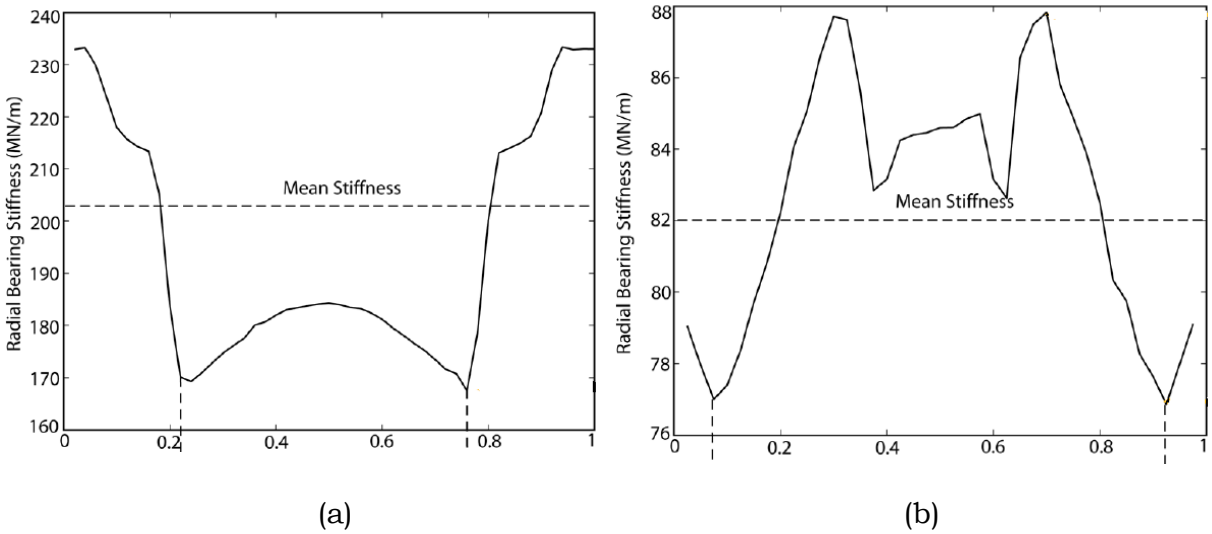

Figure 3.22 Variation in stiffness with cage rotation over 1 revolution (from *Guo* [37]) (a) roller bearing (b) ball bearing, for 4- and 5-element load sharing.

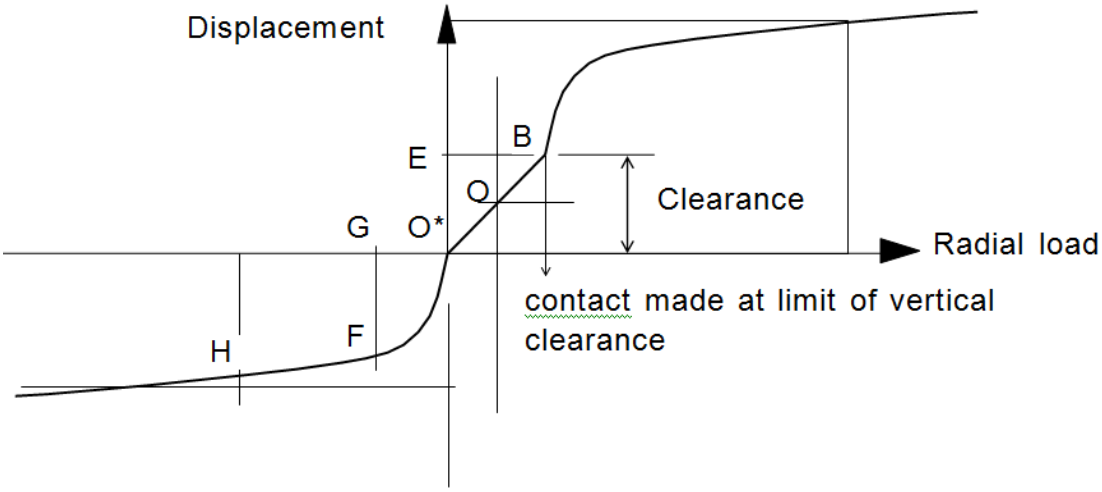

Figure 3.23 Typical displacement variation with load for a rolling element bearing

For Figure 3.23, the nominal axis of rotation provided by the drive source is at *O*. The distance *between O** and *E* represents the diametral clearance in the bearing and *B* is the point where the rolling element just contacts both inner and outer raceways, i.e. there is no clearance between the parts, at the upper vertical extreme. The point O* is where the rolling element just touches the outer race at the lowest extreme. The gravity load deforms the inner and outer raceways so that further shaft displacement occurs between O* and F, and the actual axis of shaft rotation is at F. The unbalance force leads to further deformations of the inner and outer raceways at some point H, say. As the unbalance is a rotating force then point H will move up and down the displacement curve. If the unbalance force periodically negates the rotor mass then the journal centre will move between H and B.

A new unbalance is introduced by the offset of the rotational axis due to clearance and deformation in the bearing so that should whirl take place there is some eccentricity in addition to imbalance. It is clear that the load displacement relationship (stiffness) has both linear and non-linear parts.

Harris [22] gives the following expressions for the stiffness of rolling element bearings:

$$k_{bb} = 4.77E^{-6}ZD^{1/2}\cos^{5/2}\alpha\delta_r^{1/2} \quad \text{- for ball bearings} \quad \ldots\ldots (3.8)$$

$$k_{rb} = 4.77E^{-6}ZD^{1/2}\cos^{5/2}\alpha\delta_r^{0.11} \quad \text{- for roller bearings} \quad \ldots\ldots (3.9)$$

where :

Z = number of rolling elements

D = ball or roller diameter

α = contact angle

δ = radial deflection

and $\delta_r = \frac{4.62E^{-5}F_r^{2/3}}{Z^{2/3}D^{1/3}\cos^{5/3}\alpha}$ …… (3.10)

where: F_r = the applied force

Inspection of these equations shows the stiffness of a given bearing to be a non-linear function of the applied load, F_r. These formulae are used to determine the bearing ring deformation under load and thence the bearing stiffness. Deflections from the vibrating shaft are used to calculate the restoring forces from the bearing – which are then used as input to the shaft at the next time interval in a time marching integration routine. The load is shared by a number of rolling elements and this is taken care of in the above expressions using factors derived by Stribick, 1907 [38]. However, k_{bb} and k_{rb} are the static stiffnesses, since the applied loads vary with rotation, as seen in Figure 3.19. Not only do the loadings from the shaft vary with rotation, but the number of elements supporting those loads also varies as the rolling elements scroll around with rotation of the inner ring.

In summary, analyses of the bowl and conveyor showed that their fundamental flexural modes of vibration occur at margins well above the run speed so that they can both be classed as rigid bodies. The bearings must be considered as the elements that promote rigid body modes of vibration at frequencies that contribute to the 1 x rpm and second order vibrations.

3.4 Noise and vibration

The sound field for a decanting centrifuge has many sources that include: the electric motors, the transmission, the belt guards, the hopper and cover, the sub-frame, the bearings, and windage from the rotating assembly. The windage creates a turbulent field inside the hopper and cover enclosure that acts as a stochastic force on the rotor. Randle [39] studied the sound field using sound intensity techniques and found that the greater portion of the sound can be

attributed to windage. It is surmised that a complex flow environment exists at the solids end where the discharge is radial (compared with the liquid end's axial discharge) and the protruding ports add to flow disturbance. Vibration from the rotating assembly is transmitted to parts of the machine directly by the path at the main bearings. Vibration isolators are commonly used to break the path to the subframe, but naturally these are not 100% efficient so there is some transmission. Where panels have resonant frequencies close to or matching the run speed frequency or its harmonics, then sympathetic vibration occurs. This can lead to noise generation and fatigue. In many centrifuge applications the noise is not an issue but vibration is, and for others the reverse is true. In rendering works for example, where the ambient noise level from other plant exceeds that emitted by the centrifuge, the machine can be quite noisy yet be acceptable. In municipal waste-water applications both low vibration and reduced noise emissions are acceptance criteria.

Hydrodynamic bearings generate significant stiffness and damping capacity as functions of the rotating speed and do not have the load and speed restrictions imposed by the rolling element type bearings. They are quieter in operation than the rolling element type but little work is published on the mechanics of noise generation [40, 41].

For the centrifuge being studied, the main bearings were converted to hydrodynamic oil film bearings to:

1 Demonstrate the noise reduction possible – over that from using rolling element bearings
2 Enable longer life between replacements
3 Enable higher run speeds
4 Eliminate bearing and other exciting frequencies causing resonance of attached components such as the drive and gearbox guards

Chapter 5 details the bearing design and machine modifications and Chapter 6 discusses the results of testing.

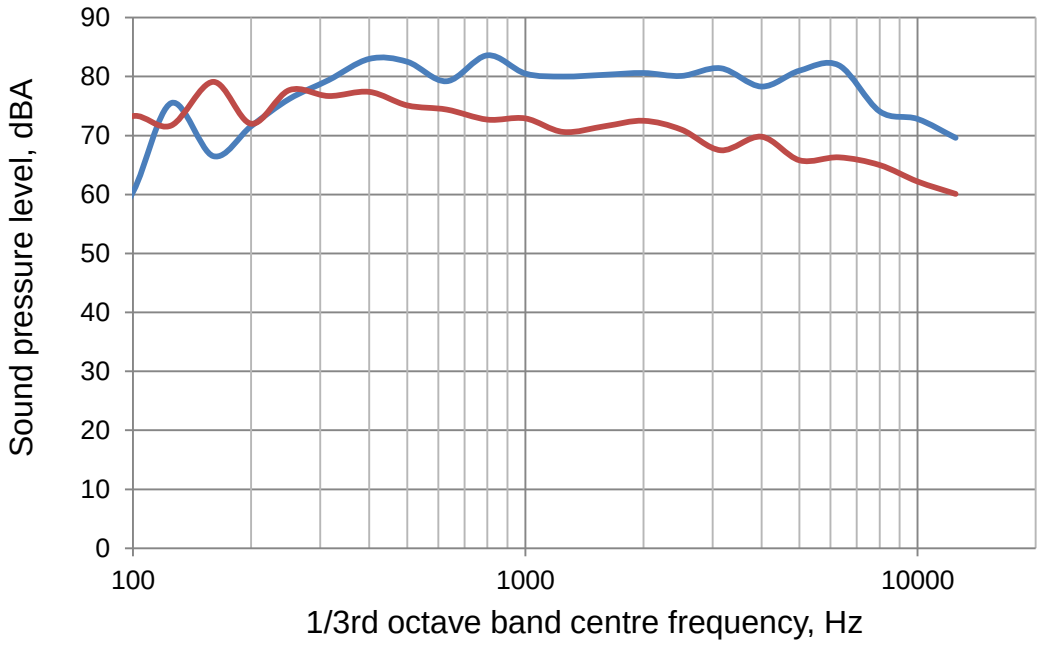

.

Figure 3.24 Comparative noise levels before (blue trace) and after (red trace) making changes to the base and bearings

The presence of a significant imbalance of the conveyor is usually detected as an audible beat – well balanced machines do not exhibit a well defined beat since the unbalanced forces are much lower. Imbalance is the primary source of excitation in the decanter centrifuge's rotating assembly that leads to vibration of the machine.

A second less well recognized source of excitation is the driving torque and its associated resisting torque. These loads are separated by the length of the conveyor and whilst the conveyor is stiff in torsion, the supporting solids end bearing is not. In the absence of a resisting torque the solids end journal is free to vibrate within the clearance zone of the bearing but is less likely to do so until there is a friction torque from scrolling out product.

Chapter 4 Routes to a solution

Figure 4.1 shows the approach used to research the problem associated with the audible beat frequency and associated high vibration levels that occur sporadically in decanter centrifuges. The diagnostic investigation included run tests and dismantling parts of the machine for metrology checks. When the diagnostic route failed to identify a specific cause then the experimental and theoretical routes were followed. The experimental study was focussed on changing those parameters that affect rotor response as detailed in Chapter 3. Similarly, the theoretical study focussed on FEA modelling whereby damping and cross coupling of bearing forces could be modified and the effects on rotor response assessed.

Chapter 5 details the modification made to the main bearings to provide damping, and Chapter 6 summarizes the testing.

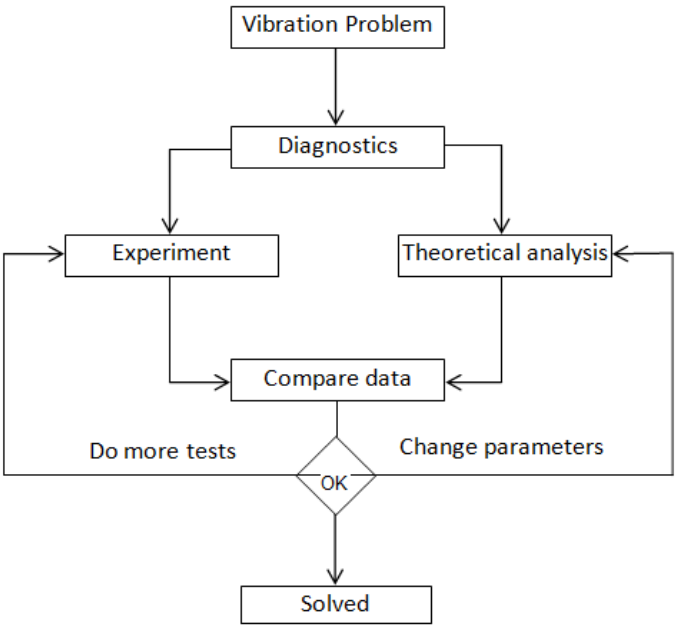

Figure 4.1 Routes to the solution

4.1 Rotor dynamics modelling

General rotor dynamic systems can be complex assemblies of shafts, discs, bearings and seals. In this respect the rotors of the decanter centrifuge are each simple systems – the complexity lies in their co-axial combination.

The rotor dynamics problem is to not only understand how the two-rotor system responds to periodic loading (unbalance) under steady state running conditions, but to determine the contributions that deformations and clearances in the bearings make. We need to quantify the severity of the effects, where the field of displacements is important for example, to avoid rubbing of the conveyor on the bowl and or conical. In the first instance though, it is necessary to identify natural frequencies and to assess their importance in relation to the normal operating speeds, determine the response to unbalance and finally the response to transients.

Differential equations can be formed that describe the time-dependent response of many mechanical systems. When a closed form solution to these equations cannot be found then a numerical method is used. There are many numerical integration procedures but they all have two common features: firstly the differential equations are only satisfied at discrete values of t (over small time intervals) and not for all time; and secondly, within each small time interval an assumption is made of the way in which variation(s) in the displacement, velocity and acceleration occur. The various integration schemes available are defined by the way in which the assumed variations are treated. The most convenient technique for evaluating the dynamic response of rotor-bearing systems, with the inclusion of non-linear bearing properties, is by a step by step integration procedure – also referred to as *time-marching* analysis.

Once the equations of motion have been derived, the model is solved by either analytical or numerical methods. The analytical approach is usually only applied in simple cases as the assumptions made in order to facilitate the solution can compromise the accuracy of the solution. The assumptions made about the boundary conditions at the bearings have the greatest influence – as indicated in Figure 2.7 of Section 2.1. The simple methods include Dunkerley, Rayleigh, and Rayleigh-Ritz and these methods compute non-rotating natural frequencies and do not include for inertia or gyroscopic effects.

Mathematical tools for analyzing the response of rotating systems (rotor dynamics) include transfer matrix and finite element methods [2]. The finite element method enables the coupling of bearing characteristics (stiffness and damping) with the rotor as well as the inclusion of static structural parts. Various software packages are available for the study of the dynamic response of rotor systems. ANSYS is one such package and was used in this present study. Some problems were encountered in its implementation however and these are discussed in Appendix E.

Figure 4.2 shows a model of the two rotor system with its applied loadings.

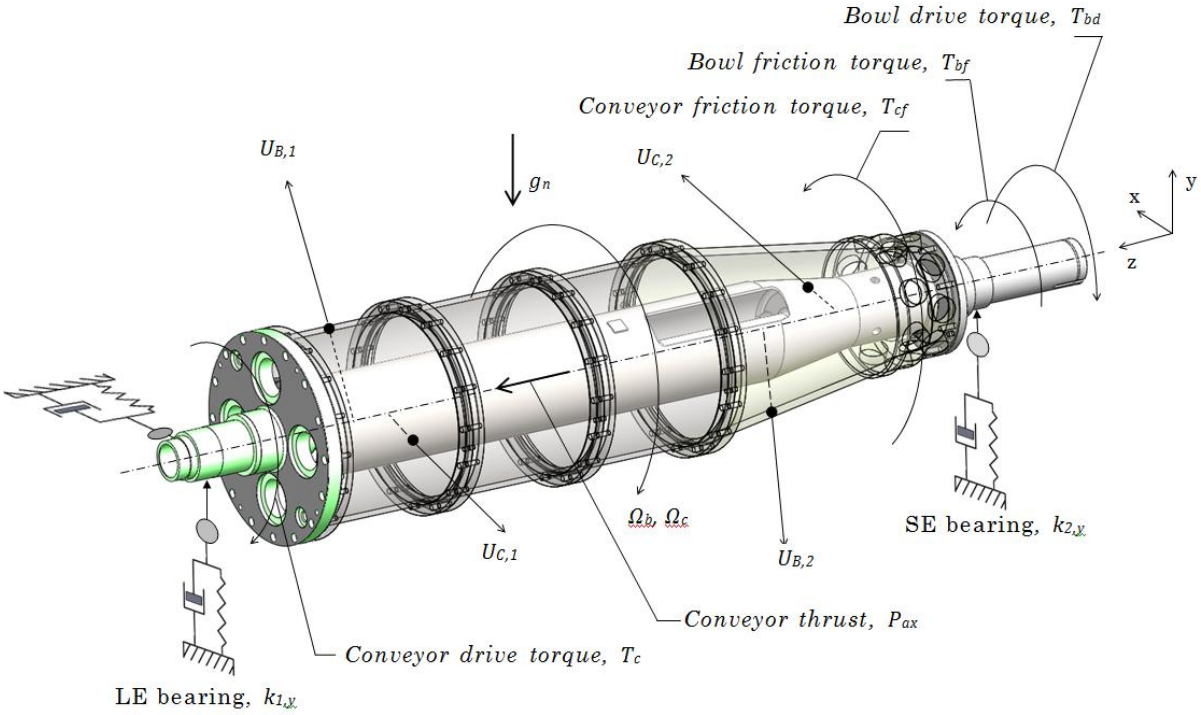

Figure 4.2 Two rotor assembly – auger shown without flights for clarity

Where the loads are:

T_{bf} - is the bowl friction torque,
T_{cf} - is the conveyor friction torque, developed on the face of the flites
T_B - is the torque required to drive the bowl, and
T_c - is the torque required to drive the conveyor
U_{ij} - are the unbalances for the bowl and conveyor, magnitude and phase
P_{ax} - is the axial load on the conveyor resulting from transport friction
F_T – is the axial thrust reaction load in the bowl
Ω_b and Ω_c are the two rotor speeds for bowl and conveyor respectively.

In general terms, the matrix equations of motion of each rotor system will be in the form [10] :

$$[\mathrm{M}]\{\ddot{u}\} + ([\mathrm{C}] + [\mathrm{G}])\{\dot{u}\} + ([\mathrm{K}] + [\mathrm{B}])\{u\} = \{F_u\} + \{F_B\} \quad \ldots\ldots (4.1)$$

$$[\mathrm{M}]\{\ddot{v}\} + ([\mathrm{C}] + [\mathrm{G}])\{\dot{v}\} + ([\mathrm{K}] + [\mathrm{B}])\{v\} = \{F_v\} + \{F_B\} \quad \ldots\ldots (4.2)$$

Where:

[M] = mass matrix

[K] = rotor stiffness matrix

[B] = rotating damping matrix (material or internal damping)

[C] = structural damping matrix,

[G] = skew symmetric gyroscopic matrix

$\{F_U\}$ = column vector of unbalance forces and gravity

$\{F_B\}$ = column vector of bearing forces, functions of velocities and displacements

$\{u\}, \{v\}$ = vectors of displacements in x and y

The corresponding schematic is shown in Figure 4.3.

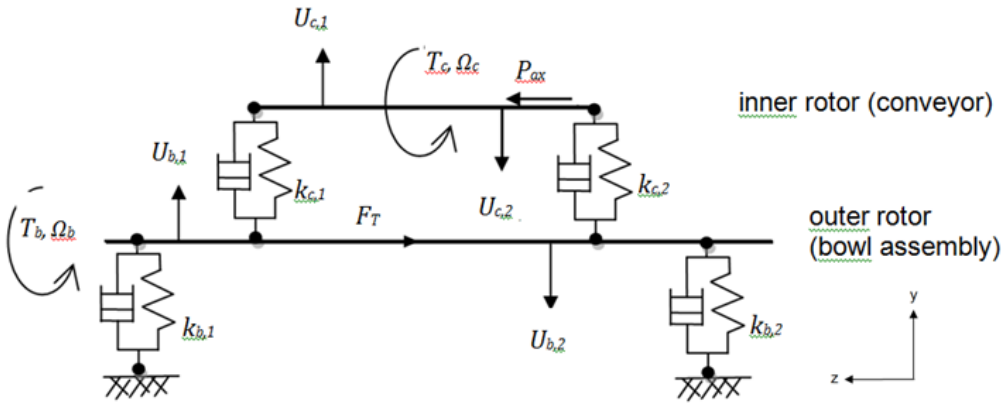

Figure 4.3 Schematic representation of dual decanter centrifuge rotors

Solutions were sought using solid models exported to ANSYS and analyzed using the Workbench GUI (graphical User Interface). This enabled the easy addition of the stiffness and damping variables together with internal or material damping using appropriately selected element types.

For two simple rigid rotor models of the decanter centrifuge, Figure 4.3 reduces to the schematic of Figure 4.4 with nodes shown at the bearing centres, mass centres of the hub discs and rotors for an analytical solution following [3]. The

displacements at nodes 2 and 4 are equal, but there is flexibility between nodes 6 and 9. Nodes 1 and 8 are considered as simple supports.

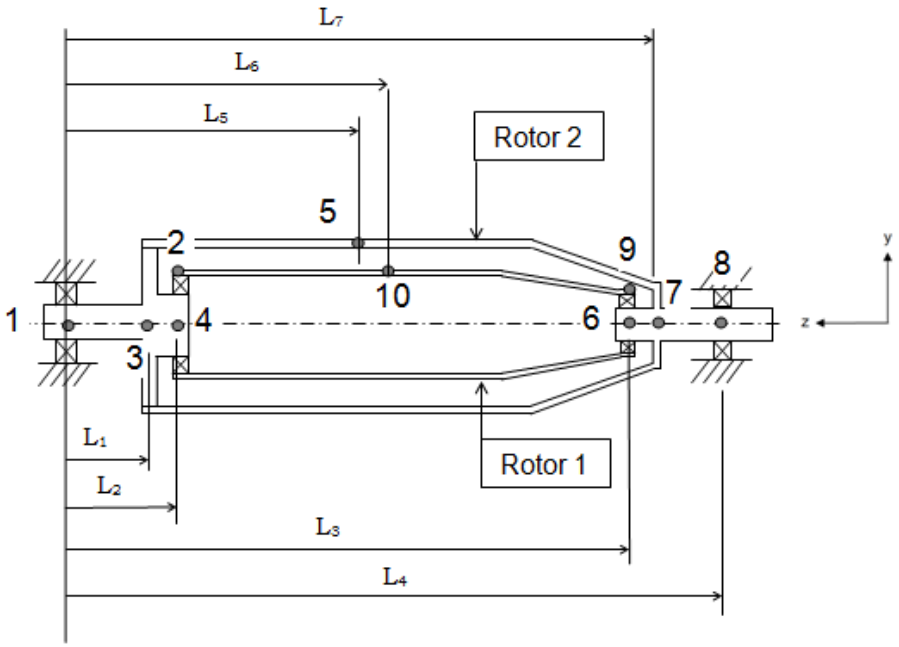

Figure 4.4 Dual rotor systems with nodal points

This is a similar problem to that of [3], where there is one intermediary flexible bearing in a multi-rotor problem. The displacements of the outer and inner rotors in the xz plane, (u_1,v_1 and u_2,v_2), are prescribed by shape functions $f_i(z) = \sin(\frac{\pi z_i}{L_i})$, where i denotes either inner or outer rotor. In terms of the generalized coordinates q_1, q_2; $u_1(z,t) = f_1(z)q_1(t)$ and $v_1(z,t) = f_1(z)q_2(t)$.

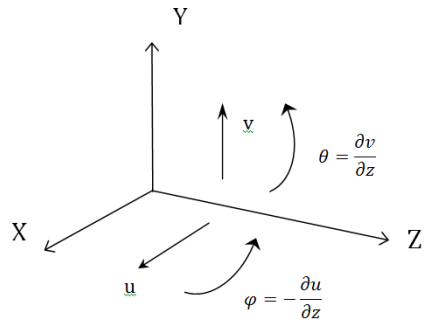

Figure 4.5 Coordinate system for the inertial reference frame [3]

From Figure 4.5, for small angles:

$$\varphi = -\frac{\partial u_1}{\partial z} = -\frac{df_1}{dz}.q_1 = g_1 q_1. \qquad \text{..... (4.3)}$$

$$\theta = \frac{\partial v_1}{\partial z} = \frac{df_1}{dz}.q_2 = g_1 q_2. \quad \text{..... (4.4)}$$

where, $g_1(z) = \frac{\pi}{L}\cos\left(\frac{\pi z}{L}\right)$.

For computation of the strain energy the second derivative is required, giving:

$$\frac{\partial^2 u_1}{\partial z^2} = \frac{d^2 f_1(z)}{dz^2} q_1(t) = h_1 q_1. \quad \text{..... (4.5)}$$

$$\frac{\partial^2 v_1}{\partial z^2} = \frac{d^2 f_1(z)}{dz^2} q_2(t) = h_1 q_2. \quad \text{..... (4.6)}$$

where $h_1(z) = -\left(\frac{\pi}{L}\right)^2 \sin\left(\frac{\pi z}{L}\right)$.

The bowl (outer rotor) is considered as rigid and its lateral (u_2, v_2) and angular displacements (ϑ_2, φ_2) are expressed as:

$$u_2(z,t) = \left(\frac{z-L_1}{L_7-L_1}\right) f_1(l_7) q_1 = f_2(z) q_1. \quad \text{..... (4.7)}$$

$$v_2(z,t) = \left(\frac{z-L_1}{L_7-L_1}\right) f_1(l_7) q_2 = f_2(z) q_2. \quad \text{..... (4.8)}$$

$$\varphi_2 = -\frac{\partial u_2}{\partial z} = -\frac{df_2(z)}{dz}.q_1(t) = -g_2 q_1. \quad \text{..... (4.9)}$$

$$\theta_2 = \frac{\partial v_2}{\partial z} = \frac{df_2(z)}{dz}.q_1(t) = -g_2 q_1. \quad \text{..... (4.10)}$$

The free modal responses for the combined rotor system are found from [3]:

$$M_1 \ddot{q_1} - \Omega(a_1 + n a_2)\dot{q_2} + k_1 q_1 = 0. \quad \text{..... (4.11)}$$

$$M_2 \ddot{q_2} + \Omega(a_1 + n a_2)\dot{q_1} + k_2 q_2 = 0. \quad \text{..... (4.12)}$$

where,

$$\Omega_1 = \Omega_b = \Omega$$

$$\Omega_2 = n\Omega_1 = n\Omega$$

$$k_1 = k_u \quad \text{..... (4.13)}$$

$$k_2 = k_u + k_v f_1^2 L_3 \quad \text{..... (4.14)}$$

$$a_1 = I_{Dz1} g_1^2(L_1) + 2\rho I_1 \int_0^{L_4} g_1^2(z)dz. \quad \text{..... (4.15)}$$

$$a_2 = I_{Dz2} g_2^2 + 2\rho I_2 \int_{L2}^{L3} g_2^2(z)dz. \quad \text{..... (4.16)}$$

and g_i are the functions of angular displacement.

Assuming solutions for eq 4.11 and 4.12 in the form

$$q_1 = Q_1 e^{rt} \text{ and } q_2 = Q_2 e^{rt} \quad \text{..... (4.17)}$$

Then the characteristic equation is:

$$M^2r^4 + (k_1M + k_2M + (a_1 + na_2)^2\Omega^2)\mathrm{r}^2 + \mathrm{k}_1\mathrm{k}_2 = 0. \quad \ldots\ldots (4.18)$$

$$where\ r = \pm j\omega_1 \text{ and } \pm j\omega_2$$

At rest, $\Omega = 0$ giving:

$$\omega_1 = \left(\frac{k_1}{M}\right)^{0.5}. \quad \ldots\ldots (4.19)$$

$$\omega_2 = \left(\frac{k_2}{M}\right)^{0.5}. \quad \ldots\ldots (4.20)$$

Under rotating condition i.e. $\Omega \neq 0$, [3] gives the rotational critical speeds as:

$$\omega_1 = \left[\frac{\omega_1^2+\omega_2^2}{2} + \frac{(a_1+na_2)^2\Omega^2}{2m^2} - \left[\left(\frac{\omega_1^2+\omega_2^2}{2} + \frac{(a_1+na_2)^2\Omega^2}{2m^2}\right)^2 - \omega_1^2\omega_2^2\right]^{0.5}\right]^{0.5}. \quad \ldots\ldots (4.21)$$

$$\omega_2 = \left[\frac{\omega_1^2+\omega_2^2}{2} + \frac{(a_1+na_2)^2\Omega^2}{2m^2} + \left[\left(\frac{\omega_1^2+\omega_2^2}{2} + \frac{(a_1+na_2)^2\Omega^2}{2m^2}\right)^2 - \omega_1^2\omega_2^2\right]^{0.5}\right]^{0.5}. \quad \ldots\ldots (4.22)$$

The assumptions imposed in order to adopt the Rayleigh approach question the usefulness of these rigid body solutions. The solutions are dependent upon the masses of equivalent uniform beams and selected stiffnesses for the flexible solids end bearing. The method has merit for comparative purposes but was abandoned in favour of using the finite element method via ANSYS/Workbench, to carry out parametric studies of the effects of the bearing characteristics. The bowl assembly and the conveyor were each modeled separately in Solid Works for manufacturing purposes and then these models were modified and imported into ANSYS Workbench. The modification involved the removal of fillets and chamfers to facilitate meshing. Symmetric properties were used first (i.e. $k_{xx}=k_{yy}=k_{xy}=k_{yx}$) followed by the asymmetric case with cross coupling. A critical speed map was prepared for the dual rotor case to observe the effect of change in bearing stiffness – see Figure 4.6.

Table 4.1 Variation of modal frequencies with bearing stiffness

Stiffness N/m	Mode 1, Hz	Mode 2, Hz
1E6	8	19.5
5E6	16.8	43.8
1E7	23.2	61.4
5E7	52.0	133.9
1E8	71.8	183.7
1E9	160.9	408

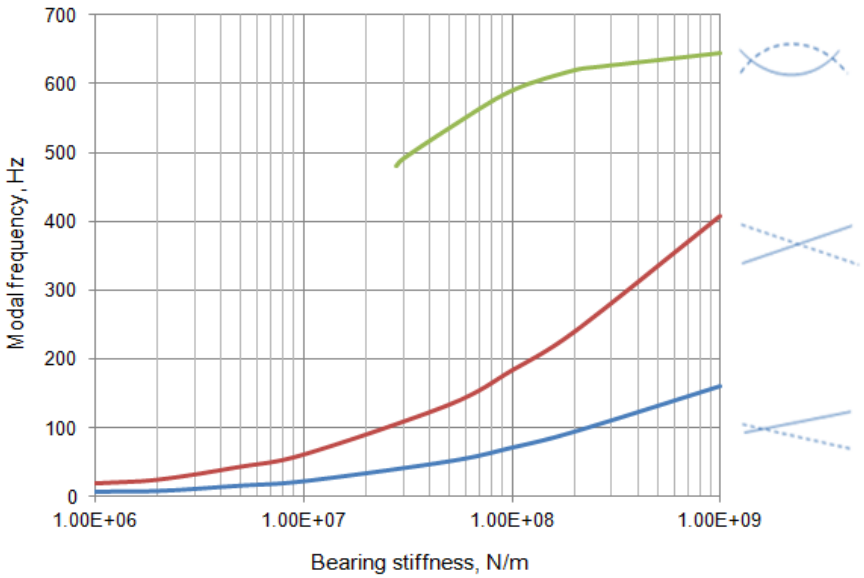

Figure 4.6 Critical speed map for the conveyor - ANSYS

The results shown in Table 4.1 and Figure 4.6 indicate that if the bearing stiffness is comparable to 7E6 N/m or lower, the first two modes for the conveyor are the rigid translational (Mode 1)and rocking modes (Mode 2) and their frequencies are comparable to the run speed (54Hz) and its first harmonic. This raises the question of whether the bearing stiffness would be as low as 1E6N/m or lower, or whether the ratings calculated by Harris [22] are truly representative of real bearings. In essence the presence of the bearing clearance means that for conveyor motion in the horizontal plane the stiffness is close to zero until the journal contacts the bearing. The effect of bearing clearance has been modeled

by having zero stiffness in the *yz* direction, maximum stiffness in the *y* direction, and cross coupling terms.

As discussed in Appendix C, it is clearly possible for the state of unbalance of the conveyor to be high and for the bearing clearances to be at the high end of the manufacturing tolerance. The combined effect is to produce a very low stiffness twice per revolution. This comes about as as gravity loading reduces the clearance at the top vertical centreline position to zero - see Figure 4.7. The horizontal component of the unbalance force causes displacement of the conveyor rotor in the clearance space of the bearing as the rotor basically pivots back and forth about the point A in Figure 4.7 i.e. at a frequency equal to twice the rotational frequency. The pivot motion would require less force for a rolling element type bearing rather than a fluid film type as friction is lower and the pivot is about a point, for a single element, rather than through a fluid damped arc of the bearing. Clearly, if the unbalance force is sufficiently high then the rotor will lift and orbit around the journal.

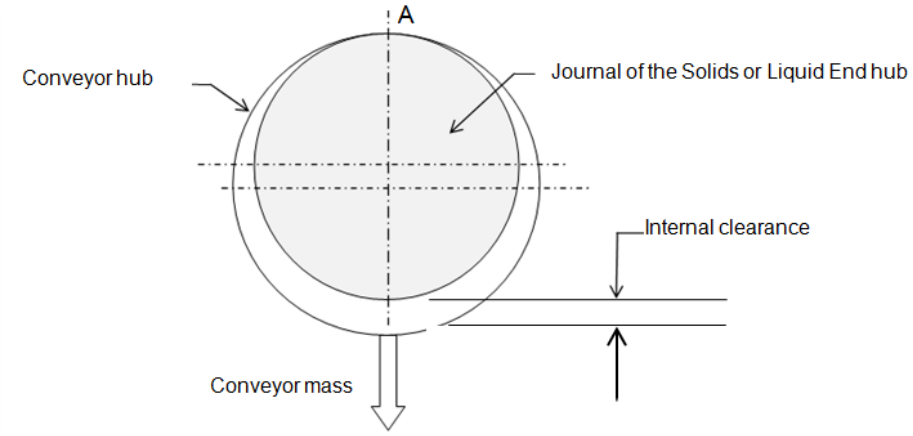

Figure 4.7 Normal conveyor bearing position

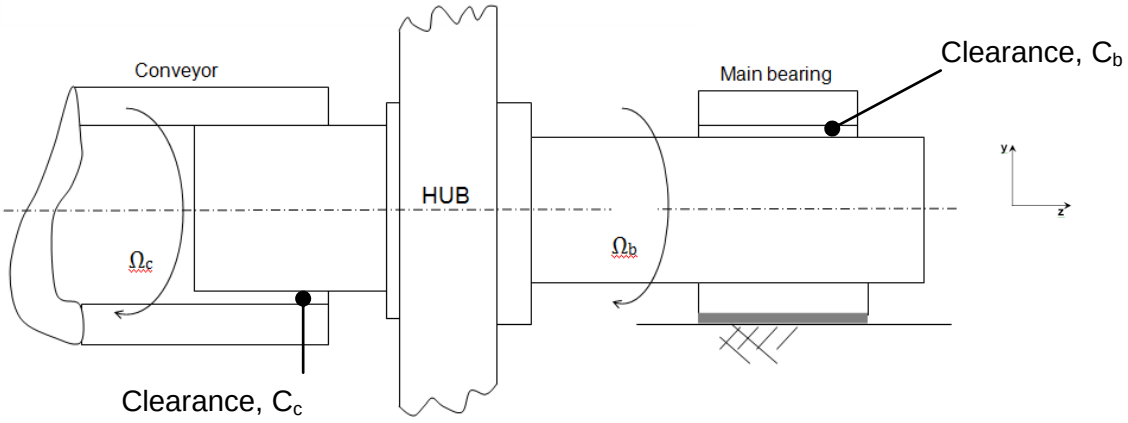

Figure 4.8 The bearing clearance positions for conveyor and bowl (main bearings)

Figure 4.8 shows the different positions for maximum clearance for the stationary rotors: C_c the conveyor bearing clearance and C_b, the main bearing clearance. For there to be motion in the vertical y direction at the external main bearings the rotor masses have to be lifted by the unbalance force in order to reduce bearing stiffness, that is, the unbalance force must be greater than the gravity load. For fluid film bearings the rotor is lifted by the hydrodynamic pressure developed with rotor rotation – but the centre of rotation can never be coincident with the bearing's centre as gravity provides a static offset. Except in cases where the shaft is vertical – as studied by Yamamoto [36].

4.2 FE Models

The simple dual rotor of Lalanne and Ferraris, Figure 4.9, was studied as the results are included in their book [3]. However, their model is limited by having symmetric bearings, using constant values and ignoring gravity, but the exercise was valuable in dealing with the support system for the two rotors on a problem that took very little computer time. A bearing housing was included in the model in order to use the bearing options available in ANSYS – this does not appear in the original case study.

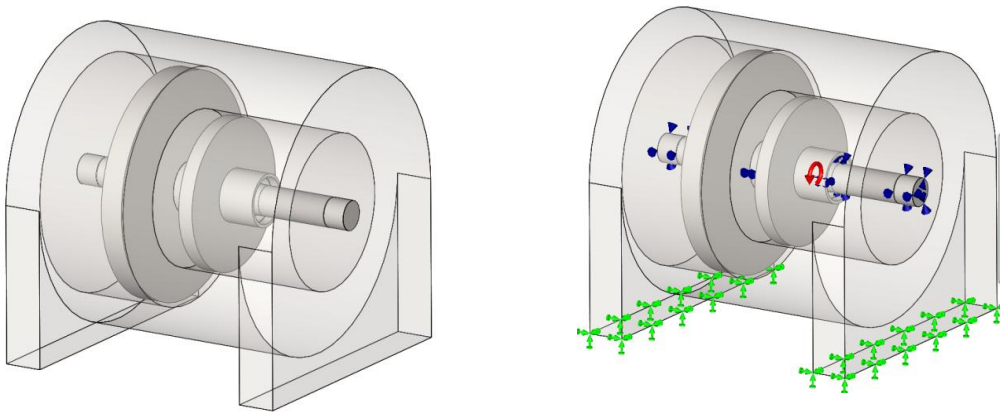

Figure 4.9 Dual rotor first model, Lalanne & Ferraris

A modal solution enabled visualization of the relative motions of the two discs. This problem did not include for rotational effects (unbalance response) but did provide confidence that the process could be applied to the centrifuge problem in a similar manner.

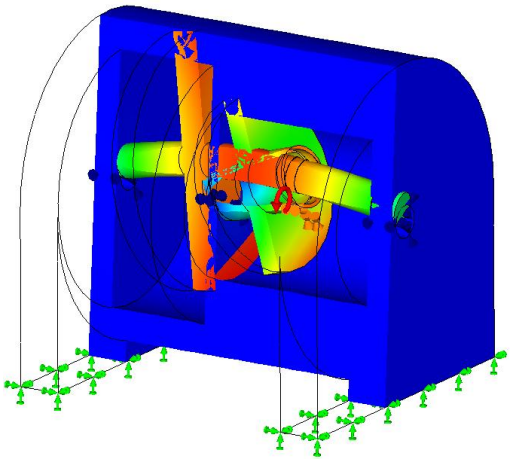

Figure 4.10 Dual rotor response – symmetric bearings

4.3 Centrifuge Rotating Assembly

Several versions of the dual rotor system model were compiled with initial variation only in mesh density in order to observe sensitivity to mesh size. Once the optimum number of elements was established the bearings were added and modal and harmonic response analyses carried out. The conveyor flights are removed but their mass is included as uniformly distributed.

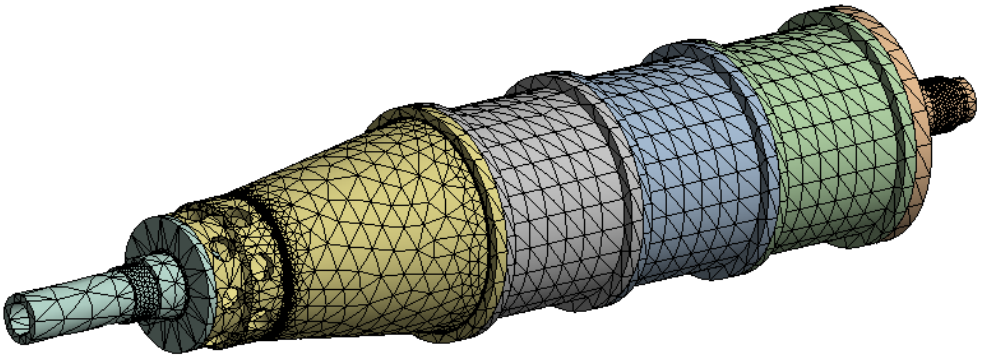

Figure 4.11 Meshed Dual rotor assembly with refinement at the bearing surfaces

The following plots from ANSYS show the dual rotor modal responses for some of the various bearing stiffness used for the critical speed map - Figure 4.6

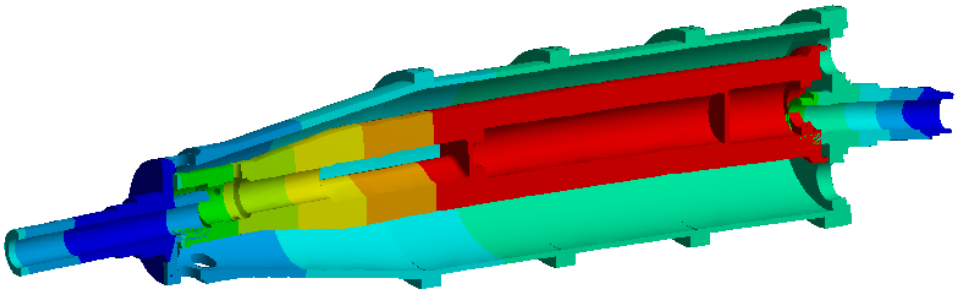

Figure 4.12 Translational mode of the conveyor, 16Hz

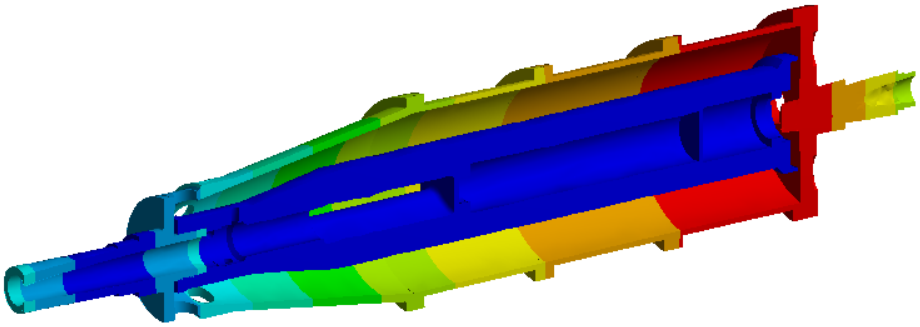

Figure 4.13 Rocking mode (conical) of the conveyor, vibration at the liquid end hub, 125 Hz

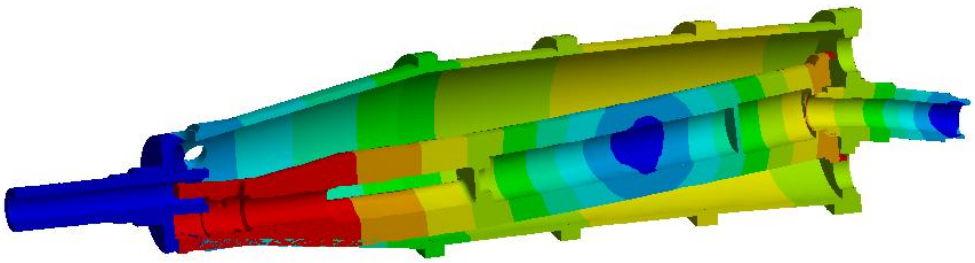

Figure 4.14 Rocking mode (conical) of the conveyor, bending of liquid end hub, 200Hz

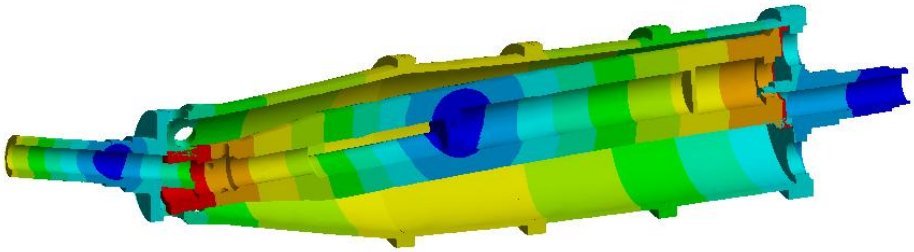

Figure 4.15 Translation of the conveyor, bending of bowl hubs, 238Hz

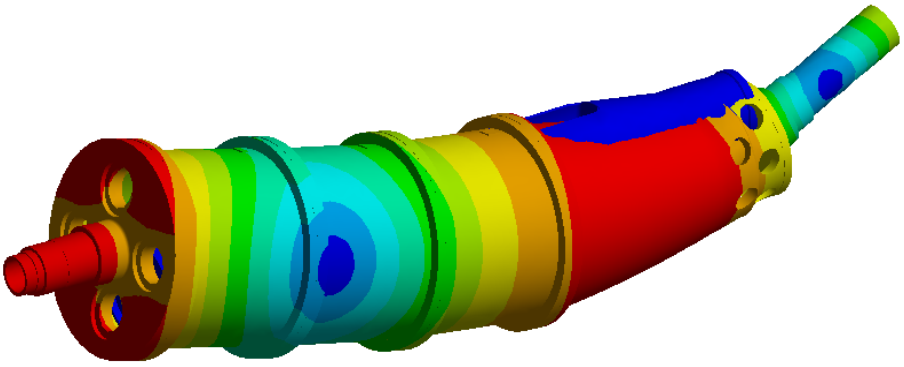

Figure 4.16 Bowl bending, 337Hz

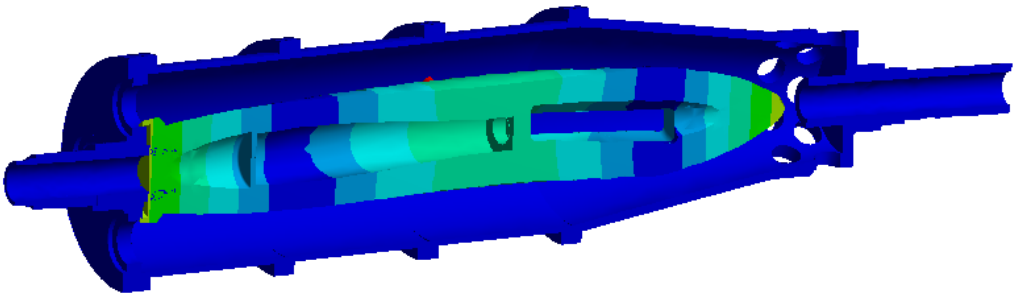

Figure 4.17 Conveyor bending, zx plane, 444 Hz

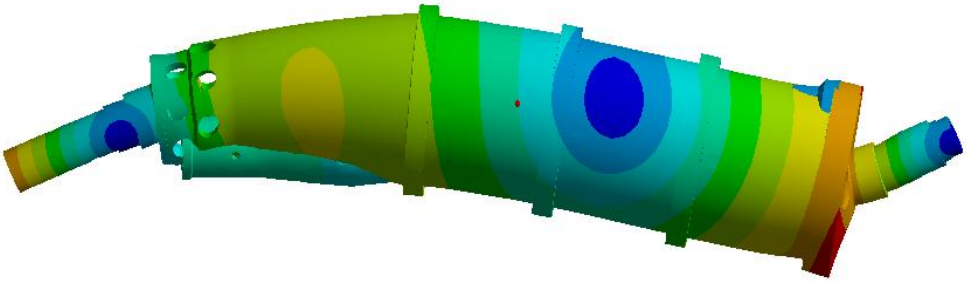

Figure 4.18 2nd bending mode of bowl, 460 Hz

Many different relative motions of conveyor and bowl assembly are apparent by varying the stiffness of the bearings. The stiffness and damping characteristics of the main bearings were kept constant and only the conveyor bearing data changed. As expected, it is possible to get any combination of motions with different mode shapes with the range of values for bearing stiffness used.

Harmonic analyses were carried out for response to unbalance, adding a dynamic couple to the conveyor. Figure 4.19 shows one plot of the response of the conveyor with rocking and bend modes, see Figure 4.14 and Figure 4.17.

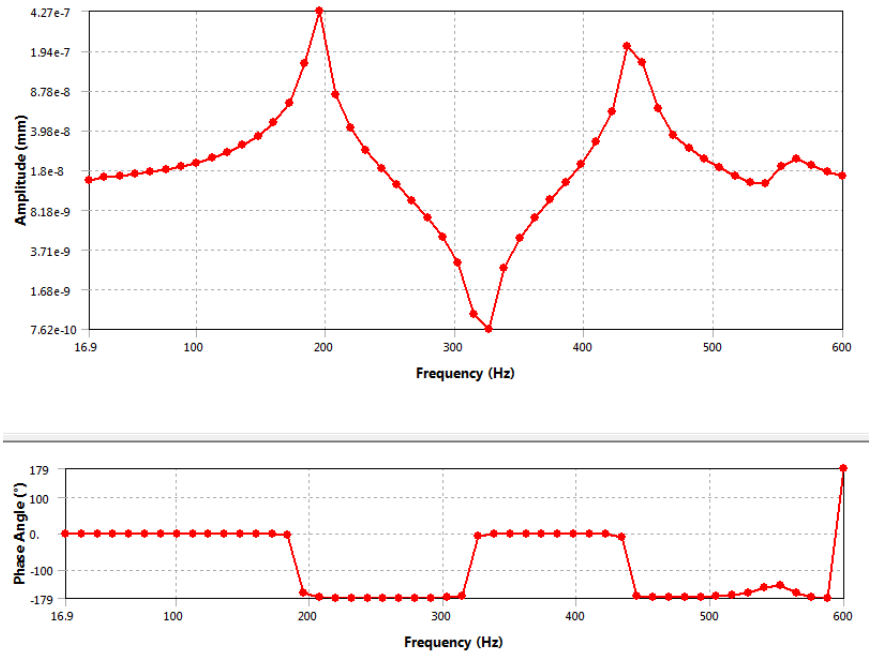

Figure 4.19 Plot of harmonic response for the conveyor with a dynamic couple

The outcome of the FEA modeling is, typically, dependent upon the input data, and whilst the geometry can be complex but well defined through CAD, the controlling parameters are the characteristics of the bearings. A parametric study shows that the mode frequencies of the rigid body motion of the conveyor ranges from below normal run speed frequency to many times higher as a result of changing the bearing stiffness. Therefore it is possible for the rigid body modes to be excited at any speed up to and including the normal run speed if the right combination of bearing stiffnesses prevails. The low stiffness in the zx plane, due to internal clearance in the bearing, is the source of the twice per revolution motion in response to unbalance.

Chapter 5 Modifications to the test machine

Several modifications were made to the centrifuge used in this study in order to be able to study the individual components of vibration from the rotating assembly – unmodified by local resonances. Appendix B details those modifications.

In order to demonstrate proof of concept, only the main plummer block bearings were changed for this study, leaving the conveyor bearings unchanged. The decision to investigate the use of hydrodynamic bearings was based on the need to improve system damping and eliminate the excitation frequencies associated with rolling element bearings. This was the methodology to reduce noise generation by treating the source rather than reducing noise by adding absorptive passive acoustic materials - as that had been attempted with poor results [39]. Once that decision for bearing conversion was made the challenge was to maintain the existing bearing centres, and the footprint of the main bearing housings. Maintaining the centre height (axis of rotation for the rotating assembly) was paramount, in order to preserve running clearances on seals and labyrinths in the case and cover.

The decanter's rotating assembly is positively located at the solids end main bearing (a deep groove ball bearing) and thermal expansion is accommodated using a cylindrical roller bearing at the liquid end. Thus in converting to fluid film bearings provision has to be included at the solid end to locate the rotating assembly. This chapter includes the design of the bearings.

There is a strong case for also converting the conveyor's rolling element bearings to journal type because the differential speed is so low – typically less than 20 rpm. An additional reason to change is because the needle roller bearing is a source of instability due to its high internal clearance and low stiffness when loaded in the horizontal plane. There are many polymer type bearing materials

available that would be suitable candidates - either dry or grease lubricated. The resistance by the manufacturer to change is probably based in the requirement to cater for the thrust load and the perceived difficulties of maintaining lubrication and cleanliness. However, if one considers the operation of rubber stern tube bearings in marine craft then neither of these concerns holds weight. Figures 5.1 and 5.2 show schematics of how journal bearings might be incorporated. Figure 5.1 shows the arrangement at the liquid end where the hub has been modified to include a thrust ring. The conveyor bore has been left as standard, along with the drive shaft and splined adaptor bush – thus enabling easy changeover of existing parts for trial of journal bearings. The bearing bush is fluted to allow debris to "drain" into the conveyor cavity and be discharged back into the bowl. Figure 5.2 shows the proposed modifications to the solids end of the conveyor hub.

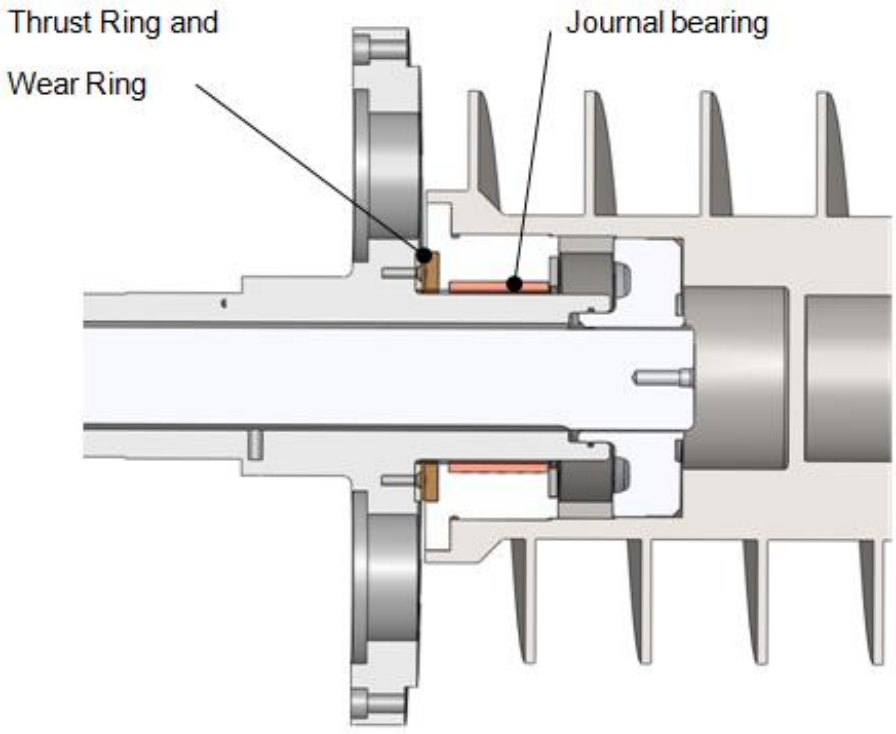

Figure 5.1 Modifications to conveyor liquid end to house fluid film bearings

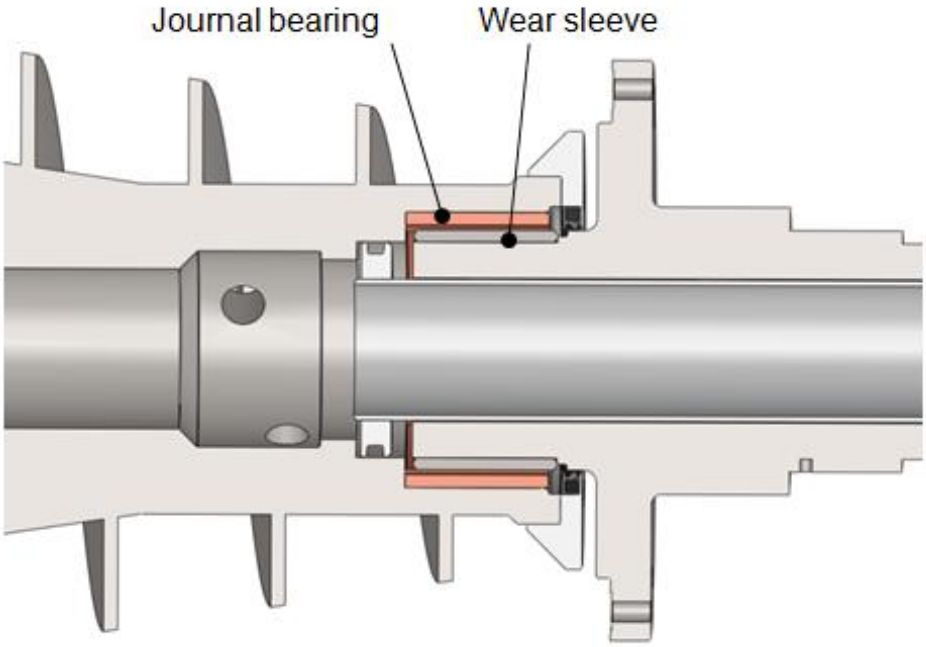

Figure 5.2 Modifications to conveyor solids end to house a fluid film bearing

Since the suggested changes to the conveyor bearings were not made for this study, in order to test the theory that conveyor vibration was due to bearing clearance a closer clearance grade type needle roller bearing for the conveyor was substituted for the C3 grade bearing normally fitted. The liquid end conveyor bearings remained unchanged. This change to a reduced clearance resulted in a considerably lower second order component of vibration – Figure 5.3. The spectrum exhibits a reduced number of the characteristic sidebands associated with the differential speed.

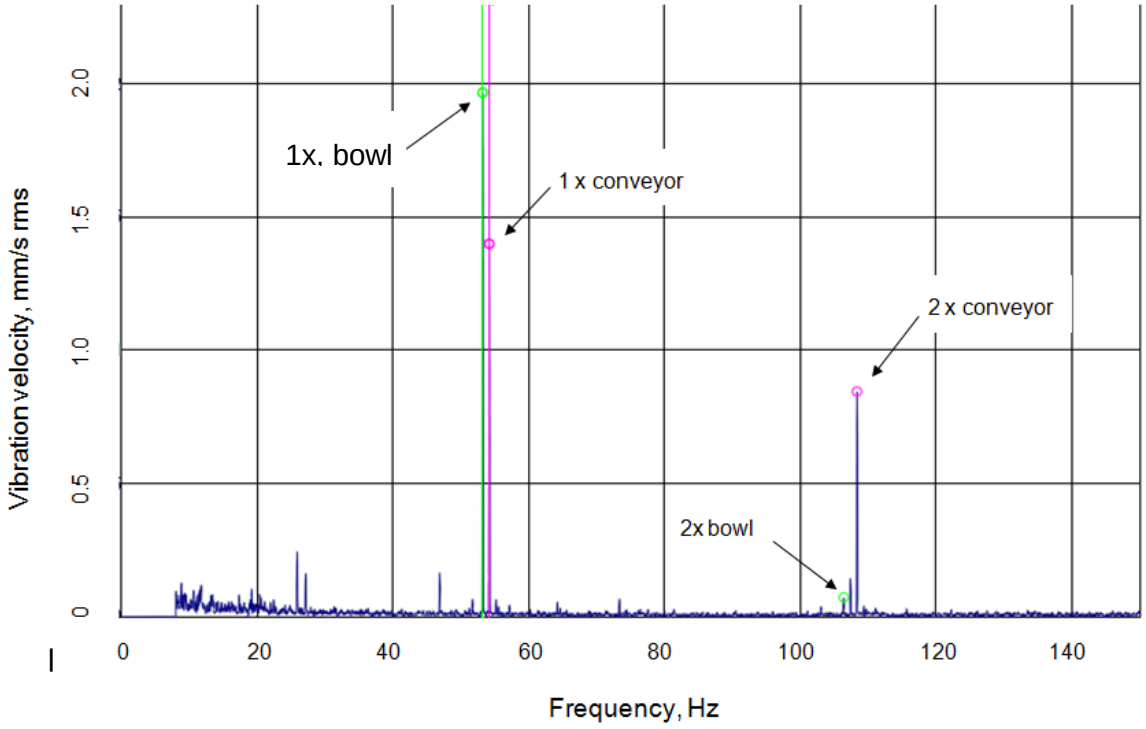

Figure 5.3 High resolution plot of vibration following fitting of smaller clearance bearing

The implication of this is that the bearing clearance affects the stiffness by modifying the arc of the bearing that takes the load i.e. a smaller or larger number of rolling elements is involved in load sharing.

5.1 Design Procedure

Design of fluid film bearings is a well established process [32], [42] but there are still challenges. For example the heat dissipated by the housing can only really be estimated (from the surface area and material mass) and so the fluid film temperature is at best an estimate. Under constant load, the film thickness is dependent upon viscosity, which in turn is temperature dependent. Thus the load carrying capacity of the bearing may be over or underestimated by assumptions made about the housing's thermal capacity. Temperature also affects the clearance/fit of the bearing in the housing, which in turn may affect the internal dimension of the bore and thus the clearance. Checklists are available to aid in the process, [43], [44], and as there are many solutions to

each situation the "correct solution" may require an iterative approach. The basic design process has the following four steps:

1. Select the bearing geometry type (cylindrical, lobed, tilting pad etc)
2. Solve the Reynolds equation to get dimensionless design data
3. Use the data to select a lubricant with a viscosity over the operating temperature range and use design flow charts to complete the design
4. Iterate if necessary.

5.1.1 Main Bearings

The design of fluid film bearing elements is straightforward as there is a plethora of published papers, guides and texts available [22], [23], [32]. An iterative process is involved as the design includes calculating a heat balance as a function of the lubricant flow. The flow must be enough to maintain an acceptable operating temperature but not require too large a clearance to do so [23].

The main controlling parameters are:

- The bearing elements have to fit inside the existing plummer blocks
- The journal sizes have to allow for wear surfaces fitted to each of the hubs
- A lubricant pump system has to be provided.

The bearing stiffness and damping coefficients are load dependent which means that the values used in computation must be updated with load changes. Transient response is one analysis where the bearing load is periodic requiring updated bearing data for each time step. A Fortran 95 code for bearing coefficients [45], was extended to include interpolation of tabulated values by incorporating a 3rd order spline function, see Appendix D. The code returns values of the coefficients, normalized oil flow, viscosity and temperature that can be imported into ANSYS using a macro (IMPORTBRG.MAC). Proprietary data for fluid film bearings, such as that from ROMAC[2] is also available by linking with ANSYS.

[2] Rotating Machines and Controls Laboratory, University of Virginia, U.S.A.

The load carrying capacity of a hydrodynamic fluid film bearing comes from the pressure developed within the film [32]. The motion of the shaft creates a divergent wedge that acts like a pump, dragging fluid into the wedge and thus increasing pressure. The presence of the wedge means that the journal centre is offset to the bearing's centre and so symmetry is not only lost but leads to cross coupled components of stiffness and damping that can lead to instability in fixed geometry bearings – see Figure 5.4. The fluid film is loaded in shear and that causes a rise in film temperature and consequent reduction in viscosity, as well as being a sink for mechanical power. In highly loaded bearings the temperature and pressure can lead to deformations of the bearings and housing that must be considered when calculating the lubricant film thickness - the centrifuge bearings are not considered to be in this category. The computational objective of the bearing analysis is to return the restoring forces that react the shaft loading. The restoring force is a function of the film pressure, which in turn is a function of the load, shaft surface speed and fluid viscosity, expressed in a non-dimensional parameter called the Sommerfeld Number S, [23], where:

$$S = \frac{\mu NDL}{W}\left(\frac{R}{C_p}\right)^2 \qquad \ldots\ldots (5.1)$$

μ= lubricant viscosity, Pa.s;
N = shaft speed, rev/s;
D= Bearing diameter, m;
L = bearing length, m;
W = bearing load, kg;
R = Bearing radius, m;
Cp = Clearance, m.

and which relates the attitude angle φ and eccentricity e as shown in Figure 5.4.

The eccentricity ratio $\varepsilon = \frac{e}{C_b}$;

where e = eccentricity; C_b = assembled clearance

The minimum film thickness $h_{min} = C_b(1 - \varepsilon)$;

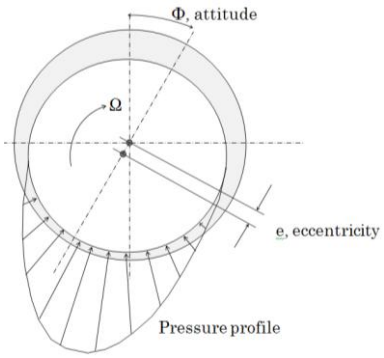

Figure 5.4 Schematic of journal and bearing

This study used plain, cylindrical bore, pressure fed, bearings. The bearings will be at the upper end of the loading capacity as the length to diameter ratio is low in order for the bearing to fit in the existing housing. For example, the selection chart in [43] indicates that a bearing diameter around 112 mm would support a load of 1300kg. Each main bearing has a proportion of the rotor weight plus a belt load: from the 37kW main drive at the solids end and from the 11kW conveyor back drive at the liquid end.

Ignoring losses, the power transmitted by a belt drive is given by [46]:

$P = \frac{2\pi N T_o}{1000}$, where, $T_o = (T_T - T_S) r_e$

And so, $(T_T - T_S) = \frac{1000P}{2\pi N r_e}$

Where T_o is the nett torque (Nm), T_T = tight side belt tension, T_S = slack side belt tension, P = 37 kW, N = 54.2 rev/s, r_e = 0.07 m (140 mm pitch diameter pulley for the main drive).

Then the 'tight side' belt tension transmitting power is (T1 – T2) =1552 N

The 'slack' side belt tension is determined from the friction coefficient and the degree of 'wrap' of the belts at the driven pulley (which in turn is determined by pulley sizes and the centre distance). Manufacturers give various expressions for finding T_s and here we use $\frac{T_1}{T_2} = e^{\mu' \alpha}$, where

$$\mu' = \frac{\mu}{SIN(\frac{\beta}{2})}$$

α is the driven pulley wrap angle = 3.49 rad (for a 500 mm centre distance), β is the pulley groove angle = 38° (determined from the belt cross section used, SPA for this case). Then, the belt force ratio = 5.5 and so T_2 = 1552/5.5, i.e. 282 N.

Then the belt loading on the bearing ($T_T + T_S$) = 1834 N. This load must be added to the bearing gravity load of 2855 N (Section 3.2.2) to give a solids end bearing load of 4688 N.

Table 5.1 Table of input data

	Description	Value		Description	Value
D	Bearing diameter, m	0.112	N	Rotational speed, rad/s	380
L	Bearing length, m	0.049	p_f	Lubricant feed pressure, bar	2.5
r	Radius of journal, m	55.93e-3	T_a	Ambient temperature, °C	25
C_b	Assembled clearance, m	0.15e-3	C_p	Machined clearance, m	0.075e-3
ρ	Density of lubricant, kg/m^3	800	W	Bearing load, N	4688

5.1.2 Calculate the dimensionless quantities

L/D; the length to diameter ratio: = 0.4375

C_p = R-r; the machined radial clearance: = 0.075e-3 m

φ= C_p/R; = 2.67e-3

$m = 1 - \frac{C_b}{C_p}$; the preload factor: ≅ 0.0

- Assume a value for T_m (the mean lubricant film temperature): = 65°C
- Calculate μ (kinematic viscosity), (or from charts, Table 5.1): = 25.9 mPa.s
- Calculate the Sommerfeld number S,

$$S = \frac{\mu NLD}{W}\left(\frac{R}{C_p}\right)^2$$ substituting in values, S = 0.477 (using SAE-30 engine oil) ..... (5.3)

Get ε, φ, Q_s, and Q_e from tabulated data by interpolation (Appendix D).

0.520; 50°; 0.37; 0.94

Q_s and Q_e are the non-dimensional side and circumferential oil flows, [23].

Table 5.1 Viscosity chart for various oils, (Saybolt Universal Seconds, SUS)*

SAE-5		SAE-10		SAE-20		SAE-30		SAE-40		SAE-50	
T, °F	ν	T, °F	ν	T °F	ν	T °F	ν	T °F	ν	T, °F	ν
38	500	35	1500	32	5000	30	10000	30	20000	40	20000
66	200	50	750	70	1000	80	1000	75	2000	95	1500
76	150	80	300	89	500	110	400	103	700	130	500
120	70	150	70	120	200	150	150	150	200	150	300
140	55	189	50	170	80	190	80	190	100	180	150
170	45	209	45	200	60	220	60	220	70	205	100
200	40	240	40	210	55	230	55	250	55	255	60
250	35			250	45	250	50				

*1N.s/m²=1Pa.s = 1000cP (=5787 SUS for ρ=850kg/m³

The oil film thickness $h_{min} = C(1 - COS\varphi)$ ..... (5.4)

Substituting in values, h_{min} = 55.6 μm

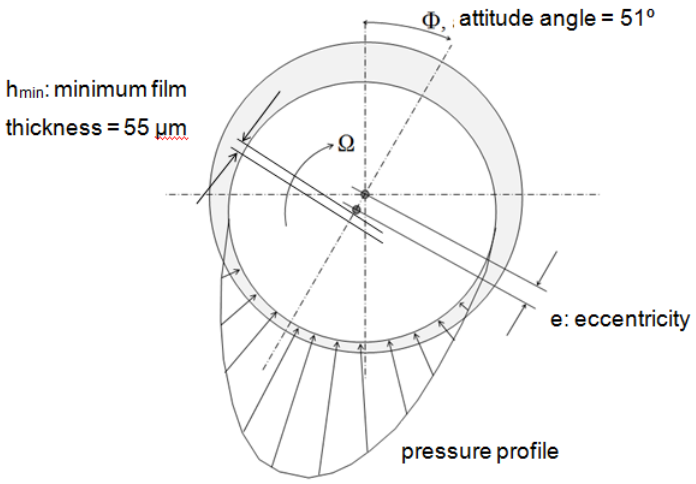

5.1.3 Calculate the oil flow

The non-dimensional oil flow Q_s, [23], is given by:

$$Q_s = q_s/(R\omega C_p L) \quad \text{..... (5.5)}$$

and so, $$q_s = Q_s R\omega C_p L \quad \text{..... (5.6)}$$

where:

Q_s = Non dimensional lubricant side flow coefficient

R = bearing radius, m

ω = shaft rotational speed, 2πN rad/s

C_p = Machined clearance, m/8

L = Bearing length, m

Table 5.2 Bearing parameters

Qs	*R*	*ω*	*Cp*	L
0.37	0.056	380	0.00015	0.05

giving, q_s = 5.9e-5 m³/s

Similarly, $q_e = Q_e R \omega C_p L$ ..... (5.7)

where:

Q_e = Non dimensional lubricant end flow coefficient

giving, q_e = 1.5e-4

The total natural oil flow is: $q_w = q_s + q_e$

and so: q_w = 2.1e-4 m³/s

The bearings are supplied with oil under pressure so there will be an additional oil flow, q_f, given by [23]:

$$q_f = \frac{8h_1^3}{\mu} p_f . Q_f \quad \text{..... (5.8)}$$

where the non dimensional oil flow coefficient Q_f is determined by the geometry of the oil feed into the bearing. For this study, the feed pressure was 240kPa, and [23] gives $Q_f \cong 0.02$

and so: $q_f \cong$ 5.95e-6 m³/s

Thus the oil flow required is q_w = 2.16e-4 m³/s, or 0.21 l/s, or 210 cc/s.

The total flow requirement from the pump is for the supply to two bearings and so the indicative oil flow rate required is 420 cc/s. The oil pump purchased for the project was a Galtech gear pump, type 1SPA4.2-D-10-NN, delivering a maximum flow of 245 cc/s at a maximum continuous working pressure of 190 bar - see Figure 5.5. Clearly this is undersized and limited the test runs as determined by heating of the bearings. Generally runs up to 25 minutes were acceptable.

(a) (b) (c)

Figure 5.5 (a) Installed oil pump, (b) needle flow control valves (c)piping to plummer block bearing

5.1.4 Heat balance

The heat generated in the bearings is dissipated by the heat flowing out with the oil H_1, and the heat transferred from the bearing housing to the surrounding air, H_2. Other heat sinks, such as flow along and into the shaft, are taken to be minor compared with the heat transferred by the oil flow.

The oil flow must be sufficient to remove the heat at a rate greater than that at which it is generated in order to avoid overheating. The cooling efficiency is also contingent upon having a large enough reservoir or heat exchanger that can cool the oil to obtain the desired inlet temperature.

The total heat flow out, $H = H_1 + H_2 + H_i$ ..... (5.9)

The H_i other contributors to heat loss are small compared with H and so they are ignored. The heat dissipated into the oil is the product of the frictional torque and the angular speed.

$$H = f_J \omega r W \quad \text{..... (5.10)}$$

Where f_J is a friction factor determined by the bearing geometry (Appendix D)

Substituting in values gives H = 4130 Watts

The net heat flowing out with the oil is given by:

$$H_1 = C\rho q(T_2 - T_1) \quad \text{..... (5.11)}$$

where

C = specific heat of oil, 1850 (J/kg°C),

ρ = density of oil, 865 (kg/m^3)

q = total oil flow, 245e-6 (m^3/s)

T_2 = oil outlet temperature, 65 (°C)

T_1 = oil inlet temperature, 50 (°C)

Setting the maximum allowable oil temperature to 65°C (to avoid degradation) and substituting in values gives

$$H_1 = 5880 \text{ Watts.}$$

The heat lost from the bearing housing surface is small, compared with that taken away by the oil flow, as the surface area of the housing is small – it typically amounts to less than 100 Watts. So, H1 + H2 is approximately 6kW which is about 10% less than the heat generated by the frictional torque. Therefore the oil flow needs to be increased in order to dissipate the heat. To improve heat rejection from the oil, the inlet temperature can be lowered by installing a water cooled heat exchanger in the oil reservoir. With a correctly sized pump then the oil temperature would not be a problem since the volume should be doubled giving a heat loss of 11.7kW.

In order to fit into the existing plummer block housings the L/D ratio (length to diameter) had to be a maximum of 0.5. Short bearings preclude the use of internal annular lubricant feed grooves as these divide the bearing surfaces into even shorter bearings and end leakage becomes a significant part of the oil flow. Instead, the oil feed groove was made around the outside of the bearing with radial feed holes into the bearing proper. The feed holes on the horizontal axis were provided with pockets – see Figure 5.6. It seemed expedient, for proof of concept, to create substitute bearings that more or less filled the space formerly occupied by the rolling element bearing and so the bearings took the form of thick walled bushes. The internal diameters were increased to allow for the addition of wear sleeves to the respective hubs.

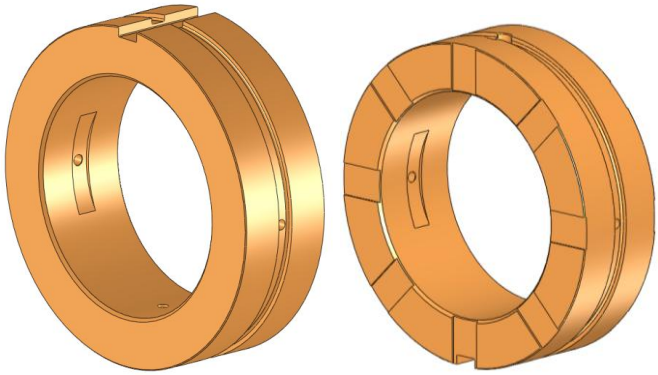

Figure 5.6 Fluid film bearing elements (left) liquid end, (right) solids end

For this study, the lubricant had to be supplied through the top of the plummer block and this precluded the option of using the pump's static pressure to lift the rotor prior to starting. In essence, once the power was supplied to the main drive motor the rotating assembly had to be coaxed into motion by pulling over by hand. This was because the oil film was squeezed out by the rotor's dead weight and the starting torque imposed by friction was too high for the current rating of the variable frequency starter. In an optimized design the layout of the bearing would be improved, incorporating hydrostatic lift and improved drainage flow. The bulky bronze bushings could be replaced by commercially available engine type shell bearings but provision would need to be made for lifting the rotor.

A locating dowel was assembled into the top of each plummer block and acted as the oil supply conduit/distributor and as the location to prevent rotation of the bearing element in the housing - see Figures 5.7, 5.8 and 5.9.

Figure 5.7 Locating dowel and oil supply connector

With a pump oil supply pressure of 8 MPa the pool size required to lift the rotor

is small (<400 mm^2) and could easily be accommodated in the bearing. The bearing design chosen in this present study was 112 mm diameter and 49 mm wide and so incorporating a pool area of 1000 mm^2 appears possible. The extension of this aspect of the bearing design was left for a future investigation.

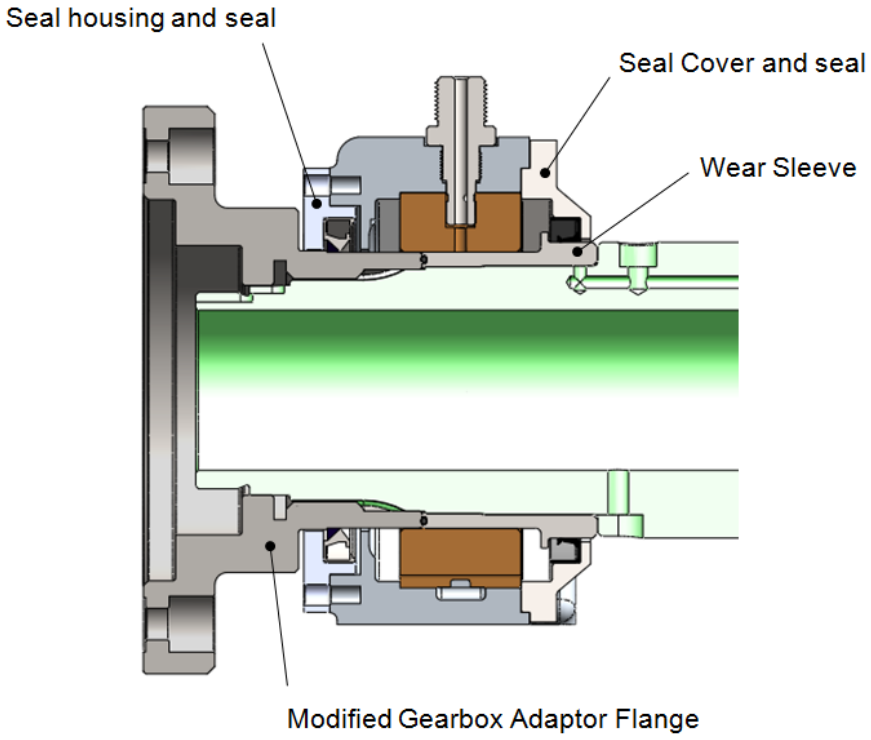

Figure 5.8 Liquid end fluid film bearing

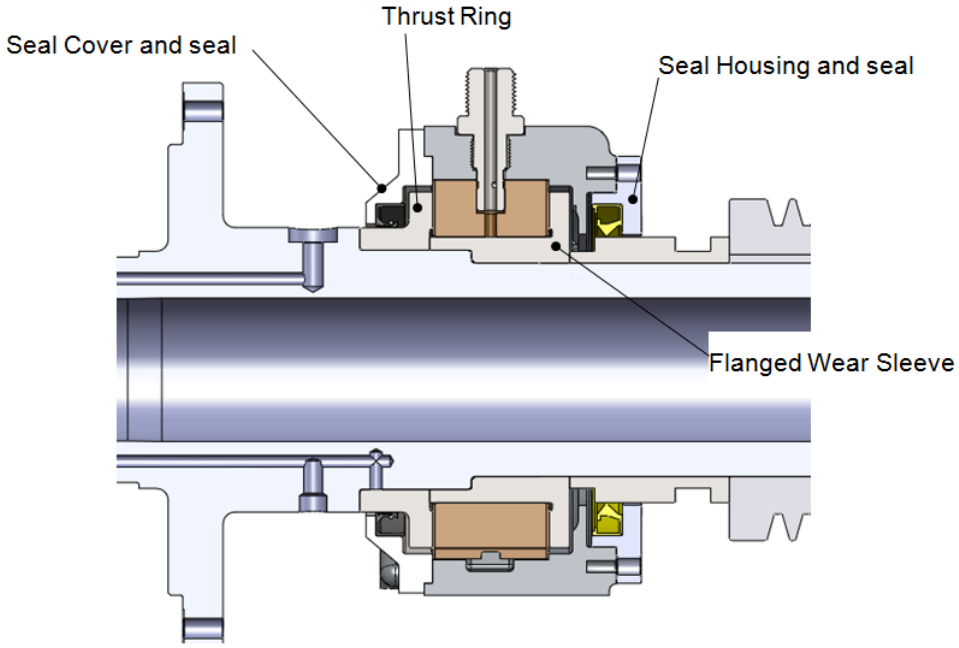

Figure 5.9 Solids end fluid film bearing for radial load and axial location

Each face of the solids end bearing, see the right of Figure 5.6 is slotted to provide thrust faces and oil drainage channels. The corresponding mating faces provided on the rotor are shown in Figure 5.9. These thrust faces provide a means of locating the rotating assembly only and are not for reacting the thrust developed by the conveyor. That thrust is taken by the angular contact bearing at the liquid end hub.

Both bearing housings were machined to provide an oil collection reservoir and drain – see Figures 5.10 and 5.11.

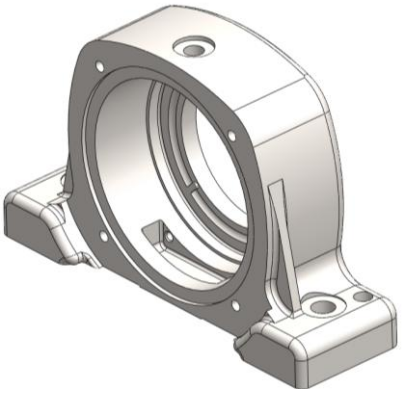

Figure 5.10 Bearing housing with reservoir

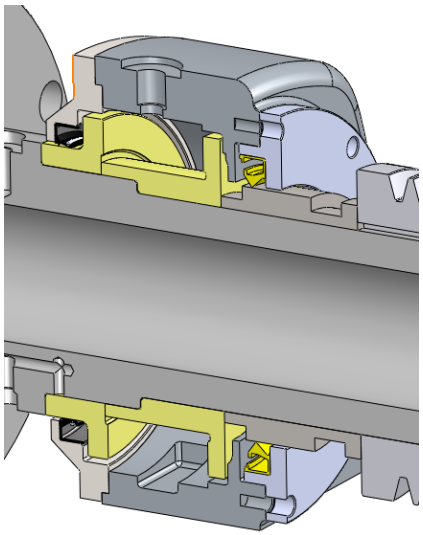

Figure 5.11 Assembled bearing – solids end, with bearing bush and dowel removed

5.2 Seals

The original rolling element bearing housings were sealed against grease egress and contamination ingress using labyrinths machined into the housing and face seals as shown in Figure 5.12.

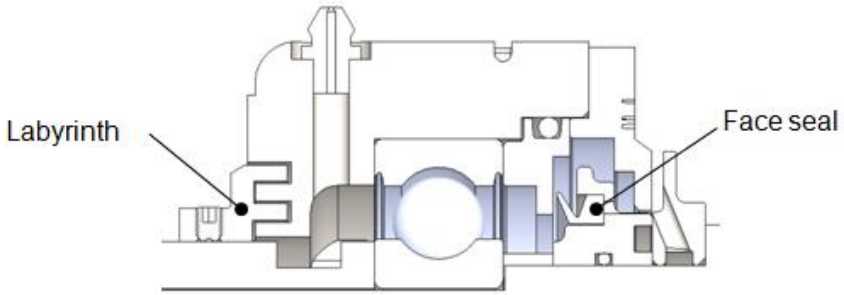

Figure 5.12 Rolling element bearing housing seals

The labyrinth was machined out and replaced by a new cover with a lip seal. The standard Pillow Block Cover, Guard Ring, Fat Valve Disc, O-ring and face seals were replaced by a new cover with a lip seal – see Figure 5.13.

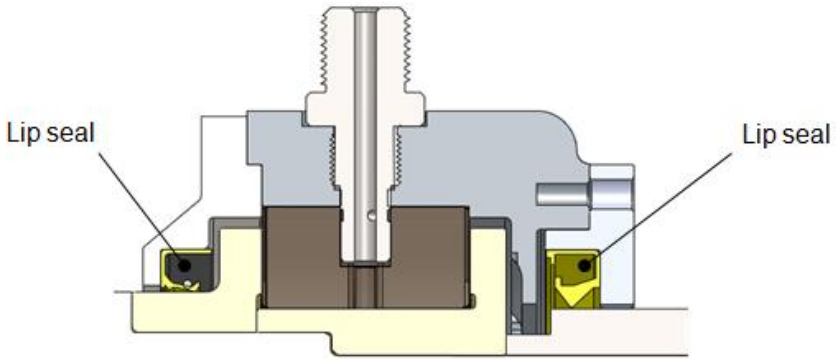

Figure 5.13 New seals for modified bearing housings (oil film)

For an operating speed of 3250 rpm, the surface velocity at the journal is 19 m/s. This is at the top end of the capacity of many seal types so finding stock items was problematic. For anticipated future designs where the operating speed is higher (e.g. up to 6000 rpm) then alternative sealing arrangements will be required.

In this chapter the physical layout of the bearing conversion has been established along with the requirements for lubrication. The conversion limits the modifications to the existing hubs and housings so that the parts can be restored after the trial.

Chapter 6 Testing

Once the new bearing design had been manufactured and fitted to the test machine a series of trial were undertaken to determine the operating vibration and noise levels. Testing was completed in the manufacturer's workshop and showed that significant reductions in noise and vibration had been achieved. The reduced vibration level shows the effect of damping and the realizable benefit of reduced excitation of attached parts e.g. the guards, due to the absence of higher frequencies in the spectrum. The associated reduced noise level is recognition of the "treat at source" approach over the passive environmental treatment approach to noise reduction in machinery.

The testing program involved measurement of vibration over a range of running speeds in addition to monitoring the shaft motion and sound level. Uni-axial accelerometers were mounted on the main bearing housings to sense vibration in the horizontal and vertical directions. Non-contacting displacement sensors were mounted adjacent to the bearing housing to sense the shaft motion. The sensors were mounted in orthogonal pairs, as required by API Standard 670 [47]. One sensor is taken as the horizontal component of shaft motion and the other as the vertical component. They are usually configured at 45º either side of the vertical centreline to avoid interference from split lines but for the centrifuge testing one sensor was on the vertical centreline and the other on the horizontal centreline.

6.1 Sound level

The sound level in front of the machine was measured when the machine was running at full speed (3600 rpm). Measurement was made using a Bruel & Kjaer type 2260 Sound Investigator fitted with a type 4189 microphone. The sound level meter was set up on a tripod with the microphone positioned 1.5 m directly in front and on the machine's centre-line, at a height of 1.2 m. This position corresponded to that used for measurement at the start of this study. This

measurement was only used to indicate the overall change in the machine's sound emission. To obtain the definitive sound power the procedure described in [39] would need to be repeated. However, the change in the character of the sound was very noticeable and many staff observing the testing asked when a full speed test would be carried out! The "before" and "after" comparison of sound emission is shown in Figure 6.1. The reduction of sound in frequency bands above 300 Hz removed the "harsh" quality associated with the standard machine, with the lower frequency content giving an impression of solidity.

The total sound level reduction achieved cannot all be attributed to the bearing change however, as the final testing included other system changes:

- The cast iron base was replaced by one made from polymer concrete (see Appendix B)
- The Hopper and Cover were supported on elastomeric isolators.

At the start of this study the overall weighted sound pressure level was 93dBA. Following the replacement of base and bearings, together with isolation of the hopper and cover, the overall A-weighted sound pressure level was 83dBA. This is a substantial reduction and at a level below the 8 hour Department of Labour's maximum continuous exposure level of 85dBA - above which hearing protection is required [48]. Measurements were taken at the centre-front of the machine, at the same location for the two conditions – 1.5 m away at a height of 1200 mm. The sound intensity study on this test machine to obtain the sound power, conducted by Randle [39], did not include the effects of the change to the main bearings and showed only marginal reduction in sound power due to the change to a polymer concrete base and isolation of the guarding. The noise reduction reported here can be taken to be due to the substitution of the oil-film journal bearings for the rolling element type.

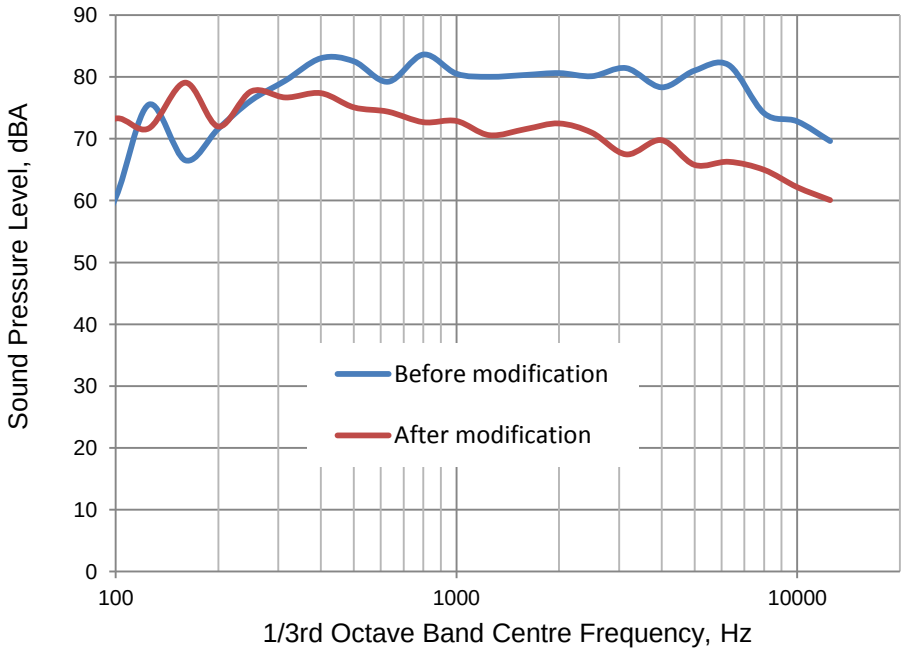

Figure 6.1 Comparison graph of centrifuge sound emissions

6.2 Vibration

Vibration measurements were made using PCB type 352C33 ICP accelerometers coupled to modular National Instruments type NI-9234 amplifiers in a cDAQ-9172 chassis. The output was input via USB to a laptop, and data collected using Labview, which was then plotted using Excel and Matlab.

The variable frequency centrifuge speed controller was set up to give a top run speed of 3625 rpm for a setting of 50 Hz. The centrifuge was operated by setting the controller in incremental steps of 5Hz, corresponding to speed increases of 362 rpm. The plots in Figure 6.2 show reduced levels of vibration at the bearings over those measured for the rolling element bearings at the start of this study.

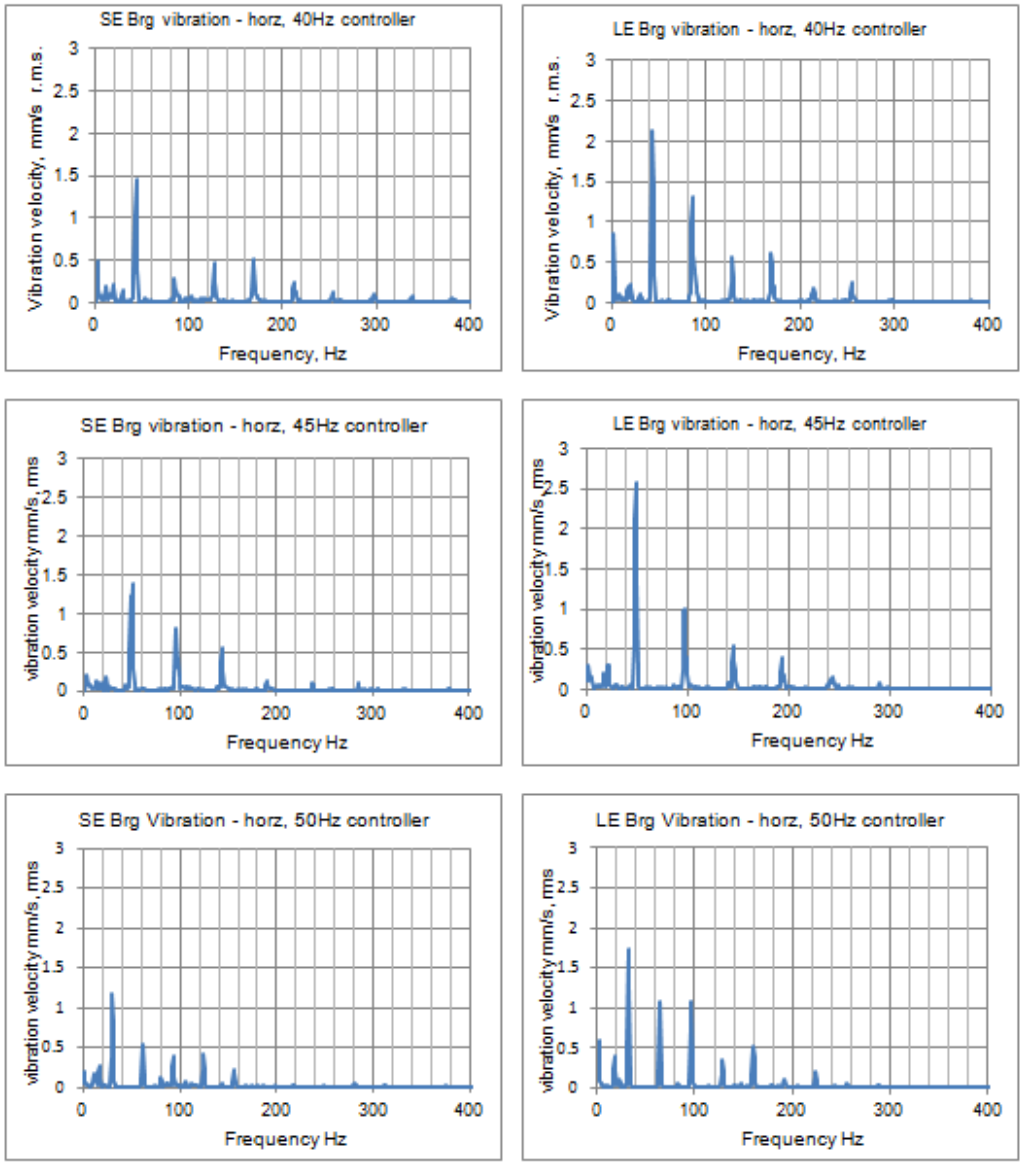

Figure 6.2 Sample plots of vibration at the main bearing housings, horizontal, mm/s, r.m.s.; (left column) Solids end, (right column) Liquid end

It is apparent from a comparison of the plots at 45 Hz and at 50Hz in Figure 6.2, that there is excitation at the liquid end causing the vibration there to be higher than for the solids end, which reduces with increasing speed. It is possible that this derives from or is a combination of the tension in the back-drive's v-belts, eccentricity of the gearbox, drive belt resonance (as the belt tension is high), or residual unbalance of bowl, conveyor or both. Several different frequencies can result from belt problems [25]. A belt with a high tension acts like a tight

vibrating string and if one of the lower modes of vibration coincides with the drive frequency then resonance will occur. An unbalanced belt will generate vibration at the frequency of its lap speed i.e. the speed at which it rotates around the two pulleys, which can be estimated by:

$$belt\ speed = \pi . driver\ pulley\ [rpm] . \frac{driver\ pulley\ pitch\ diameter}{belt\ length} \quad \ldots\ldots (6.1)$$

For the test machine the pitch diameters are: driver pulley is 355 mm, belt length 2240 mm. At 3625 rpm, the belt speed is 1805 rpm (30.1 Hz).

This is somewhat below the rotor speed but could coincidently occur at or close to half rotor speed with the appropriate geometry. The plot in Figure 6.2 for full test speed of 3260 rpm shows a vibration frequency slightly higher than half the run frequency. Therefore belt vibration as the source has the higher probability than whirl in the oil film – since that frequency would be around 0.47 of the run speed (28Hz). The close proximity of two possible sources of excitation would exacerbate any oil whirl condition if present. During testing, vibrating belts can be visualized using a strobe if this is suspected from diagnostic checks - unfortunately, one was not available for these tests. For this study, the matter was not pursued further as the vibration levels were acceptable to the manufacturer and in compliance with industry standards.

Plotting the rotor response versus speed, Figure 6.3, shows an apparent resonance frequency at approximately 2800 rpm. Although the vibration level is highest at the liquid end bearing it is possible that the source is at the solid end main bearing. This is because the main drive load at the solids end is high (40 kW) and the solids end main bearing could act as a node with a mechanical advantage appearing due to the difference in distances between the two main bearings and the solids end drive belt tension load. There was an expectation of the liquid end main bearing experiencing higher vibration than that at the solids end due to a mechanical break-down. This came about because the oil supply was lost during one test and the rotor almost seized on the bearing – requiring a clean-up machining pass that opened the bore to give a diametral clearance of +0.2 mm. Thus the liquid end main journal would run at a higher eccentricity, resulting in a lower stiffness.

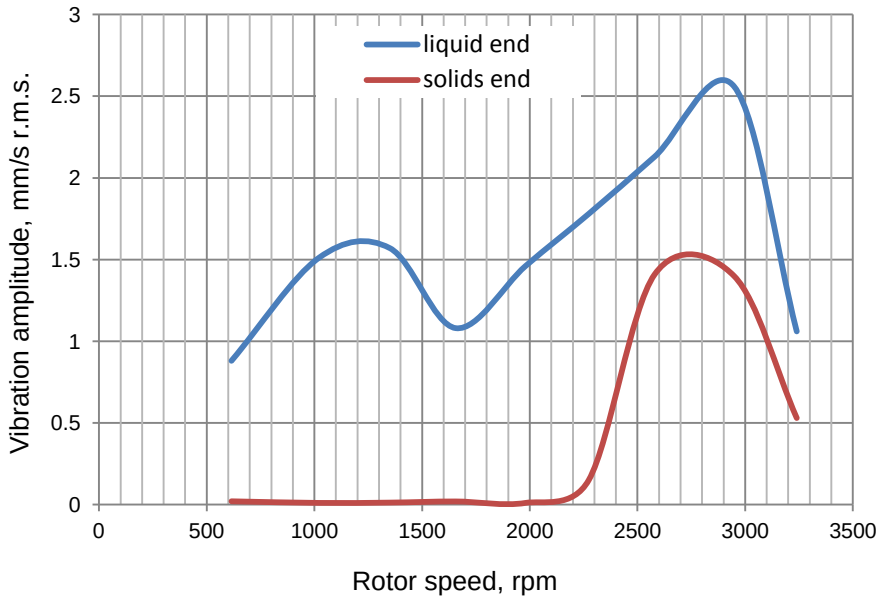

Figure 6.3 Plot of unbalance response

Whilst the plots of Figures 6.2 and 6.3 give indications of the relationship of vibration with rotational speed, it is usually more advantageous to view the data as a cascade or waterfall plot – Figure 6.4. In most applications of this type of chart, the spectra are recorded during a run-up or run-down of the machine at some increment (or decrement) of the rotational speed. The speed is sensed by a proximity probe using a reference on the shaft (often reflective tape or a keyway). Then the normal x-y plots are stacked along the z-axis to form the cascade. Many signal analyzers have this capability as an intrinsic function. Plotting data in this fashion gives a fast pictorial way to see the components related to rotational speed and the system natural frequencies. In Figure 6.4 the three dotted lines are for 1x, 2x, and 3x the rotational speed. Components related to the rotational speed are on lines angled to the frequency axis where natural frequency components are on lines normal to it. Figure 6.4 does not really have a sufficient number of traces to form a descriptive plot but the trend appearing in Figure 6.3 is apparent on a plane formed along the 1x rpm axis.

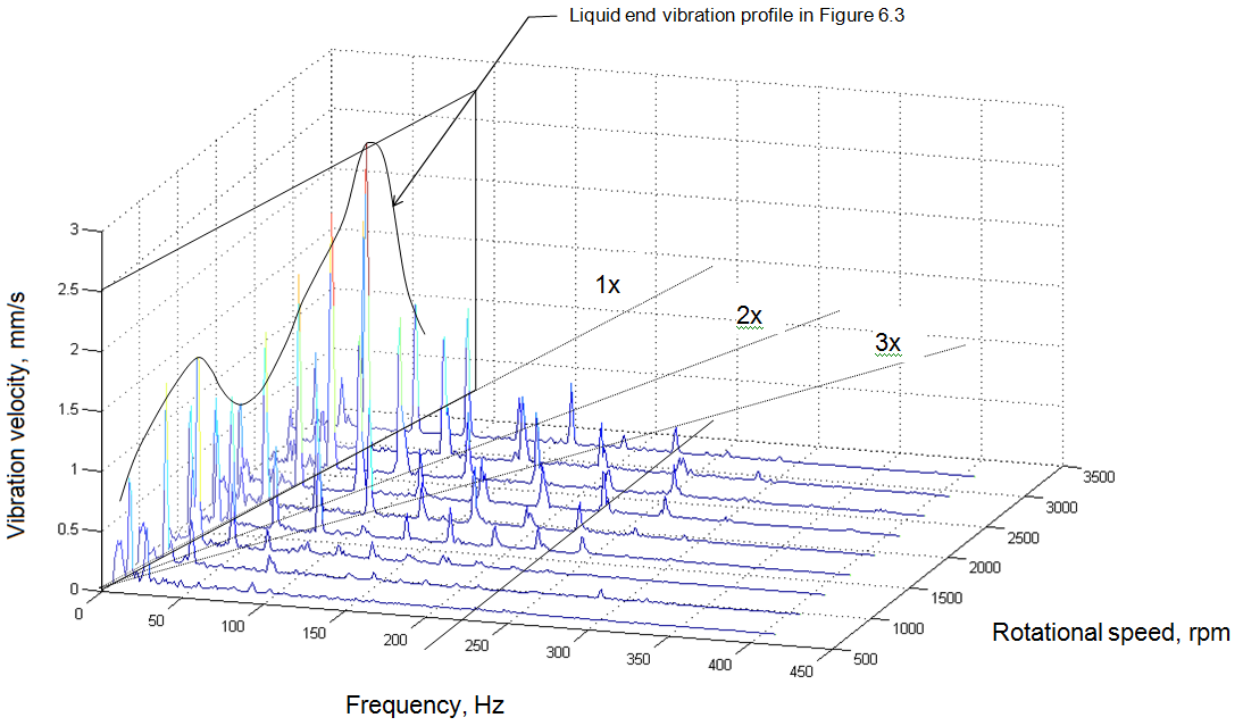

Figure 6.4 Waterfall plot of vibration test data

A review of the data shows that the vibration level has decreased – particularly at the troublesome solids end, over that from readings taken at the start of the study – see Figure 6.5. Some of this is attributable to a better state of balance but the fluid film bearings generate damping forces that can significantly reduce vibration.

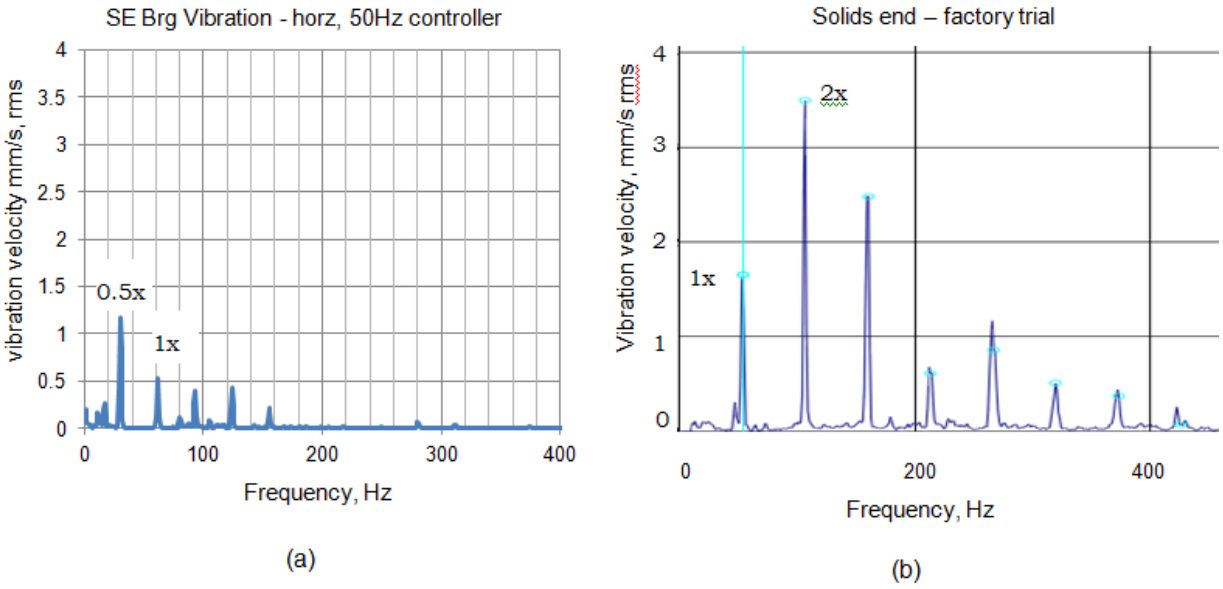

Figure 6.5 Comparison of vibration spectra at the solids end, (a) after modification and (b) before modification

6.3 Shaft motion

The shaft motion data shows two different responses for the main bearing journals, but in both cases the motion is within about 10% of the bearing clearance.

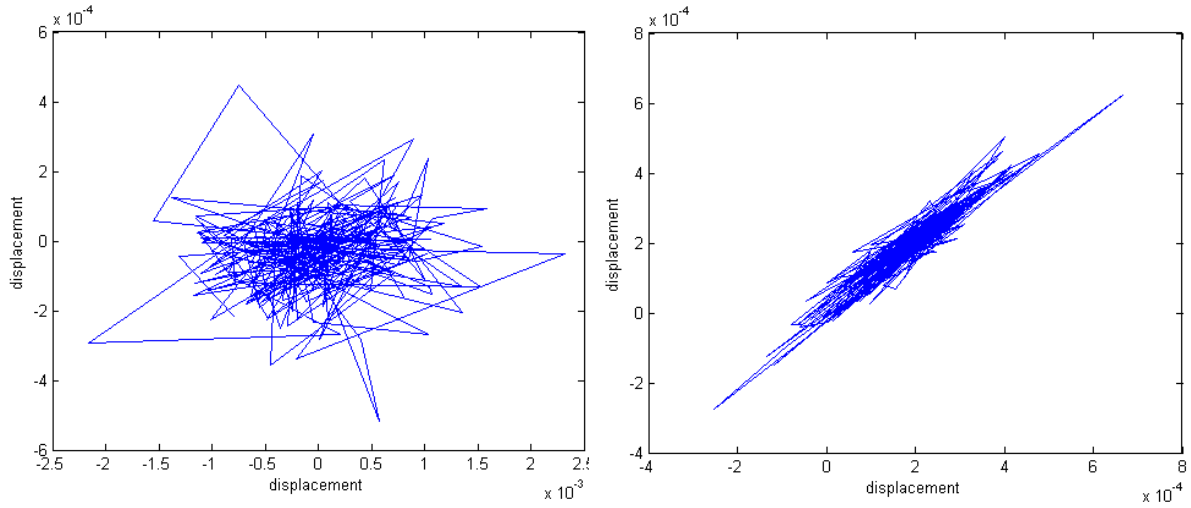

(a) **(b)**

Figure 6.6 Shaft motion plots (a) liquid end, (b) solids end, at 3600rpm

The plot traces indicate a high level of noise that could be attributable to surface irregularities, as none of the displacement probes could be located on the smoothest part of the respective shafts.

Figure 6.6 shows that the two bearings have different stiffnesses as indicated by the general shapes of the two plots. The solids end plot shows a higher motion horizontally than vertically, which is a reflection of the vertical load (the drive-belt load and deadweight of the rotor). The liquid end plot is more circular (but very noisy), indicating roughly equal stiffness in the horizontal and vertical directions. A FFT plot of the displacement data for the liquid end shows a very low 1x rpm (60 Hz) component of vibration but a higher level at 30Hz. This is consistent with an orbital motion in the bearing (called oil whirl) that occurs around 0.47 x rpm, as a result of the clearance being too high.

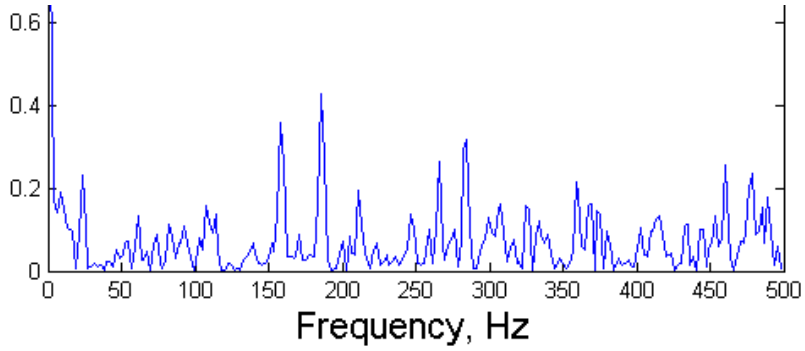

Figure 6.7 Frequency spectrum of LE main journal displacement at 3600rpm

The testing program demonstrated the effectiveness of hydrodynamic bearings to support the rotating assembly, by achieving a significant reduction in noise level, a reduction in the magnitude and frequency content of the vibration spectrum, and a change in the character of the noise emission to that of a “less harsh” nature.

Chapter 7 Conclusions and recommendations

7.1 Summary

Vibration at the solids end was reduced substantially by changing the conveyor bearing to a closer tolerance needle roller bearing, i.e. one with a smaller internal clearance. In effect this provides a stiffer support. The balance was improved which in turn reduced the level of vibration. The incidence of a high second order vibration has been explained as being contingent on a combination of factors that must prevail simultaneously and that are: a large bearing clearance, a low mass loading, and a high level of unbalance. The bearing clearance and unbalance are amenable to control but the low mass loading of the solids end needle roller bearing is an inherent property that can only be resolved by a design modification.

This study set out to solve a perplexing vibration problem and to then go on to reduce noise and vibration in the decanter centrifuge. The objectives have been achieved and ongoing work identified.

- When appropriately designed, fluid film bearings have the advantages of being lower cost and longer life than rolling element type and can be fitted into a smaller space. As has been demonstrated, both the main bearings and the conveyor bearings are candidates for conversion to fluid film bearings.
- When the main bearings are converted to fluid film bearings then the rotor needs to be hydrostatically lifted prior to starting and a small lift pump must be provided. This would also cater for the time between idle and the run speed, at which full hydrodynamic lubrication is achieved.
- The sound level was reduced by 10dBA.
- The audible beat is caused by the phasing of the unbalances of the two rotors. If a beat is audible then it is an indicator of a high level of unbalance of the conveyor - for which the most probable cause is journal run-out.

- The overall vibration levels at the main bearings were reduced by at least a factor of 2 by changing to oil film bearings.

7.2 Effect of the feed

The vibration phenomenom that has been the subject of this study manifests under no-load (not processing) and as such is a problem at start up and during the cleaning process at the end of processing, i.e. potentially twice per day. During processing the vibration level reduces but is not mitigated. The contribution that the product feed makes is through its solids fraction. When the solids are transported to the solids end discharge, the conveyor becomes centred in the bowl and loaded in compression, stabilizing the rotor. This compression load is reacted by the thrust bearing at the liquid end hub. When there is no product and therefore no thrust loading, the conveyor is "free" to vibrate within the clearance ranges at both liquid and solids end bearings. This condition is the one that creates both a starting problem (tripping the vibration safety switch) and generating the audible high beat frequency noise emission. The presence of a high second order component of vibration, in the spectra of the bearing vibration on a new machine that is operating on product, is a strong indicator that the conveyor is unbalanced – with an associated high probability that there is run-out in the journal(s). Balancing in-situ will be ineffective. This study has shown that the remedy is to fit a closer tolerance bearing at whichever hub displays the higher vibration level. If the vibration is still high and with a second order component, then machining run-out of the hubs is the source.

7.3 Machining errors

The review carried out during this study showed that the journal surfaces of the hubs can fall outside the tolerance for concentricity shown on the manufacturing drawing. The resulting shaft run-out affects the condition of balance of the conveyor so that, whatever state the balance was in following the shop balancing procedures, the assembled conveyor is significantly unbalanced. In the present manufacturing process the approach has been to try to achieve a better condition of overall balance by making corrections to the bowl. However, improvements are extremely hard to achieve because of the slowly varying position of the conveyor's

unbalance due to the differential speed and a long time is spent attempting to converge on a solution.

This study has shown that in cases where the journal run-out exceeds the specified machining tolerance then the vibration spectrum will show a high level of unbalance for the conveyor and this will need to be corrected using the procedure given in Appendix C. In cases of gross run-out the offending hub(s) will need to be changed or re-machined. The occurrence of out-of-tolerance parts should be logged and correlated with either QA inspection or sampling plans in order to determine if there is an underlying cause e.g. a machine common to all "bad" parts.

7.4 Assembly errors

Generally, the errors attributable to the assembly are due to tolerance build-ups rather than the assembly procedure itself. This is particularly so for the bowl sections where the spigot fits (G in Appendix C, Figure C.5) may be assembled with the maximum deviations all on the same axial alignment. However, these accumulations (from run-out) can be corrected for by balancing. A deviation from squareness of the mating faces leads to misalignment that generates a 2x rpm vibration component together with vibration in the axial direction. This latter source was not shown to be a problem during this study.

The incidence of out of tolerance hub journals raises three important questions:

1 What is the sensitivity of the response of the centrifuge as a function of the machining tolerances?
2 Are the currently specified tolerances consistently achievable by the range of machining centres used to manufacture the parts?
3 Is there a correlation with a particular machining centre from which the parts are sourced? In other words, does the same machine periodically produce out of tolerance parts?

This study found that the vibration problem is attributable to the state of balance of the conveyor, which in turn is a function of the clearances in the bearings and journal eccentricity. Any imbalance due to assembly of the bowl is easily

remedied in-situ but the conveyor requires a new approach as detailed in Appendix C.

7.5 Bearing designs

This study has shown that the journal bearings used for this study were adequate for proof of concept, for production machines the recommendation is to increase their length. This lowers the pressure loading but also reduces the oil side leakage as a percentage of total oil flow – effectively reducing oil temperature. The increased size of the bearing and housing could be used to advantage to arrange for hydrostatic lift of the rotor prior to starting. The conversion from rolling element bearings to fluid film bearings does however require the addition of an oil supply pump and reservoir – although the latter could be incorporated into the subframe.

The conversion of the conveyor bearings to fluid film bearings should be considered in conjunction with alternative forms of lubrication. Modern plc (programmable logic controller) and variable frequency drives enable the two rotors to be run up to speed together so that the conveyor bearings are only exposed to the differential speed. In any case, this is the situation for decanter centrifuges that have fixed drive ratios driven by one motor i.e. there is no separate back drive motor. The bearings can easily be changed for one or other type of polymer bearing that is capable of running dry or is pre-lubricated. A further option is to arrange lubrication by water (always available in processing plants) or by the process fluid itself. The recommendation for future work is to progress the proposed bearing arrangements appearing at the start of Chapter 5 with, perhaps, readily available bushings – such as the metal-polymer or solid-polymer bearings from Glacier Garlock Bearings (distributed by Dotmar Engineering in New Zealand).

7.6 Final remarks and recommendations

This study has shown that the noise and vibration emissions from the decanter can be reduced substantially by using fluid film bearings as the primary form of rotor support, and by carrying out improvements to the conveyor's state of balance. Hydrodynamic bearings generate many fewer frequency components than rolling element bearings and this study highlighted the elimination of a

large number of higher frequencies formerly in the vibration spectra. Earlier studies [39] showed these higher frequencies to subsequently excite add-on parts (such as the gearbox cover) and ultimately cause fatigue. Hydrodynamic bearings add substantially to system damping and this study showed reductions in both noise and vibration. Subjectively, the character of the "sound" emitted by the machine is different and of a "softer" nature. The implication is that further noise reduction would follow conversion of the conveyor bearings to fluid film type. However, there is a limit to the gains in noise reduction from bearing changes as windage noise generated by the rotating assembly ([39]) is high. Therefore one would not expect to be able to realize further gains in noise reduction unless the threshold from windage was also reduced. The change of the conveyor's rolling bearings to journal bearings should thus first be evaluated based on performance and cost benefits with noise reduction being an added advantage - until such time as the windage noise is addressed.

7.6.1 Recommendations

1 Many pumping systems work with water lubricated bearings (Thorndon, Sulzer, Mikasa) and the present study should be extended to investigate using water as the lubricant for the conveyor bearings. Water is always readily available in processing industries where centrifuges are in common use and a water circulating system is more environmentally attractive than using grease or oil lubricants.

2 Lubrication by a non-Newtonian fluid is another possibility that should be investigated with the aim of using the process fluid. Example processes where this could be trialled are fish oil recovery, wool scour liquor extraction, fruit and vegetable juice processing. The general guide to bearing selection [42] lists process fluids as an option for consideration. Once the centrifuge is running the lubricant could be drawn off the liquid pool using a scoop similar to that used to extract a third phase in multi-phase separators. The machine's start-up and shut-down periods would be facilitated by using water.

3 The mechanism of instability in the solids end needle roller bearing should be investigated as a non-linear problem.

4 The design of the bearing must be extended to include hydrostatic lift of the rotor prior to starting.

References

1. Donohue, B., *Investigation of Vibration in a 1456 Decanter Centrifuge*, 2004: Christchurch, New Zealand.

2. Rao, J.S., *History of Rotating Machinery Dynamics*2011: Springer.

3. Lalanne, M., Ferraris, G., *Rotordynamics Prediction in Engineering*. 2nd ed2001: John Wiley and Sons.

4. Pham, M.H., Bonello, P., *An impulsive receptance technique for the time domain computation of the vibration of a whole aero-engine model with non-linear bearings.* Journal of Sound and Vibration, 2008. **318**: p. 592-605.

5. Bonello, P., Pham Minh Hai., *A receptance harmonic balance technique for the computation of the vibration of a whole aero-engine model with non-linear bearings.* Journal of Sound and Vibration, 2009. **324**(1-2): p. 221-242.

6. Kamenicky, J.M., E.; Zapomel, J., *Numerical Analysis of Dynamic Properties of Nonlinear Rotor Systems of Aircraft Jet Engines.* International JOurnal of Rotating Machinery, 2000. **6**(5): p. 333-343.

7. Hai, P.M.B., P., *A computational parametric analysis of the vibration of a three-spool aero-engine under multifrequency unbalance excitation.* Trans. ASME, Journal of Engineering for Gas Turbines and Power, 2011. **133**(July 2011).

8. Childs, D.W., *Turbomachinery Rotordynamics: Phenomena, Modeling and analysis.*1993: John Wiley & Sons, Inc.

9. Kappaganthu, K., Nataraj, C., *Nonlinear modeling and analysis of a rolling element bearing with a clearance.* Communications in Nonlinear Science and Numerical Simulations, 2011. **18**((2011)): p. 4134-4135.

10. Ehrich, F.F., *Handbook of Rotordynamics*1992: McGraw-Hill.

11. Records, A.a.S., K., *Decanter Centrifuge Handbook*2001: Elsevier.

12. Bell, G.A., *Analytical treatment for optimisation of the operation of the decanting centrifuge*, in *Mechanical Engineering*2013, University of Canterbury: Christchurch, New Zealand.

13. Fleming, D.P., Murphy, B.T., Sawicki, J.T., Poplawski, J.V. *Transient Response of Rotor on Rolling Element Bearings with Clearance*. in *Seventh International Conference on Rotor Dynamics*. 2006. Vienna, Austria.

14. Tiwari, M., Gupta, K. and Prakash, O., *Effect of radial Internal Clearance of a Ball Bearing on the Dynamics of a Balanced Horizontal Rotor.* Journal of Sound and Vibration, 2000. **238**(5): p. 723-756.

15. Gupta, T.C.G., K.; Sehgal, D.K., *Nonlinear dynamics and chaos of an unbalanced flexible rotor supported by deep groove ball bearings with radial clearance*, in *ASME Turbo Expo 2008, Power for Land, Sea and Air*2008, ASME: Berlin, Germany. p. 321-333.

16. Yamamoto, T.I., Y., *Theoretical discussions on vibrations of a rotating shaft with nonlinear spring characteristics.* Ingenieur Archiv, 1977. **46**: p. 125-135.

17. Villa, C.V.S., Sinou, J-J., Thouverez, F., *Investigation of a rotor-bearing system with bearing clearnace and hertz contact by using a harmonic balance method.* Journal of the Brazilian Society of Mechanical Sciences and Engineering, 2007. **29**(1): p. 13.

18. Friswell, M.I.P., J.E.T.; Garvey, S.D.Lees, A.W., *Dynamics of Rotating Machines*2010, New York: Cambridge University Aerospace Series.

19. Ishida, Y.a.Y., T., *Linear and Nonlinear Rotordynamics - a modern treatment with applications*2012: Wiley-VcH.

20. Smith, D.M., *The motion of a rotor carried by a flexible shaft in flexible bearings.* Proc. Royal Society, London, UK., 1933. **Series A, V142**: p. 92-118.

21. Eshleman, R.L.a.E., R.A, *On the critical speeds of a flexible rotor.* Trans. ASME, Journal of Engineering for Industry, 1969. **91**(4): p. 1180-1188.

22. Harris, T.A., *Rolling Bearing Analysis*. 4th ed2001: John Wiley & Sons.

23. Someya, T.E., *Journal Bearing Data Book*1989, London, U.K.: Springer-Verlag.

24. Tiwari, R.L., A.W. Friswell, M.I., *Identification of dynamic bearing parameters: A review.* Shock and Vibration Digest, 2004. **36**(2): p. 99-124.

25. Mitchell, J.S., *Introduction to Machinery Analysis and Monitoring*1993: Pennwell Books, USA.

26. Ruddy, A.V., *The dynamics of rotor bearing systems*1979: University of Leeds.

27. Ruddy, A.V.a.S.-S., D., *An Introduction to the Influence of the Bearings on the Dynamics of Rotating Machinery.* Tribology International, 1980. **Oct 1980**.

28. Kim, B.O.a.L., A. S, *Rotordynamic Characteristics and Vibration Reduction of an Industrial Decanter Centrifuge*, in *The 8th IFToMM International Conference on Rotor Dynamics*2010, KIST: Seoul, Korea.

29. Thompson, W.T., *Theory of vibrations with applications*. 2nd ed1981: George Allen & Unwin.

30. McCallion, H., *Vibration of linear mechanical systems*1973: Longman.

31. Lazovic, T.R., M.; Mitovic, R., *Mathematical model of load distribution in rolling bearings.* FME Transactions 2008, 2008. **36**: p. 189-196.

32. Hamrock, B.J., Schmid, S.R., Jacobson, B.O., *Fundamentals of Fluid Film Lubrication*2004: Marcel Dekker, Inc.

33. Yang, J.H., S.Z.; Wang, L.Q., *Dynamic Balancing of a Centrifuge: Application to a dual rotor system with very little speed difference.* Journal of Vibration and Control, 2004. **10**: p. 1029 - 1040.

34. Upadhyay, S.H.H., S.P.; Jain, S.C., *Analysis of nonlinear phenomena in high speed ball bearings due to radial clearance and unbalanced rotor effects.* J. of Vibration and Control, 2010. **16**(1).

35. Childs, D.W., *Twice-running-speed Response due to Elliptical Bearing Clearances.* Trans ASME Journal of Vibration and Acoustics, 2003. **125**: p. 64-67.

36. Yamamoto, T., *On the critical speeds of a shaft.* Memoirs of the Faculty of Engineering, Nagoya University, 1954. **6 (2)**.

37. Guo, Y., *Rolling element bearing stiffness matrix determination*, in *Gearbox Reliability Coallaborative Meeting 2102*2012, NREL.

38. Stribick, R., *Ball bearings for various loads.* Trans ASME 1907. **29**: p. 420-463.

39. Randle, P., *Assessment of Sound Sources - 1456 decanting centrifuge*, 2011, University of Canterbury: Christchurch, New Zealand.

40. Kim, B.-H.R.D.-G.K.K.-W., *Effects of design parameters on the noise of rotor-bearing systems.* Tribology International, 2004. **37**(2004): p. 599 - 605.

41. Kim, B.-H.R.K.-W., *Acoustical properties of hydrodynamic journal bearings.* Tribology International, 2003. **36**(2003): p. 61 - 66.

42. ESDU, I., *65007 - General guide to the choice of journal bearing type*, 2002: London, U.K.

43. Welsh, R.J., *Plain Bearing Design Handbook*1983: Butterworths.

44. ESDU, I., *84031 - Calculation methods for steadily loaded axial groove hydrodynamic journal bearings*, 1991: London, U.K.

45. Donohue, B., *The response of rotor systems to seismic excitation*, in *School of Mechanical Engineering, Applied Mechanics*1984, Cranfield: U.K.

46. Hannah, J., ; Hillier, M.J., *Mechanical Engineering Science*1985, Great Britain: Pittman.

47. Institue, A.P., *Machinery Protection Systems*, 2001: U.S.A.

48. Labour, D.o., *Approved Code of Practice for the Management of Noise in the Workplace*, 2002, NZ Govt: Wellington, New Zealand.

49. United, C. *http://www.unitedcentrifuge.com/products/centrifuges/centrifuges-overview.html*. 2012.

50. www.viscotherm.com. *Viscotherm*.

51. Institute, A.P., *Tutorial on the API Standard Paragraphs Covering Rotor Dynamics and Balance (An introduction to lateral critical and train torsional analysis and rotor balancing)*, 2010.

52. Cloud, C.H. *Design Audits of Machinery: Rotor Dynamics*. in *21st Ethylene Producers'*. 2009. Tampa, Florida, USA.

53. Schultz, H.a.N., R.-G. , *Designing Machine Tool Structures in Polymer Concrete*. International Journal of Cement Composites and Lightweight Concrete, 1983. **5**(3): p. 203-207.

54. Orak, S., *Investigation of vibration damping on polymer concrete with polyester resin*. Cement and Concrete Research, 2000. **30**: p. 171-174.

55. Mani, P.G., A.K.; Krishnamoorthy, S., *Comparative study of epoxy and polyester resin-based polymer concretes*. International Journal of Adhesion and Adhesives, 1987. **7**(3): p. 157-163.

56. Wowk, V., *Machinery Vibration: Balancing*1995: McGraw Hill, Inc.

57. ISO, *1940-1: 2003. Mechanical vibration -- Balance quality requirements for rotors in a constant (rigid) state -- Part 1: Specification and verification of balance tolerances. International Standards Organisation*

58. *Balance Quality Requirements of Rigid Rotors: the practical application of ISO1940/1*. 2009; Available from: www.irdbalancing.com/downloads/techpaper1balqualityreqmts.pdf.

59. Barbedo, J.G.A.L., A, *Estimating Frequency, Amplitude and Phase of Two Sinusoids with Very Close Frequencies*. World Academy of Science, Engineering and Technology, 2009. **35**: p. 740-747.

60. Zeng, S.W., X.-X., *Unbalance identification and field balancing of dual rotors system with slightly different rotating speeds*. Journal of Sound and Vibration, 1998. **220**(2): p. 343-351.

61. Someya, T., *Journal-bearing databook*1988: Springer-Verlag.

Appendix A The working principle of the decanting centrifuge

Centrifugation is the mechanization of the natural sedimentation process of settling out the solids in a liquid suspension. A beaker of slurry suspension, Figure A.1, if left on a bench for some time will naturally settle out into its component parts under the action of gravity, with the heavier particles settling at the bottom.

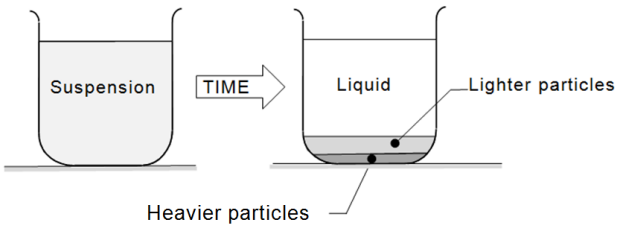

Figure A.1 Illustration of gravitational separation or sedimentation

Ponding must be used for separating out large volumes of suspension by gravity - see Figure A.2 for example. This is where the term 'pond' is derived for the product suspension in a centrifuge [11].

Figure A.2 Settling pond (Kaponga, South Taranaki, NZ)

Large volumes for processing this way need large areas of land and sufficient time for the natural process to take its course. Whilst this solution might be acceptable in rural districts where land is cheaper, in urban areas where land is expensive it makes more sense to mechanize the process and centrifugation is one option that is used as an alternative. In addition, for many applications there are environmental aspects that prevent the use of natural settling and so mechanical methods are mandatory. In industrial processing, centrifugation is much faster at separating out suspensions than settling tanks or ponds, but the machine cost has to be offset by the value of the throughput. The removal of solids must match the rate at which effluent is produced. Centrifuges are ideal for the continuous separation of suspensions and the solid bowl type is referred to as the decanting centrifuge.

In the decanting centrifuge, the feed enters at the axis of rotation and usually has a relatively low velocity - around 1 m/s. It falls into the rotating hub of the conveyor where it is accelerated to the tangential velocity of the conveyor hub and discharged into the pond surface in the bowl – see Figure A.3 and A.4. The heavy particles are flung to the bowl wall, rapidly achieving the result of the process depicted in Figure A.1.

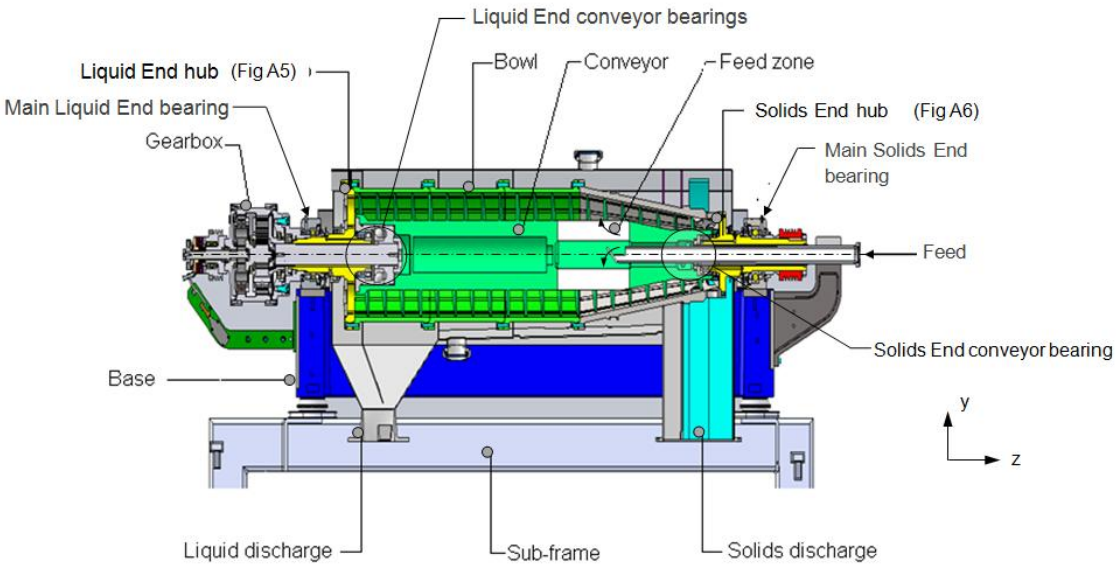

Figure A.3 Cross-section through a typical decanter centrifuge

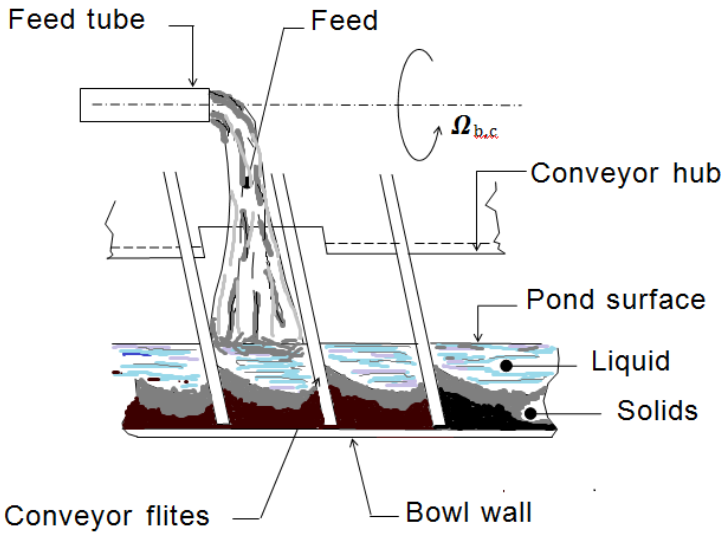

Figure A.4 Illustration of the feed zone – conveyor transporting product from left to right

The liquid's free (pond) surface is not constrained by pressure and once at the level of the discharge dams it flows in the opposite direction to the moving solids – in the spiral gap between flights and out through the discharge ports – see Figure A.5. A video depiction of the process can be found on the website for United Centrifuge Ltd [49].

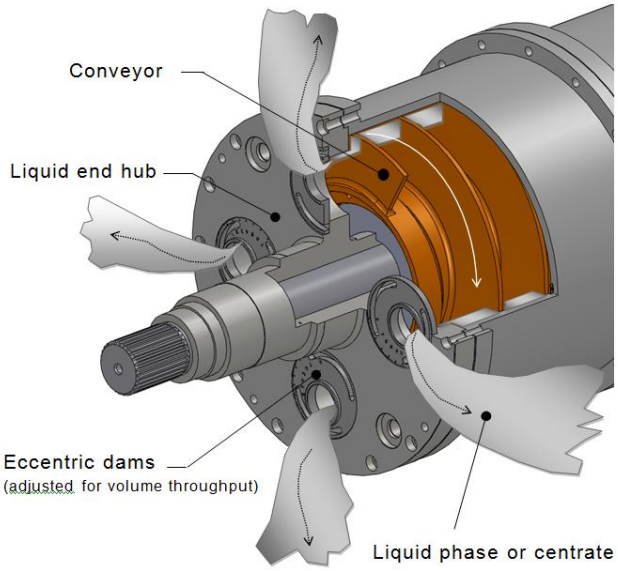

Figure A.5 Discharge of the liquid phase (or centrate) via adjustable eccentric dam plates

Correspondingly, the solids component is pushed out the discharge ports, by the conveyor, at the opposite end of the machine – see Figure A.6. A substantial thrust force is developed as a result of the solids product being compressed by the dual actions of the centrifugal force and translation against the dry surface of the conical (Figure A7).

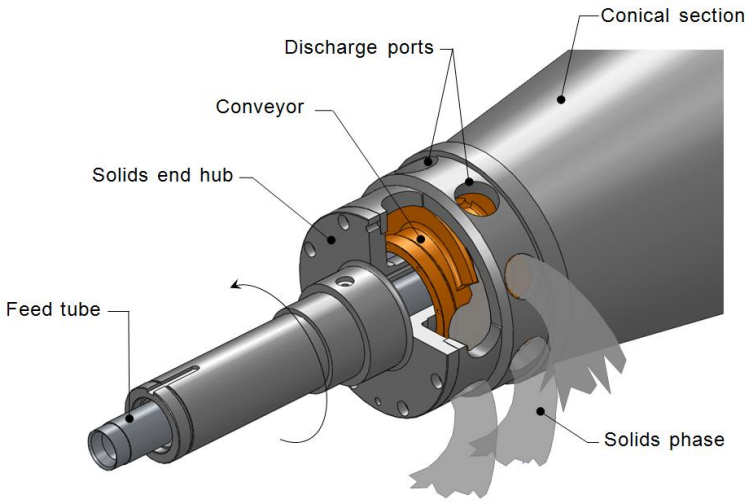

Figure A.6 Discharge of the solids phase via radial ports

The centrifuge process appears to be simple but the centrifuge itself is a complex assembly. It is important to understand the relationship between the variables that control the process as these affect the dynamic response of the machine. For example, increasing the speed to increase throughput, increases the centrifugal loading as the square of the increase. The result is that a higher density solids loading is generated at the bowl wall leading to increased friction from transport by the auger. The torque required to transport this denser product may exceed the rating of the gearbox – for which case protection is provided through a drive disabling clutch. The centrifuge rotor is different to other rotating machines as it is essentially a type of pressure vessel. The pressure develops at the bowl wall due to rotation and varies linearly with the radius. Thus the highest pressure is at the largest radius and the heaviest particles collect there. The slenderness ratio is of the order of 4:1, with relatively light loads for the bearings. The highest load for the bowl is from tension resulting from the compression load generated in the conveyor by the action of lifting and translating the *dry* solids up the conical slope to discharge.

There is little difference between models from different manufacturers and the parts that are fundamental to the working of the centrifuge are:

- the base/support structure, with or without a sub-frame but vibration isolated
- the bearings
- the rotating assembly
- the transmission and
- the feed tube

The rotating assembly is housed in an enclosure that allows access through a hinged lid and provides ducts in the lower half for discharge of the separated products.

The transmission includes the belt drives to the main and back-drive motors, the gearbox, and the driveshaft for the conveyor. For the machine used in the current study the rotating assembly is driven by electric motors through v-belts. Larger machines can also be driven by specialty hydraulic motors, see [50] for example.

Referring to Figure A.3, the conveyor auger screw is supported on bearings that in turn, are supported on journals at the liquid end and solids end hubs. A splined shaft connects the gearbox and conveyor through a clearance bore in the liquid end hub. At the liquid end there is also an internal thrust bearing that reacts the thrust load. At the solids end the conveyor is supported on a needle roller bearing, mounted on the solids hub. The solids end hub has a large bore to accommodate the feed tube. The effect of the two hollow hub bores is to make the supporting bearings of larger diameter for the applied loads than would result for solid shafts. As a result, the bearings are lightly loaded.

The depth of the pond (the amount of product in the bowl) is only determined by the setting of eccentric weirs/dams in the liquid end hub – see Figures A.4 and A.7. The deeper the pool then the more product there is in the bowl and the shorter the beach. The upper free surface of the pond has the smallest radius; the bottom surface of the pond is at the bowl wall and is subject to the pressure developed by centrifugal force. In effect, the decanter centrifuge is a rotating pressure vessel with the pressure above the pond being atmospheric.

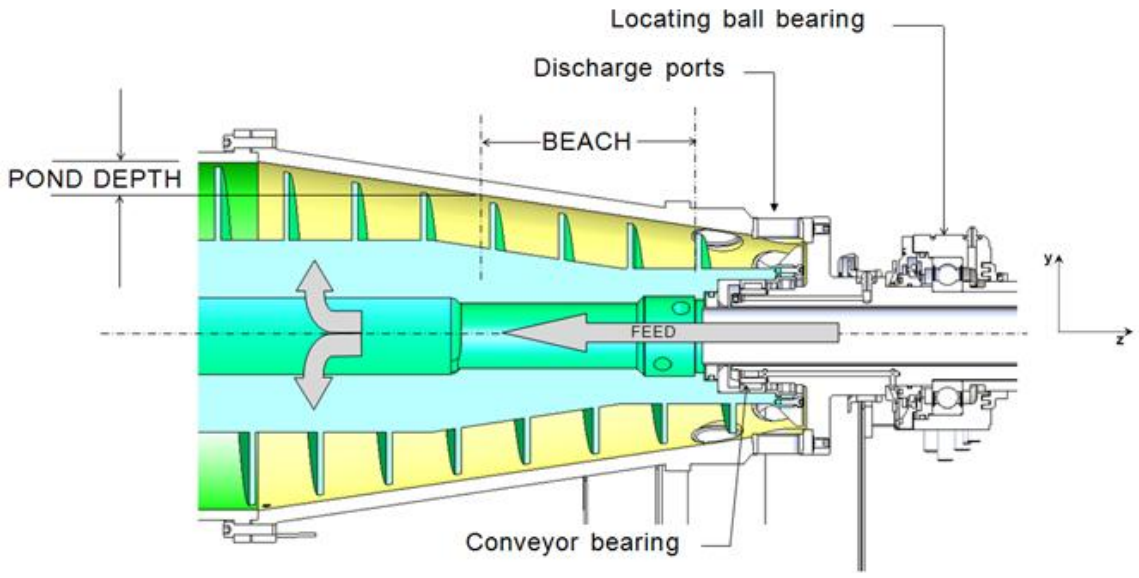

Figure A.7 Sketch showing dry beach area of the conical at the solids end (Note: the feed tube is not shown)

The liquid and solids end hubs are supported on plummer block bearings at each end of the machine. For the machine in this study the solids end main bearing is a locating deep groove ball bearing and the liquid end main bearing is a cylindrical roller bearing. The cylindrical roller bearing allows axial growth of the rotating assembly with temperature rise; some machines, such as those used in rendering processes, operate with product at 90°C.

The conveyor is driven by an electric motor (referred to as the back drive) through v-belts to an epicyclic gearbox at the liquid end and the bowl is driven via v-belts and an electric motor at the solids end. The belt-drives are not shown on the cross-section in Figure A.6 but the drive motors can be seen in Figure A.8 below - the belt-drives are located under the white sheet-metal guards at either end.

Figure A.8 An external view of a decanter centrifuge

The epicyclic gear produces a high torque (typically 2000 to 4000 Nm) low speed output that drives the conveyor, which rotates at a speed between 1 to 60rpm different to that of the bowl. For the conveyor to lift and push the solids out from the bowl there has to be a difference in speed. Thus the two rotors are asynchronous. The conveyor may be run faster or slower than the bowl depending upon the conveyor design.

Appendix B The Polymer Concrete Base

It seems almost impossible to imagine a situation where a complex assembly would not have parts that can be excited to resonance by the dynamic effects of its components. If these effects can be identified then stiffening or adding damping can be used to modify the part(s) to avoid resonance. In the case of the decanter centrifuge, high levels of vibration were measured on the cast iron base and the gearbox guard. Fatigue failures of some the attachments points of gearbox guards have been recorded. One recurrent problem with the centrifuge under review is that the standard base is resonant at the normal run speed for the machine. All bases are not cast with the same core positions and so some machines are problematic where others are satisfactory. The early part of this project was concerned with establishing a stiff foundation for the rotating assembly in order to avoid the signal modification caused by resonances.

Residual unbalance of the rotating assembly is the primary excitation force and the resonance condition of the base means that high levels of vibration result from the unbalance. Unbalance is discussed in Appendix C. Beside the fatigue issues associated with this high level of vibration there is an associated control problem that results from tripping of the vibration switch. The switch signals an alarm condition when unbalance is increasing and shuts down the machine when a pre-set level is exceeded. When a resonant condition exists with the base then the switch trips during machine run-up and it becomes impossible to start the machine without by-passing the safety switch.

The main bearing housings that support the decanter's rotating assembly are mounted directly onto machined surfaces of the cast base and there is no opportunity for isolation of the unbalanced forces. The sub-frame is isolated however so that no vibration (or very little) is transmitted to the floor. A finite element analysis of the base showed the first vibration mode to be in torsion and therefore not likely to be identified using the normal uni-axial vibration

measurements taken horizontally at the bearings. The standard base is a web stiffened casting of grade G250 grey cast iron, as shown in Figure B.1, weighing around 470kg. The response of the cast iron base was determined experimentally by Randle [39] as part of a parallel study to reduce noise emission.

The problems associated with the base led to this study undertaking a review of the design. The objective was to determine what changes needed to be made in order to mitigate the modal response and to then assess whether a new approach was required.

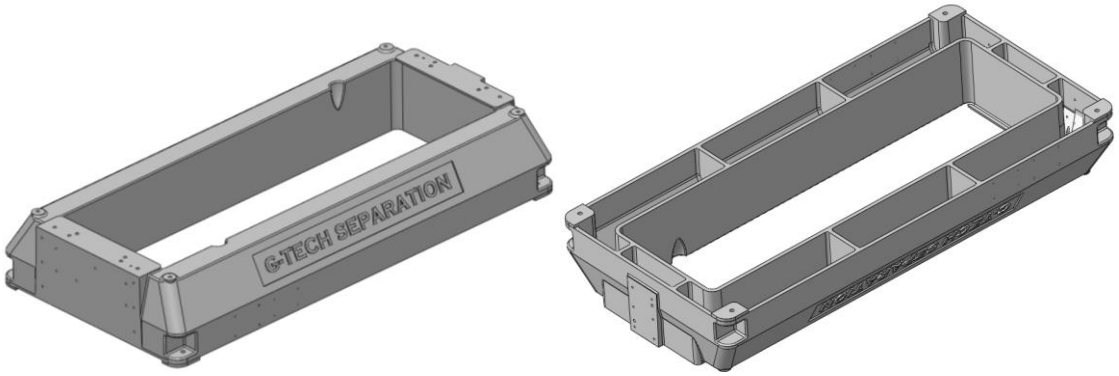

Figure B.1 Two views of the standard cast iron base showing exterior and interior surfaces

The vibration sensed at the main bearings is composed of the primary contributions from the rotating assembly and the bearings, and is modified by the characteristics of the attached static components - guards, hopper and cover and the base-frame. Where the static components have natural frequencies that are harmonically linked to the exciting frequencies then higher levels of vibration are expected. It is necessary to separate out the amplification, due to the static components, from the measured vibration in order to study the response of the rotating assembly to unbalance. Other options are to stiffen and damp the base, or modify the static components, to reduce or mitigate the unwanted additional vibration.

In addition to *Randle's* work, frequency and mode studies were carried out for the base on its own and for the assembly, using a Solid Works model (shown in

Figure B.1) and the finite element software ANSYS. The natural free response of the base was determined by impact tests using an impact hammer and accelerometers. From Figure B.2 it is seen that the major free response of the base in the horizontal direction occurs at 60Hz, with further important modes occurring at 150Hz and 182Hz. Organizations such as the American Petroleum Institute (API) [51] specify safe margins for the operation of rotating systems and typically give a separation margin for run speeds to be outside 15% of a critical speed [52].

For the decanter centrifuge, not only is the normal run speed too close to the base's 60Hz natural frequency but the maximum design run speed for the machine is 4000rpm (66.7Hz) and so there is further cause for concern.

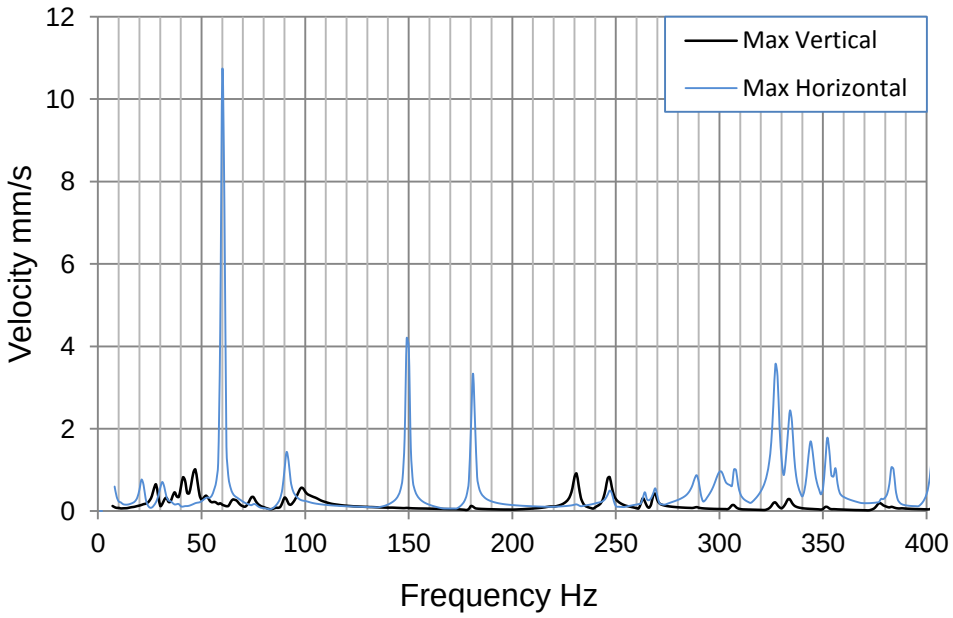

Figure B.2 Spectrum of free vibration for the bare cast iron base

Animation of the modes of vibration using ANSYS was used to study the vibration in order to understand the motion resulting from modal displacement during normal operation of the centrifuge. The objective was to find out whether the base could be modified in some way so that excitation of the low frequency modes could be avoided by making small changes to the casting pattern. The first two significant modes for free vibration (from FEA) occur at 37Hz and 54Hz – see Figure B.3. These modes are most likely to be excited by residual out of

balance of the rotating assembly. Other minor modes may occur in other than the vertical direction, indicating that further measurements are required in different planes. That is, a proper modal study is required in order to fully characterize the base. However, in lieu of this the FEA study can be used to identify modes that can then be checked on the real base. The ANSYS study showed the presence of a strong mode in torsion at 37Hz that would only practically be detected by using more than one accelerometer and taking phase measurements in addition to vibration level.

Centrifuges are normally only fitted with a switch (to detect vibration that exceeds a preset allowable maximum and isolates the machine) or horizontally mounted accelerometers at the bearings for condition monitoring. The switch is mounted on a side rail that has a bend mode at 54Hz – Figure B.3(b). The accelerometers are coupled to a plc controller to monitor vibration and/or log bearing condition. Methods proposed for modifying the base included stiffening by welding plates on the underside of the rails and adding stiffeners to the corners of the casting.

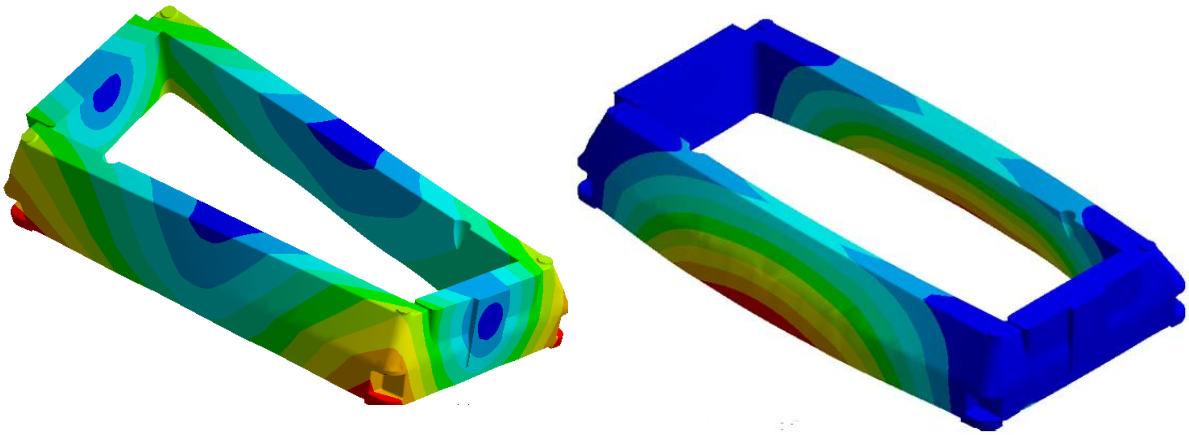

(a) (b)

Figure B.3 The first two mode shapes from an ANSYS FEA analysis
(a) torsion at 37Hz, (b) side rails out of phase bending at 54Hz

These modifications were found to raise both the in-phase and out-of phase rail bending modal frequencies out of the sensitive range but also raised the torsion mode from 37 Hz to 51 Hz and so into the troublesome range. A second torsion mode was introduced at 85 Hz by the corner stiffeners. Both these frequencies are expected to shift upwards when assembled components were bolted to the

base and the prospect of resonance seemed inevitable. The run tests showed the close proximity of the lowest natural frequencies to the normal run speed – see Figure B.4.

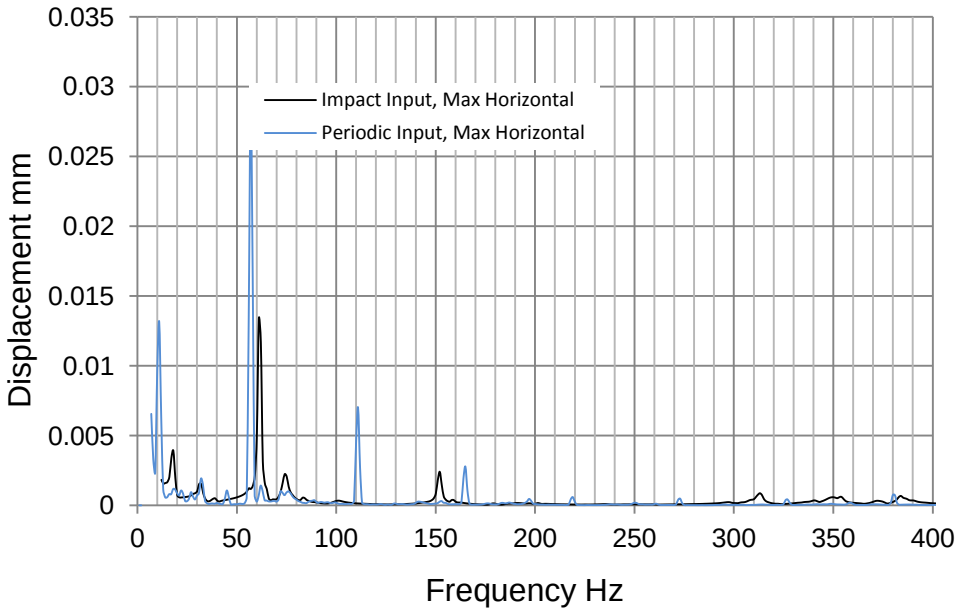

Figure B.4 Plot showing comparison of the horizontal displacements for impact and run responses (assembled machine)

The static add-on components (the drive guards, hopper and cover) were isolated in order to reduce their excitation and subsequent effects on the base. This necessitated selection of appropriate rubber isolators together with modifications to the case for their mounting – see Figure B.5. The hopper and cover have labyrinth plates to seal the discharges and have clearances of a few millimeters from the rotating bowl – Figure B.6. The deflection of the hopper and cover on rubber mounts therefore had to be properly controlled in order to avoid contact of the labyrinths with the bowl. The working height of the isolators was therefore made adjustable.

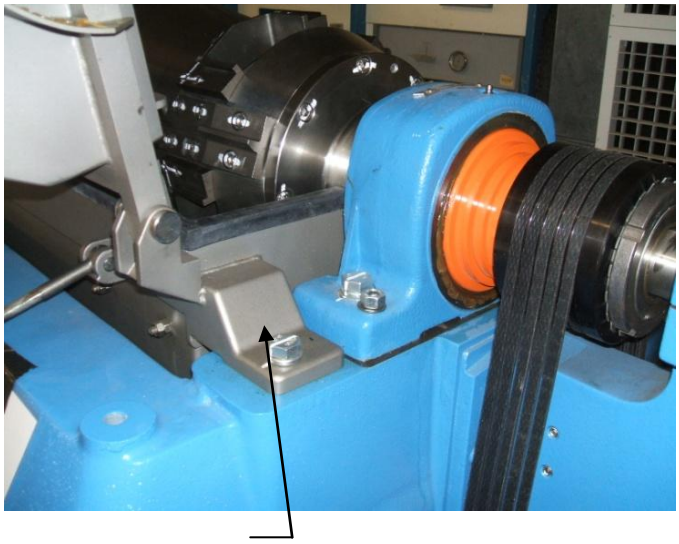

(a) Standard attachment of the case and cover to the cast iron base (Note: the position of the mounting foot is standard)

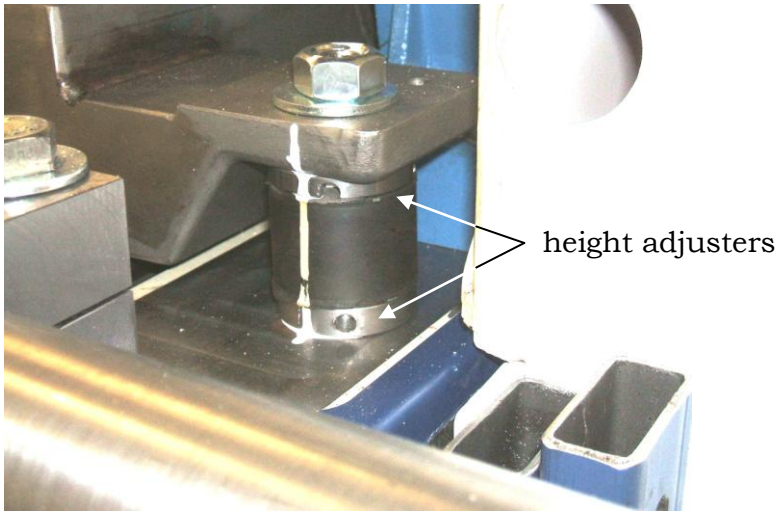

(b) Rubber isolator mount under the case mounting foot (Note: the foot has been reversed and re-welded to the case)

Figure B.5 Mounting of the case (a) standard (b) modified

Having isolated the static components, the cast iron base-frame itself was still troublesome in that the first three modes of vibration were found at frequencies of 31Hz, 52Hz, and 104Hz. Tests showed that it was not possible to effectively modify the behaviour of the base-frame through stiffening or the addition of tuned mass dampers. A decision was then made to fabricate a new base with improved properties. After review of the options a composite material of polymer (epoxy) concrete was chosen. The selection was based on the material having a

much higher damping capacity than cast iron together with good compressive and tensile properties. A controlling requirement was that the test base be designed to have the same external dimensions as the cast iron version and preferably be no heavier.

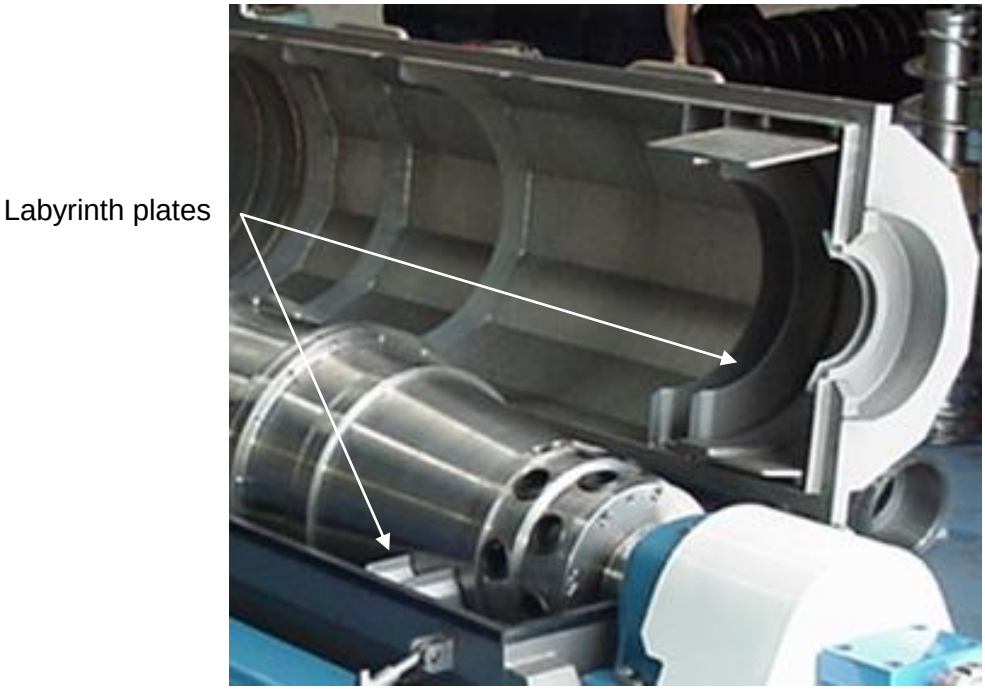

Figure B.6 View inside case and cover showing the labyrinths

Polymer concrete

Much work has been conducted on the use of polymer concrete for machine and tool bases – e.g. lathes and milling machines [53]. Basically the cement fraction is replaced by a polymeric binder, usually polyester or epoxy resins. However, for this application, polyester was discounted as a possible binder because of the likelihood of cracking of the thick section [54] and of being more water absorbent than epoxy [55]. Pure epoxy resins are also brittle but they can be enhanced by the addition of plasticizers, which mitigate the incidence of cracking. Aggregates and sand form the major part of the material matrix that is bound together with the resin. Following [55], test samples were made using different fractions of the resin binder, keeping the mass contents of the sand and aggregate constant – Table B1. One sample also included chopped strand fiberglass. Figure B.7

shows the appearance of two of the test bars, which were of rectangular cross-section 100 x 50 mm and 600mm long. The samples were room cured for 24 hours, where the ambient temperature was between 22°C and 25°C. Standard 3-point bend testing was conducted to determine the flexural strengths for comparison published data.

Table B.1 Test sample constituents

Component	Mass (grams)	Flexural Modulus MPa
Aggregate, stone pebbles 5-15mm	2300	
Aggregate ,stone pebbles <5mm	2300	
Sand (washed, river)	2300	
1 Resin, epoxy, 10%	690	15.9
2 Resin, epoxy, 7.5%	518	16.3
3 Resin, epoxy, 5%	345	14.2
4 Resin, epoxy, 10%+ 1% fibreglass	690 + 69	10.8

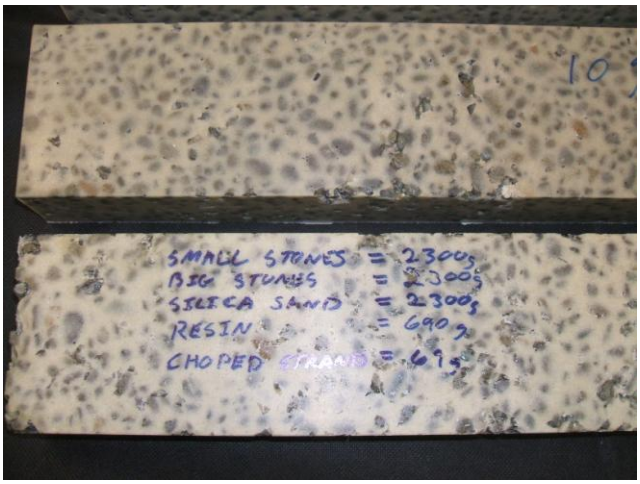

Figure B.7 Appearance of sample polymer concrete test bars

At 16.3MPa, the flexural modulus was highest for the 7.5% epoxy sample – the comparative value for Portland cement concretes is 3 to 5 MPa. The effect of the added glass fibre filler was to lower the flexural strength by some 20%, with microscopy showing a lack of adhesion. The data is in line with the results of [55] but of lower value and is attributed to the use of larger stones in the

aggregate. The testing gave confidence in the preparation and manufacturing processes and so a full size base was made.

The mould for a full sized base was constructed from marine grade ply by ASP Limited Figure B.8, and the metal inserts were fabricated by Bellmor Engineering Limited – Figure B.9.

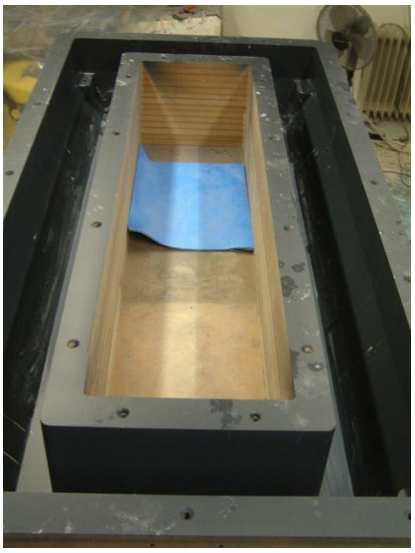

Figure B.8 Base mould

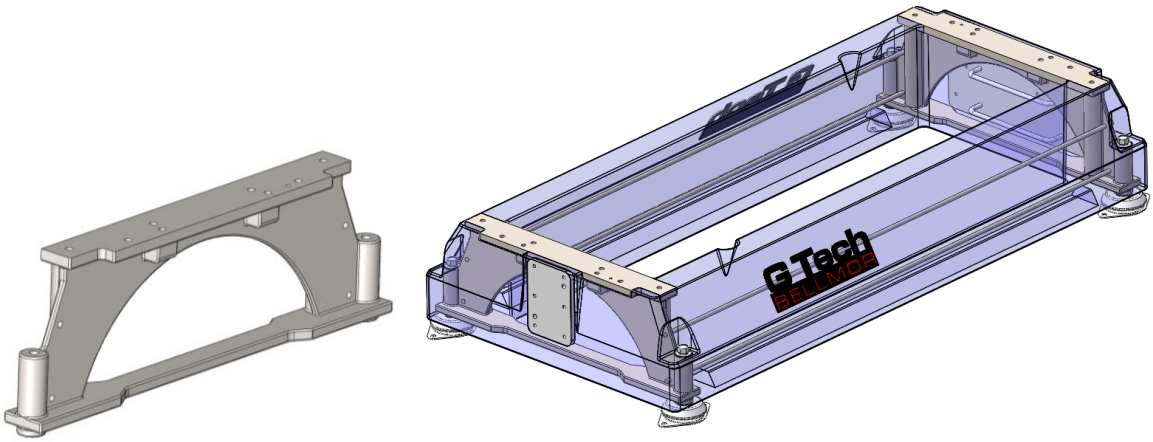

(a) (b)

Figure B.9 (a) Metal insert (b) inserts connected by rebar in cast base

The mass of the new base was almost identical to the original cast iron version and is of the same external dimensions - only the corner features are different. Figure B.10 shows a visual comparison between the two versions of the base.

The casting is released from the mould in an almost finished state, having a coloured exterior and decals included in the gel coat. Some finish machining of the metal inserts was required in order to ensure compatibility with the existing rotating assembly bearing centres and fixing points for the guards and other add-ons.

A parallel project was being carried out at the University of Canterbury by *Randle* [39], into the sound field produced by the decanter centrifuge and into ways to reduce its intensity. *Randle* noted that there was no reduction in sound emission due to installation of the new base but that there was significant reduction in most frequency bands for vibration – Figure B.11.

Figure B.10 Comparison between (top) test machine with a cast iron base and (bottom) test machine with an epoxy concrete base

Referring to Figure B.11, it can be seen that the dynamic responses at 54Hz and 108Hz (1 and 2 times rpm) have been more than halved, making for better

conditions for the assessment of the rotating assembly – a common run speed is 3250 rpm (54.2 Hz). The higher frequencies have been significantly reduced and much less likely to contribute to tripping of the vibration switch.

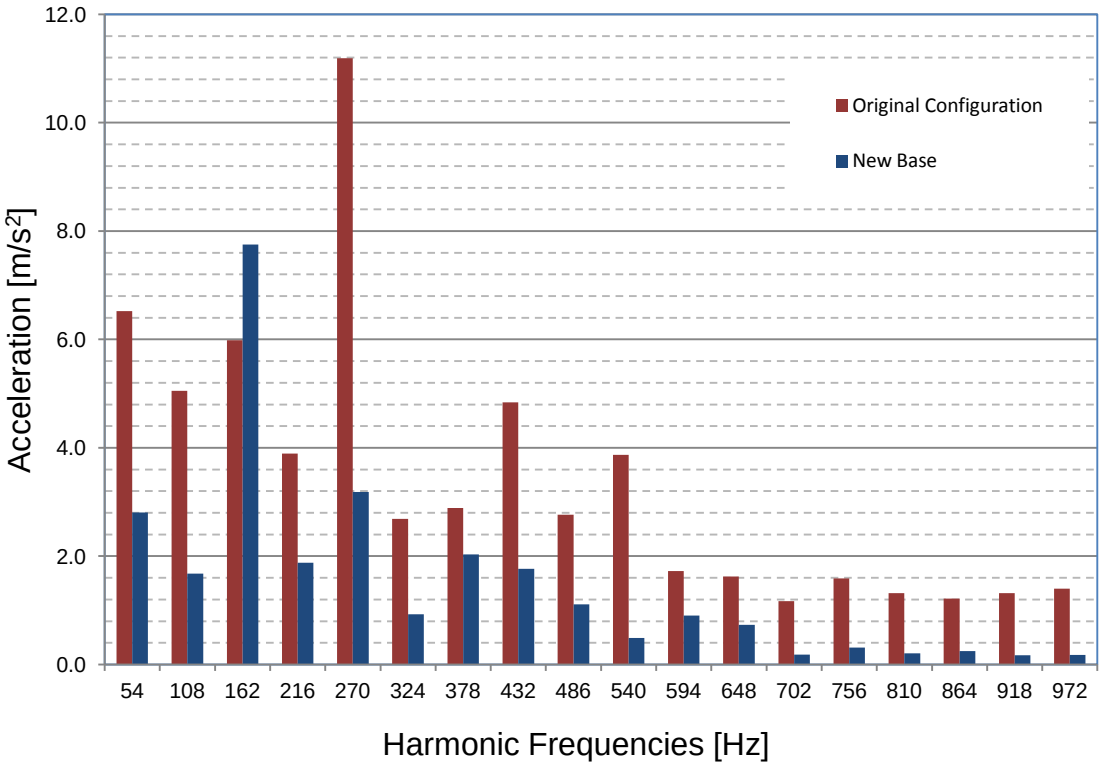

Figure B.11 Spectral plot showing comparison of frequency components for the two types of base (*extracted from Randle, 2011*)

Appendix C Rotating Assembly Unbalance

Background

The states of balance for the rotors of a decanting centrifuge are very important because the inner rotor cannot easily be accessed for trim correction in an assembled machine. The residual unbalance is the primary source of vibration generation. Taking measurements of the vibration at the main bearings gives only a snapshot of the machine condition as the vibration amplitude changes as a result of the differential speed of the inner and outer rotors. This leads to the cyclic variation in unbalance as detailed in Chapter 3. The two rotors each balanced separately and correctly to a specified grade in a balancing machine will, when assembled, result in an assembly that will periodically have high and low levels of residual unbalance.

As the running speed of rotating equipment increases then the force due to residual unbalance increases as the square of the increment – e.g. double the speed leads to four times the force. It was shown in Chapter 3 that where the residual unbalance was significant then the centrifugal force could equal or exceed the gravity force of the rotor mass at the bearing. Excitation by residual unbalance is one of the most common causes of vibration problems in industry and international standards exist to introduce control into the manufacturing cycle whereby the residual unbalance of rotating parts are able to be specified [56]. A range of machines for static and dynamic balancing of rotors is available and most include programs that enable balancing to the international standard limits. It would seem then that there would not be a problem with balancing of the two rotors of the centrifuge and this is true – to a degree. The bowl is able to be spun whilst resting (or being mounted) on the main journals and so able to be balanced as an assembly – see Figure C.1.

Figure C.1 Balancing a bowl assembly

However, for the conveyor the process is more difficult and comes about because in the assembled machine the conveyor runs on bearings that are mounted on journals that are parts of the hubs of the bowl assembly. Therefore in order to run the conveyor on its own, in a balancing machine, it must temporarily be fitted with mandrels as shown in Figure C.2.

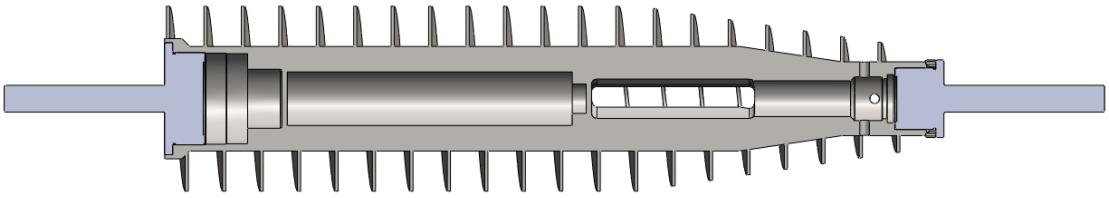

Figure C.1 Conveyor with balance mandrels fitted

Figure C.2 Conveyor in Schenk balancing machine

The mandrels themselves must be balanced – to a better degree than the balance quality required for the conveyor. It is also of vital importance that the axes of the mandrels are aligned and co-linear. The balance quality for different types of rotor is specified in international standards – see for example Table C.1, extracted from ISO 1940 [57], (which is also ANSI STD S2-19). However, some industries require better grades than those specified in Table C.1, even for the same components. For example, the oil and gas industry (API) and the military (MIL-STD) both use standards that have more precise limits [58].

Table C.1 Balance quality grades for different rigid rotor types

Balance Quality Grade	Rotor Description
G0.4	Disks, spindles and armatures of precision grinders. Gyroscopes.
G1	Small electrical armatures with special needs. Grinding machine drives. Tape recorder and phonograph drives.
G2.5	Steam and gas turbines, merchant main turbines, rigid turbo-generator rotors, turbo-compressors, machine-tool drives, large and medium electrical armatures with special needs, small electrical armatures, turbine driven pumps.
G6.3	Process plant machine parts, merchant marine main turbine gears, centrifuge drums, fans, aircraft gas turbine rotors, fly wheels, pump impellers, machine-tool and general machinery parts, normal electrical armatures, engine components under special needs
G16	Drives shafts with special needs, crushing machinery parts, agricultural machinery parts, car, locomotive and truck components, six or more cylinder engine crankshafts and drives with special needs, dredge or slurry pump impellers.

Centrifuge drums are listed in the G6.3 quality grade. However, it is generally recommended that the conveyor be balanced to G2.5 [28]. This is because it is so difficult to correct for imbalance once the machine is assembled. This still only partially helps the situation though since further imbalance results from machining run-out of the journals.

The specified balance quality grade is the product of the permissible residual unbalance and the rotational speed. For G6.3 this means that the total

permissible residual unbalances applied at the correction planes must add up to a maximum of 6.3 mm/s. The permissible unbalance is split between the correction planes in the ratio as determined by the positioning of the planes about the centre of gravity for the machine – see Figure C.3.

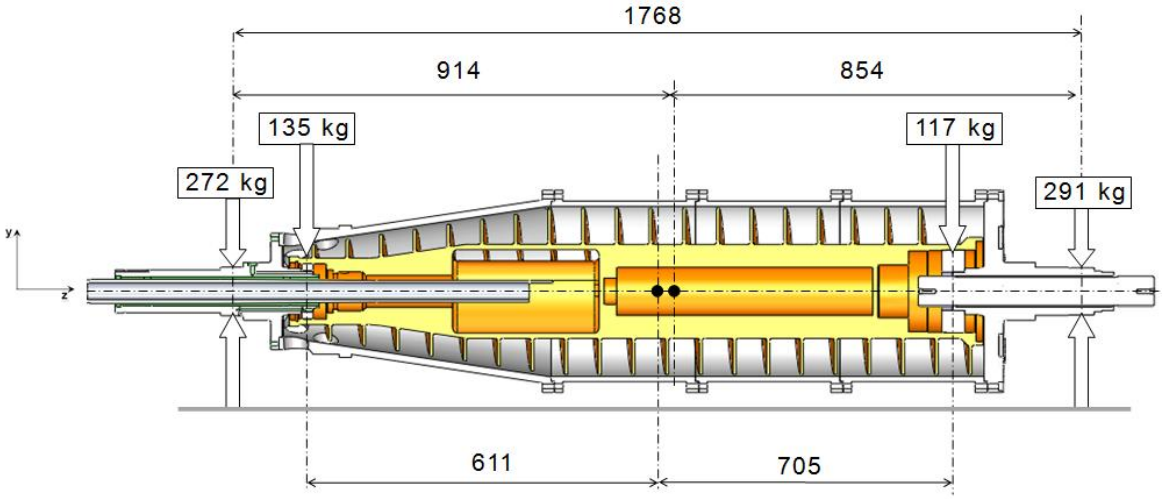

Figure C.3 Distribution of mass for the GTech1456 decanter centrifuge (Note: the main bearing loads include the mass of the conveyor)

The balance grade must be converted to a permissible level for each correction plane and expressed in terms of mass and radius. From [57], the permissible unbalance in gram.mm is given by:

$$U_{per} = 9549 * G * \left(\frac{W}{N}\right)$$

- 9549 = a constant
- W = the rotor weight (or the bearing's share) in kg
- N = the operating speed in rpm
- G = the balance quality grade, mm/s

The ISO standard includes a graphical representation of EQ-C.1, an extract of which is shown in Figure C.4, with the red lines showing the centrifuge selection at 3250 rpm. The graph shows that the total permissible residual unbalance is approximately 20 g.mm/kg, or 20 μm centre of gravity offset.

For the Liquid End this translates into (20*291) or 5820 g.mm and for the Solids End (20*272) or 5440 g.mm. The correction radius is of the order of 200mm and

so the mass unbalance will be of the order of 25 grams. Thus this would be easily achievable, since 25 grams is a significant weight (a piece of steel 25 mm x 25 mm x 5 mm) - except that the unbalance is now composed of the residual unbalances of the bowl and of the conveyor. Correcting only for the bowl at this stage will leave the conveyor uncorrected. If there is no unbalance introduced by the assembly (fits, alignments, run-outs) then the state of balance of the conveyor should be close to that obtained in the balancing machine.

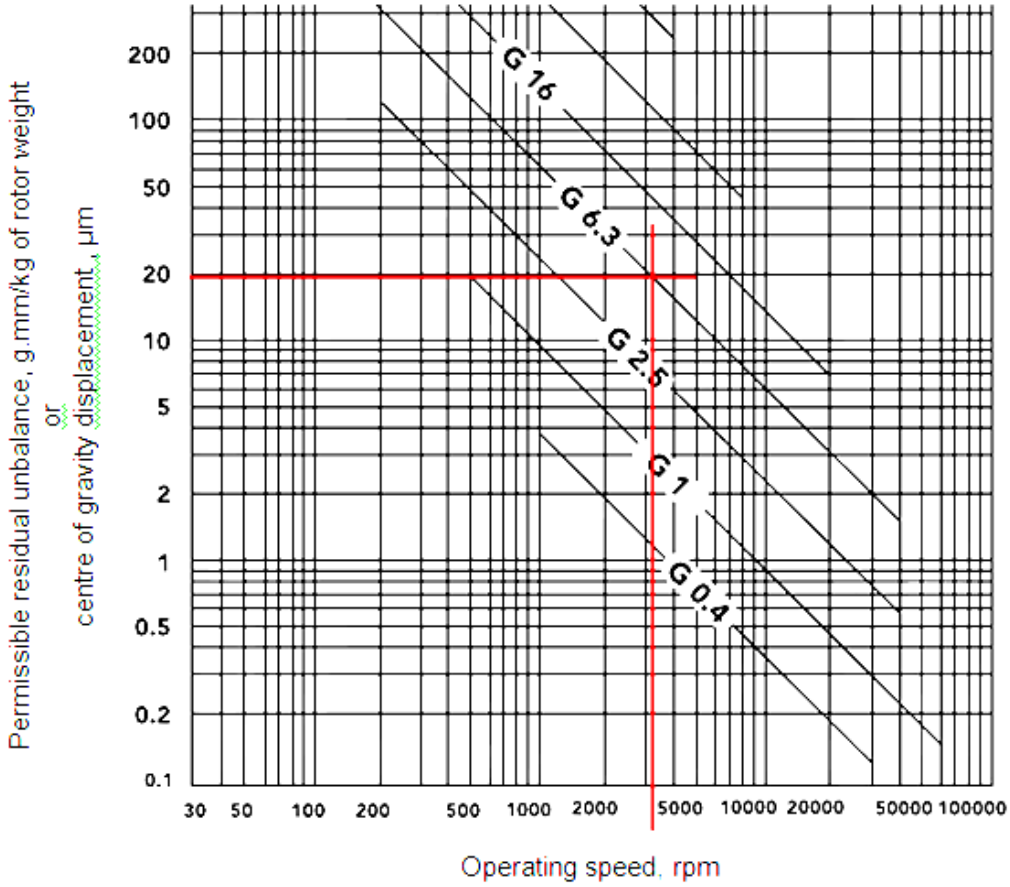

Figure C.4 Permissible Unbalance selection chart extract

Components of unbalance

The assembly contributors to imbalance include alignment, fits, mass inhomogenieties in castings, and machining tolerances and errors. The conveyor radial support at the liquid end hub is surface B in Figure C.5. Immediately we see that the concentricity of B relative to the rotation reference A is of paramount importance in defining the axis of rotation of the conveyor. The

position of that axis is further compromised by any lack of concentricity of surface C, which defines the position of the radial cylindrical roller bearing.

If we assume that the mass distributions of the conveyor and the bowl were symmetric about their respective axes then any unbalance would be due to the machining tolerances or errors. For example,

- radial run-out for the conveyor, C and D not being concentric
- run-out and deviation from squareness of the journal B, (surface F from surface B and B from A).
- radial run-out of the bowl, G and E not concentric

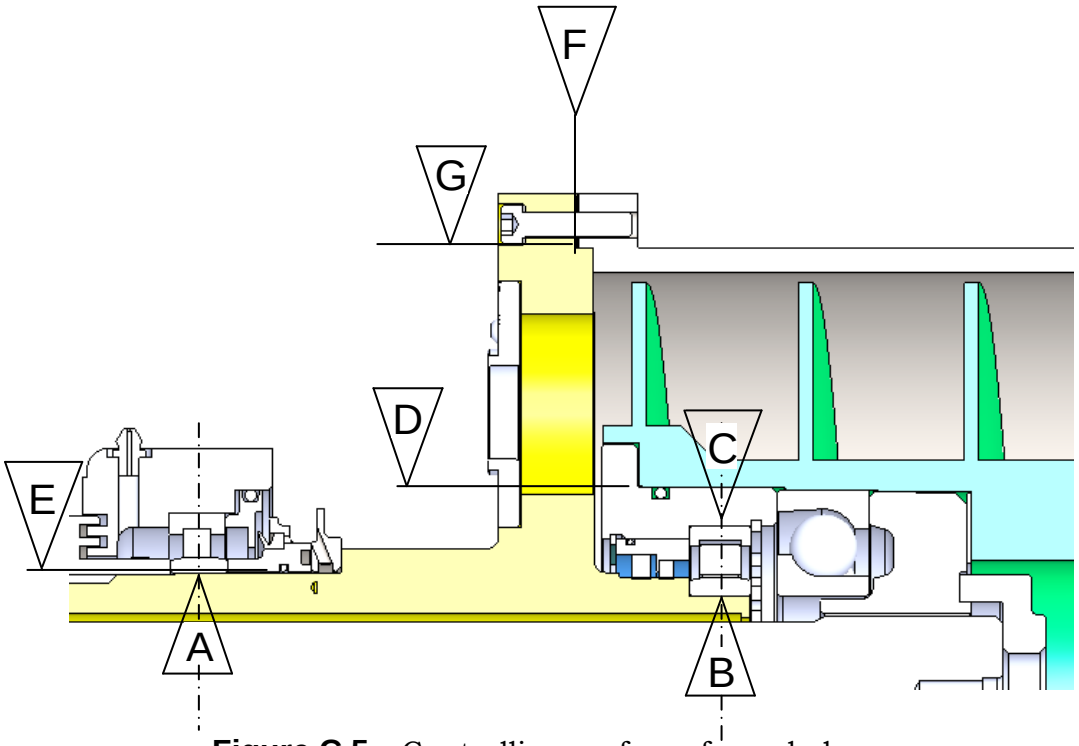

Figure C.5 Controlling surfaces for unbalance

Thus the tolerances of machining are important in defining the nominal state of balance for the assembled machine – prior to any corrective action. There can never be zero unbalance except by chance, as it is impossible to machine without error.

The situation for the conveyor is compounded by the presence of clearance in the radial rolling element bearing; this means that the axis of the conveyor and the axis about which the body rotates are not coincident. Therefore, however well the conveyor is balanced in a balancing machine, it will always be

unbalanced when assembled into the bowl assembly. The degree of unbalance will depend on both the bearing clearance and the bearing journal's run-out. Typical clearances for the conveyor bearings are:

- NU216 cylindrical roller – 65µm to 100µm
- NKI85 needle roller – 75µm to 110µm

These clearances show that the conveyor can move radially between 32µm and 55µm from a neutral position i.e. the axis of rotation. This state represents an unbalance between 8065 g.mm and 13860 g.mm; a centrifugal loading between 930N and 1600N (or roughly 35 to 65% of the rotor mass) is the result.

Separating the unbalances

Once the parts have been machine balanced and assembled then field balancing methods are used to carry out a trim balance. This usually involves modal or influence coefficient techniques derived from using test weights applied in turn to the correction planes of the bowl. This however does not correct for any unbalance of the conveyor.

A new method was developed to separate the conveyor and bowl unbalances since the phase and magnitude cannot simply be separated out from signals at the main bearings. This is because the two rotational frequencies are very close. Typically there might be 10 rpm difference and so the frequency difference is just 0.17 Hz. The combined unbalances can be expressed as:

$$\begin{aligned} U &= U_b + U_c \\ &= A_1 e^{(\omega_1 t + \theta_1)i} + A_2 e^{(\omega_2 t + \theta_2)i} \end{aligned}$$

where, U_b is the unbalance of the bowl, U_c is the unbalance of the conveyor, A_1 and A_2 are the magnitudes of the vibration of the rotating assembly at the bearing for the correction plane under consideration, ω_1 and ω_2 are the rotating speeds for the bowl and conveyor respectively with the phase angles being θ_1 and θ_2.

There is no dynamic balancing instrumentation available that will separate out the components of close frequency unbalances in a multi rotor assembly and whilst there are several estimation methods [59], they are unsuitable for

centrifuge balancing. This is mainly because separating the close frequencies requires long sampling times in order to capture at least one whole beat; this may be detrimental to the safety of the machine.

As shown in Chapter 2, the unbalances of the two rotors pass into and out of phase, creating a beat phenomenon that requires long measurement periods to visualize. Vibration instrumentation typically only takes snapshots of data. The method developed for this project is simple to carry out, but correcting the conveyor is still problematic since access to it is very difficult once it is assembled. Having said that, Zeng and Wang [60] advocate applying correction weights through the porting and whilst this would be difficult, it would be possible if the conveyor carried tapped holes into which correction weights could be fastened.

The method developed for this present study involves disconnecting the drive to the conveyor so that it is basically locked to the bowl. This is done in four steps so that the conveyor can be locked at 90º increments from some convenient reference point marked on the bowl. Four steps is the recommended minimum and more steps would allow a better resolution of the result - but requires more run time. At each step a run is made and the vibration is measured at the main bearings. The results are plotted as vibration amplitude versus locking position for the conveyor – refer Figure C.6. From the plot the cyclic nature of the unbalance response change is clear. The point of minimum vibration occurs where the conveyor unbalance is 180º out of phase with the bowl unbalance. Similarly, the point of maximum vibration occurs when the two unbalance components are in phase. The bowl unbalance is constant for all the test runs and so is given by the average value of the responses – in the example of Figure C.6, the bowl unbalance is 2.9 mm/s at the Solids End (SE) and 3.3 mm/s at the Liquid End (LE). The conveyor unbalances are half the ranges: 2.3mm/s at the SE and 2.5 mm/s at the LE. For this case the phase angles are close to 0º for the bowl component at the SE and 270º at the LE and these phase angles are measured relative to the convenience mark put on the bowl to register the position of locking.

Currently, the conveyor must be removed from the bowl to effect any balance correction and then reassembled in the same disposition relative to the bowl.

However, fixing points for correction weights could be included by a simple design change, allowing in-situ correction.

Attention must be paid as to whether the vibration signal is displayed as r.m.s. or peak as the calculated weight will be under estimated if using an r.m.s value.

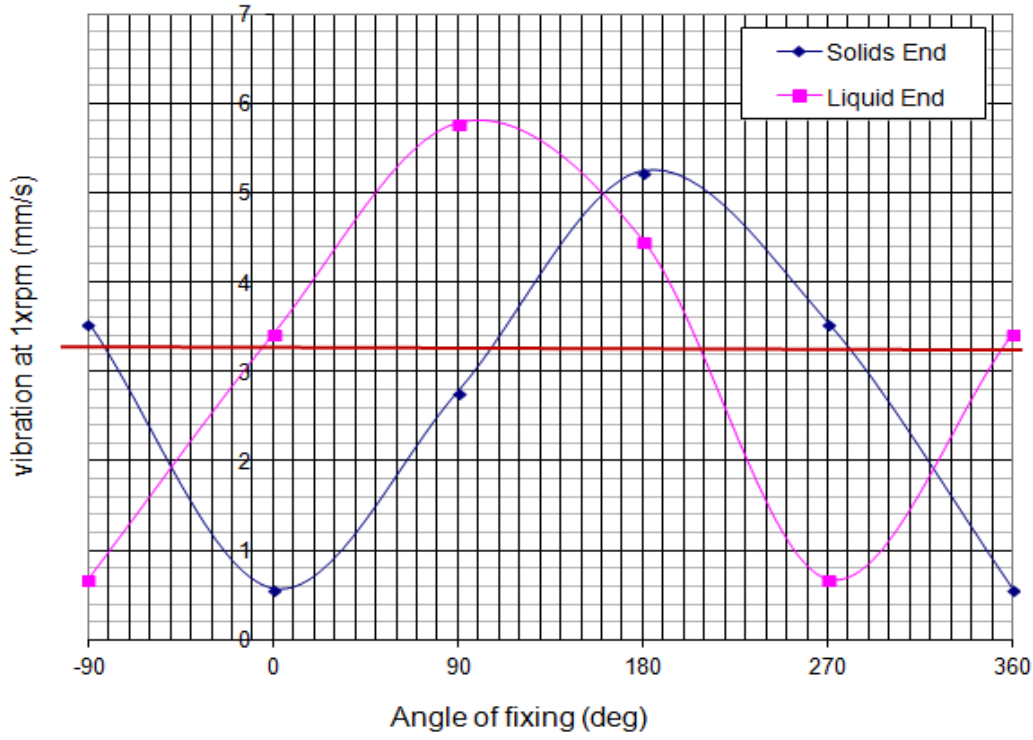

Figure C.6 Plot of unbalance response for 4 fixed positions of the conveyor

Test weight size

Considering just the bowl from the above example, the component of vibration velocity measured at the bearings is 2.9 mm/s for the solids end where the component of bowl mass is 137kg. If the vibration was measured as r.m.s. then it should be converted to the peak value, i.e. 4.1mm/s. Then, if we assume that all that vibration is at the bowl speed (or look at the FFT spectrum and take the magnitude of the 1x bowl speed component), the vibration acceleration is found by multiplying by the rotational frequency. In this example,

$$acceleration = \frac{4.1 * 3250 * 2\pi}{60}$$

i.e. the acceleration is 1.4 m/s^2.

The force generated by that acceleration is: 137kg x 1.4m/s^2, i.e.192 N

Taking a balance correction radius as 0.173m (from the conical section) then the mass required to null the vibration generated force is:

$$m = \frac{192 * 36E5}{0.173 * (3250 * 2\pi)^2} \text{ grams}$$

i.e. $m = 9.6$ gram

The process is repeated in a similar manner for the other corrections and then all the corrections should be applied together.

Appendix D Fortran Program for calculation of the bearing characteristics

The bearing solver was extracted from the finite element program DROROS (dynamic response of rotor systems), compiled by the writer in Fortran F77. The basic layout of the subroutine SRFBRG is shown in Figure D1.

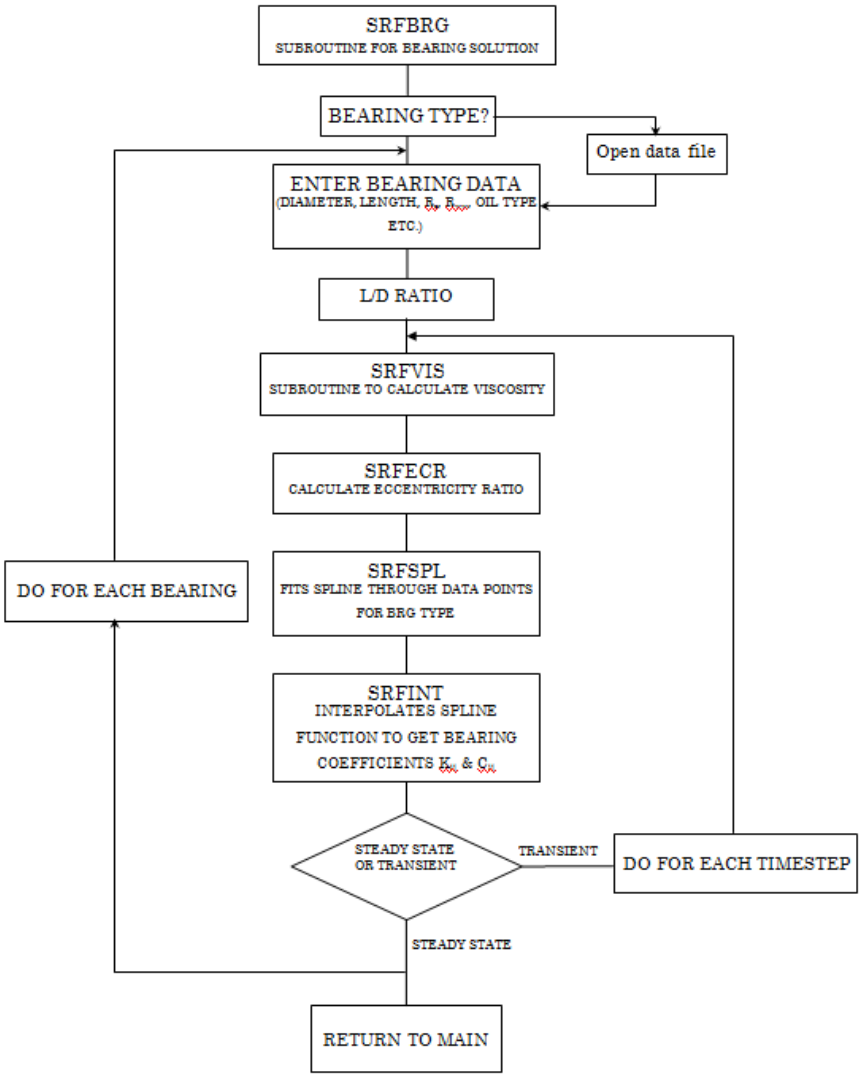

Figure D.1 Structure of subroutine SRFBRG

This program is not a full bearing solver but interpolates tabulated values from Someya [61] (that are finite difference solutions) based on input geometry data and lubricant dynamic viscosity.

The geometry of the bearing, clearance, and oil type are inputs with outputs as functions of the Sommerfeld number, $S = \frac{\mu NDL}{W}\left(\frac{R}{C}\right)^2$. The data output are:

ε – eccentricity ratio (eccentricity/clearance)

φ – attitude angle

Q_s, Q_e – non dimensional oil flow coefficients, for side and circumferential flows

f_J - journal friction coefficient

K_{ij} – stiffness coefficient

C_{ij} – damping coefficients

When the subroutine is included in the main program, the eccentricity (*e*) is derived from the rotor displacement at the bearing. For this study the routine was used to iterate the bearing temperature to get lubricant feed rate, eccentricity ratio and the coefficients. Based on this data a suitable circulating pump was sized and purchased.

Most rotor software programs use fixed averaged values for the stiffness and damping coefficients so that the analyses of transients can only be approximations that may be misleading if the bearing's characteristics change significantly with eccentricity.

Table D1 Dynamic characteristics of journal bearings – calculated data, [23]

S	cylindrical bearing with two axial grooves L:D=0.5												
	static characteristics					spring coefficients				damping coefficients			
	ε	ϕ	Qs	Qc	fJψ-1	Kxx	Kxy	Kyx	Kyy	Cxx	Cxy	Cyx	Cyy
5.96	0.075	82.600	0.066	1.000	111.500	1.770	13.600	13.100	2.720	27.200	2.060	2.060	14.900
4.43	0.100	80.400	0.088	0.999	83.000	1.750	10.300	9.660	2.700	20.600	2.080	2.080	11.400
2.07	0.200	71.600	0.170	0.999	39.500	1.880	5.630	4.410	2.560	11.200	2.220	2.220	6.430
1.24	0.300	64.100	0.243	0.997	24.400	2.070	4.270	2.560	2.340	8.500	2.320	2.320	4.730
0.798	0.400	57.500	0.309	0.986	16.400	2.390	3.750	1.570	2.170	7.320	2.240	2.240	3.500
0.517	0.500	51.100	0.366	0.967	11.300	2.890	3.570	0.924	2.030	6.810	2.100	2.100	2.600
0.323	0.600	44.700	0.416	0.939	7.750	3.650	3.620	0.427	1.920	6.810	2.080	2.080	2.060
0.187	0.700	38.200	0.459	0.900	5.130	4.920	3.880	0.235	1.830	7.320	2.160	2.160	1.700
0.135	0.750	34.900	0.478	0.875	4.070	5.900	4.110	0.258	1.800	7.650	2.100	2.100	1.460
0.0926	0.800	31.200	0.496	0.846	3.130	7.350	4.460	0.527	1.780	8.170	2.050	2.050	1.240
0.0582	0.850	27.200	0.510	0.806	2.300	9.560	4.920	0.805	1.730	9.120	2.060	2.060	1.060
0.0315	0.900	22.700	0.524	0.758	1.560	13.800	5.760	1.240	1.720	10.600	2.030	2.030	0.846
0.00499	0.975	12.500	0.543	0.663	0.543	43.300	9.610	4.260	1.990	22.400	2.930	2.930	0.637

Listing

```
PROGRAM BRG
!       TESTED ON 23 SEPT 2010 - OK
REAL SOM, IEPS, IPHI, IQS, IQE, IFRIC
REAL ISTXX, ISTXY, ISTYX, ISTYY, IDMXX, IDMXY, IDMYX, IDMYY
CALL BEARING(SOM, IEPS, IPHI, IQS, IQE, IFRIC, ISTXX, ISTXY, ISTYX, ISTYY, &
        IDMXX, IDMXY, IDMYX, IDMYY)
PRINT*,SOM
PRINT*,IEPS
PRINT*,IPHI
PRINT*,ISTXX, ISTXY, ISTYX, ISTYY
PRINT*,IDMXX, IDMXY, IDMYX, IDMYY
STOP
END
!
!-----------------------------------------------------------------------
SUBROUTINE BEARING (SOM, IEPS, IPHI, IQS, IQE, IFRIC, &
        ISTXX, ISTXY, ISTYX, ISTYY, IDMXX, IDMXY, IDMYX, IDMYY)
!       computes the Sommerfeld duty parameter for the given speed and
!       oil type, and calls an interpolating routine to determine the
!       eccentricity ratio and the eight oil-film force coefficients.
!       A cubic spline function is first fitted to tabulated data from
!       Someya before interpolating
!
CHARACTER BTYPE*5
PARAMETER (PI=3.141592654)
INTEGER NSOM, OT
REAL LDR, PLOAD, TSNUM(20), TEPS(20), TPHI(20), TQS(20), TQE(20), TFRIC(20), &
        TSTXX(20),TSTXY(20), TSTYX(20), TSTYY(20),TDMXX(20), &
        TDMXY(20), TDMYX(20), TDMYY(20)
REAL YP1(20), YP2(20), EPS2(20), SOM, PHI2(20), QS2(20), QE2(20), FRIC2(20), STXX2(20),STXY2(20),
STYX2(20)
REAL STYY2(20), DMXX2(20), DMXY2(20), DMYX2(20), DMYY2(20), &
        IEPS, IPHI, IQS, IQE, IFRIC
REAL ISTXX, ISTXY, ISTYX, ISTYY, IDMXX, IDMXY, IDMYX, IDMYY
REAL OMEGA2, DIA, CP, TMPIN, RW, PFEED, GLENGTH, AVEL, ATMP, TMP
!-----------------------------------------------------------------------
CALL BRGDAT(BTYPE, LDR, PLOAD, NSOM, TSNUM, TEPS, TPHI, TQS, &
        TQE, TFRIC, TSTXX, TSTXY, TSTYX, TSTYY, TDMXX, TDMXY, TDMYX, TDMYY)
CALL INPUT(BTYPE, DIA, CP, OT, TMPIN, OMEGA2, RW, PFEED, GLENGTH, &
        AVEL, ATMP, TMP)
!       Determine coefficients of 3rd order spline through tabulated values
CALL SPLINE(TSNUM, TEPS, NSOM, 2.E30, 2.E30, EPS2)
CALL SPLINE(TSNUM, TPHI, NSOM, YP1, YP2, PHI2)
CALL SPLINE(TSNUM, TQS, NSOM, YP1, YP2, QS2)
CALL SPLINE(TSNUM, TQE, NSOM, YP1, YP2, QE2)
CALL SPLINE(TSNUM, TFRIC, NSOM, YP1, YP2, FRIC2)
CALL SPLINE(TSNUM, TSTXX, NSOM, YP1, YP2, STXX2)
CALL SPLINE(TSNUM, TSTXY, NSOM, YP1, YP2, STXY2)
CALL SPLINE(TSNUM, TSTYX, NSOM, YP1, YP2, STYX2)
CALL SPLINE(TSNUM, TSTYY, NSOM, YP1, YP2, STYY2)
CALL SPLINE(TSNUM, TDMXX, NSOM, YP1, YP2, DMXX2)
CALL SPLINE(TSNUM, TDMXY, NSOM, YP1, YP2, DMXY2)
CALL SPLINE(TSNUM, TDMYX, NSOM, YP1, YP2, DMYX2)
CALL SPLINE(TSNUM, TDMYY, NSOM, YP1, YP2, DMYY2)
!       determine viscosity and calc the Sommerfeld Number
```

```
CALL VISC(OT, TMP, VIS, ODENS, OHEAT)
SOM=(VIS*OMEGA2*2*PI*DIA*GLENGTH/(60*RW))*(DIA/2*CP)**2
!          interpolate the tabulated values for the discrete Sommerfeld Number
CALL SPLINT(TSNUM, TEPS, EPS2, NSOM, SOM, IEPS)
CALL SPLINT(TSNUM, TPHI, PHI2, NSOM, SOM, IPHI)
CALL SPLINT(TSNUM, TQS, QS2, NSOM, SOM, IQS)
CALL SPLINT(TSNUM, TQE, QE2, NSOM, SOM, IQE)
CALL SPLINT(TSNUM, TFRIC, FRIC2, NSOM, SOM, IFRIC)
CALL SPLINT(TSNUM, TSTXX, STXX2, NSOM, SOM, ISTXX)
CALL SPLINT(TSNUM, TSTXY, STXY2, NSOM, SOM, ISTXY)
CALL SPLINT(TSNUM, TSTYX, STYX2, NSOM, SOM, ISTYX)
CALL SPLINT(TSNUM, TSTYY, STYY2, NSOM, SOM, ISTYY)
CALL SPLINT(TSNUM, TDMXX, DMXX2, NSOM, SOM, IDMXX)
CALL SPLINT(TSNUM, TDMXY, DMXY2, NSOM, SOM, IDMXY)
CALL SPLINT(TSNUM, TDMYX, DMYX2, NSOM, SOM, IDMYX)
CALL SPLINT(TSNUM, TDMYY, DMYY2, NSOM, SOM, IDMYY)
RETURN
END
!
!-------------------------------------------------------------------------------
SUBROUTINE BRGDAT (BTYPE, LDR, PLOAD, NSOM, TSNUM, TEPS, TPHI, TQS, &
          TQE, TFRIC, TSTXX, TSTXY, TSTYX, TSTYY, TDMXX, TDMXY, TDMYX, TDMYY)
!
!          routine to read the bearing data from user disc file
!-------------------------------------------------------------------------------
CHARACTER BTYPE*5
INTEGER NSOM
REAL TSNUM(20),TEPS(20),TPHI(20), TQS(20), TQE(20), TFRIC(20), TSTXX(20), &
          TSTXY(20), TSTYX(20), TSTYY(20),TDMXX(20), TDMXY(20), TDMYX(20), TDMYY(20)
REAL LDR, PLOAD
OPEN(9,STATUS='OLD', FILE='BEARING.DAT')
!          READ DATA
READ(9,*) BTYPE
READ(9,*) LDR
READ(9,*) PLOAD
READ(9,*) NSOM
DO I=1,NSOM
          READ(9,*)TSNUM(I), TEPS(I), TPHI(I), TQS(I), TQE(I), TFRIC(I), TSTXX(I), &
          TSTXY(I), TSTYX(I), TSTYY(I), TDMXX(I), TDMXY(I), TDMYX(I), TDMYY(I)
END DO
CLOSE (9)
RETURN
END
!-------------------------------------------------------------------------------
SUBROUTINE INPUT(BTYPE, DIA, CP, OT, TMPIN, OMEGA2, RW, PFEED, GLENGTH, &
          AVEL, ATMP, TMP)
!          READ DATA FROM INPUT.DAT
CHARACTER BTYPE*5
PARAMETER (PI=3.141592654)
INTEGER OT
REAL DIA, CP, TMPIN, OMEGA, RW, PFEED, GLENGTH, AVEL, ATMP, TMP
OPEN(1, STATUS = 'OLD', FILE='INPUT.DAT')
READ(1,*)BTYPE
READ(1,*)DIA, CP, OT, TMPIN, OMEGA, RW, PFEED, GLENGTH, AVEL, ATMP, TMP
CLOSE(1)
OMEGA2=OMEGA*2*PI/60
RETURN
END
```

```
!-------------------------------------------------------------------------------------
SUBROUTINE SPLINE(X,Y,N,YP1,YPN,Y2)
INTEGER N, NMAX
REAL YP1, YPN, X(N), Y(N), Y2(N)
PARAMETER (NMAX=50)
!       Given arrays x(1:n) and y(1:n) containing a tabulated function, i.e. Yi=f(x),
!       with x1<x2<....<xN, and given values YP1 and YPN for the first derivative of the ! interpolating
function at points 1 and N respectively, this routine returns an
!       array y2(1:N) of length  N which contains the second derivatives of the
!       interpolating function at the tabulated    points xi.  If YP1 and/or YPN are
!       equal to 1x10^30 or larger, the routine is signalled to set the corresponding
!       boundary condition for a natural spline, with zero second derivative on that
!       boundary.  Parameter:NMax is the largest expected value of N.
INTEGER i, k
REAL P,QN, SIG, UN, U(NMAX)
IF (YP1.GT..99e30)THEN
        Y2(1) = 0.
        U(1) = 0.
ELSE
        y2(1) = -0.5
        u(1) = (3./(x(2)-x(1)))*((y(2)-y(1))/(x(2)-x(1))-yp1)
END IF
DO 11 i=2, N-1
        SIG = (x(i)-x(i-1))/(x(i+1)-x(i-1))
        P = SIG*Y2(i-1)+2
        Y2(i) = (SIG-1.)/P
U(i) = (6.*((Y(i+1)-Y(i))/(X(i+1)-X(i))-(Y(i)-Y(i-1))/(X(i)-X(i-1)))/(X(i+1)-X(i-1))-SIG*U(i-1))/P
11 END DO
IF (YPN.GT..99E30)THEN
QN = 0.
UN = 0.
ELSE
QN = 0.5
QN = (3./(X(N)-X(N-1)))*(YPN-(Y(N)-Y(N-1))/(X(N)-X(N-1)))
END IF
        Y2(N) = (UN-QN*U(N-1))/(QN*Y2(N-1)+1.)
DO 12 k=N-1, 1,-1
        Y2(k) = Y2(k)*Y2(k+1)+U(k)
12 END DO
RETURN
END
!
!-------------------------------------------------------------------------------------
SUBROUTINE SPLINT(xa, ya, y2a, N, x, y)
INTEGER N
REAL x, y, xa(N), y2a(N), ya(N)
INTEGER k, khi, klo
REAL a, b, h
        klo=1
        khi=N
1       IF(khi-klo.GT.1)THEN
        k = (khi+klo)/2
                IF(xa(k).gt.x) THEN
                khi = k
                ELSE
                klo = k
                END IF
        GOTO 1
```

```
END IF
h = xa(khi)-xa(klo)
IF(h.eq.0) pause 'bad xa input in splint'
a=(xa(khi)-x)/h
b=(x-xa(klo))/h
y=a*ya(klo)+b*ya(khi)+((a**3-a)*y2a(klo)+(b**3-b)*y2a(khi))*(h**2)/6.
RETURN
END
!-------------------------------------------------------------------------------------
!
SUBROUTINE VISC(OT, TMP, VIS, ODENS, OHEAT)
!       this routine returns the value of oil viscosity for the film
!       operating temperature (TMP), degC, and oil type (OT), C and N are constants
!       see Fuller 1956, Theory and Practice of Lubricaton for Engineers
!
REAL TMP, VIS, ODENS, OHETA, N, C, T
INTEGER OT
IF(OT.EQ.1)THEN
        C = 10.51149252
        N = -3.78437522
ELSE IF(OT.EQ.2)THEN
        C = 10.29448279
        N = -3.673593294
ELSE IF(OT.EQ.3)THEN
        C = 10.2125765
        N = -3.615466856
ELSE IF(OT.EQ.4)THEN
        C = 10.01085103
        N = -3.528224427
ELSE IF(OT.EQ.5)THEN
        C = 9.940544906
        N = -3.491387949
ELSE IF(OT.EQ.6)THEN
        C = 10.06435601
        N = -3.521275375
END IF
ODENS = 875.0
OHEAT = 2000.0
T = TMP*1.8+491.67
VIS = (10**(10**(N*ALOG10(T)+C))-0.8)*ODENS*1E-6
RETURN
END
```

Appendix E Rotor dynamics in ANSYS

This appendix has been included to show how to insert bearings into a solid model in ANSYS Workbench and highlights other features that are difficult to implement. Rotor dynamics analysis in ANSYS Workbench is not straightforward and although there is extensive documentation for the Mechanical APDL Classic module of ANSYS there is nothing for Workbench. The "help" tab in Workbench is linked to Mechanical APDL and many of the features available in APDL are accessible to Workbench users by adding command snippets. These snippets are APDL code inserted where appropriate and some can be copied from the examples included in the Mechanical APDL manual. It is not clear how ANSYS adapts the snippet commands that are written for beam type elements when the model has been prepared in a CAD package. For example, the COMBIN214 bearing element is basically a 2-node linear spring element (or 3-node for non-linear problems) but can be "mapped" to a bearing journal area on the solid model.

The rotor dynamics solution process using ANSYS software is outlined in Figure E.1 and Figure E.2. With the introduction of the Work Bench GUI, importing complex models into ANSYS has been made straightforward. However the latest ANSYS manual on rotor dynamics is version 12.0, 2009, where this study used Workbench version 14.5, 2012.

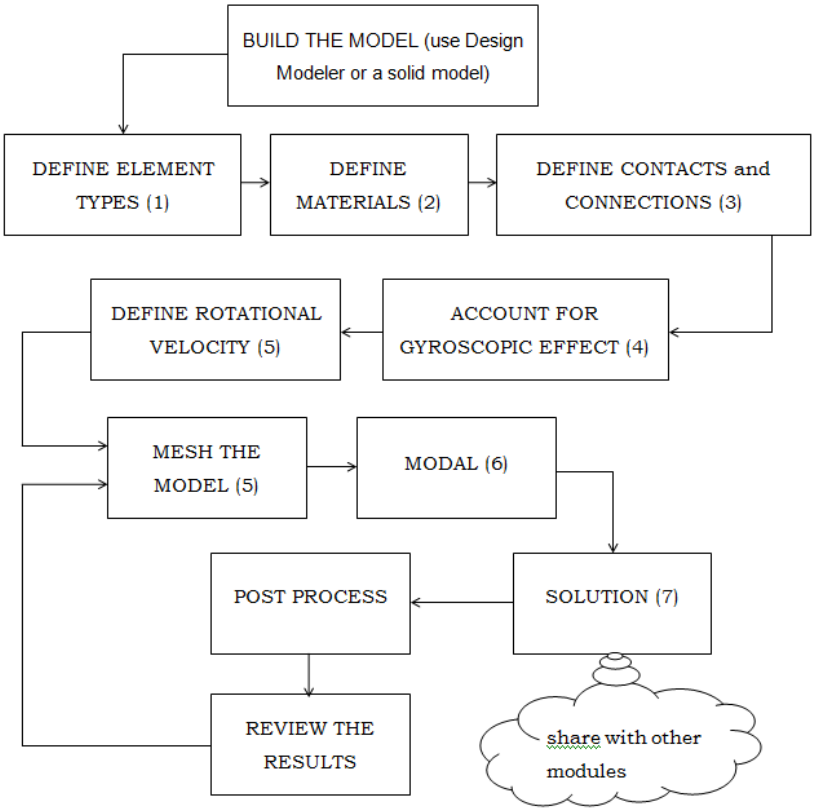

Figure E.1 Solution process for a rotor dynamic problem

NOTES:

1. Element can be program selected or can be altered by APDL command snippet in the MODAL module
2. Material type is imported with the model or defined using APDL command snippet
3. Bearings are only body to ground, body to body bearings connections are made as joints (bushings) unless in an assembly
4. The Coriolis component is included in the damping matrix, so a damped solution must be selected. The QRDAMP (reduced) eigen-solver must be used if the modal study is to be followed by an harmonic analysis.
5. Size control and face mapping are required for bearing surfaces to ensure nodes lie in the plane of the bearing centre
6. Ensure correct use of Rotational Velocity, Analysis Settings and entry of any APDL commands in this module.
7. A Campbell Diagram can be selected from the drop down menu

Figure E.2 Notes to be read in conjunction with Figure E.1

One example that is problematic is the insertion of unbalance forces for a harmonic analysis. Applying an unbalance force at a node cannot be done simply in Work Bench as node numbers do not appear to be able to be displayed. In APDL code the unbalance is inserted as:

```
f0 = [unbalance]        ! kgm
INODE = node(  )
f, INODE, fy, f0        !real component
f, INODE, fz,,-f0       !imaginary component
finish
```

INODE is the node number at which the unbalance is to be applied. Whilst this node is readily identified in code where the model is generated in APDL, this node number cannot be directly determined from Work Bench. Two options are:

- Open the model in Design Modeler and generate additional points and save as *named selections*. Those named selections are then used in Work Bench as the nodal positions at which to apply the unbalance f0.
- Alternatively small patches where unbalances are to be applied can be constructed on the solid model and then turned into named selections in Work Bench – Figure E.3.

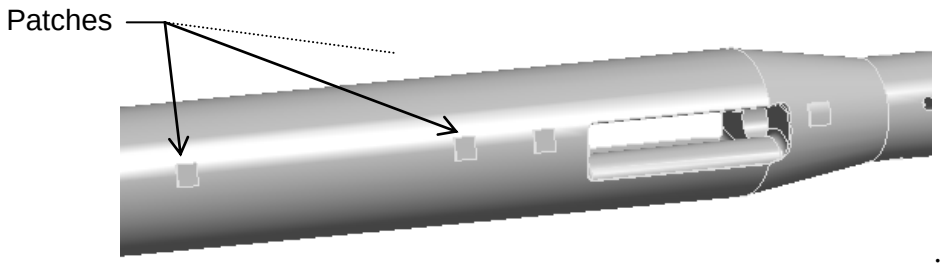

Figure E.3 Model altered to include patches for application of unbalance forces

ANSYS constructs the equations of motion from the input data (the model) and assembles the mass, stiffness and damping matrices using additional data input via the Work Bench GUI. In the simplest case the system equations are solved to obtain the static modal response. That is, the response without rotational effects such as gyroscopics and unbalance.

The modal response depends upon the way the rotor is supported and so bearing connections are added with appropriate stiffness and damping

characteristics to obtain a Campbell diagram. The Campbell diagram plots the critical speeds against rotor speed – Figure E.4. A critical speed map can also be plotted to show the effect on modal frequency of varying the bearing stiffness using the macro *CRITSPEEDMAP.MAC* .

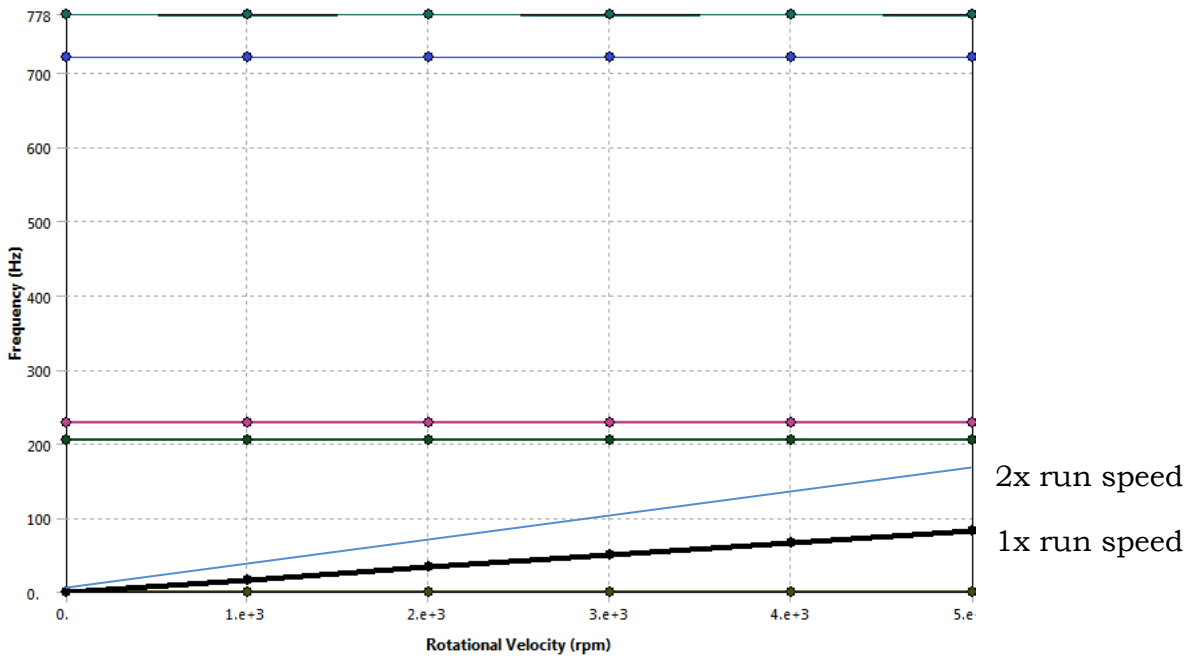

Figure E.4 Campbell diagram for the conveyor model on flexible bearings

The Campbell and critical speed plots give an insight into the range of operating speeds for which a problem might be expected. Radial lines for run speed and its harmonics are plotted on the Campbell diagram see Figure E.4, and if they intersect with a critical speed line then a resonance will occur. For the example shown a problem is not evident. However, for lower bearing stiffness the first mode frequency falls to a lower value and resonance is possible.

Since the critical speeds change with bearing stiffness then a table of the bearing's characteristics must be inserted as APDL script. A macro is available that enables importing tabular data – *IMPORTBEARING1.MAC*.

The rotating system can be considered as composed of two rigid rotors and so the rotors were first analyzed as separate systems to assess the effects of different bearing stiffnesses on each of their responses. The individual rotor models are meshed and modal studies carried out to obtain the free-free responses, refining the meshes as required to obtain consistent results. When

mounted in bearings the lowest modal frequencies will be much lower than for the free-free case – as shown in a typical critical speed map (Chapter 4), and so the model must be extended to study the effects of the bearings.

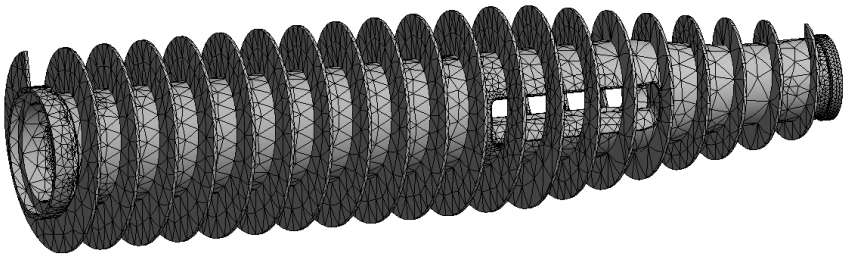

Figure E.5 Meshed model of the complete conveyor

Solid Works models for the conveyor with and without flights were prepared for the study. Laboratory tests and a structural FEA indicated that the flights did not contribute in any significant way to flexural strength of the conveyor and so they were omitted from later models – Figure E.5 and E.6. The mass of the flights cannot be ignored as it constitutes about 20% of the conveyor's finished weight and so the density of the material used in the FEA modeling process was increased appropriately.

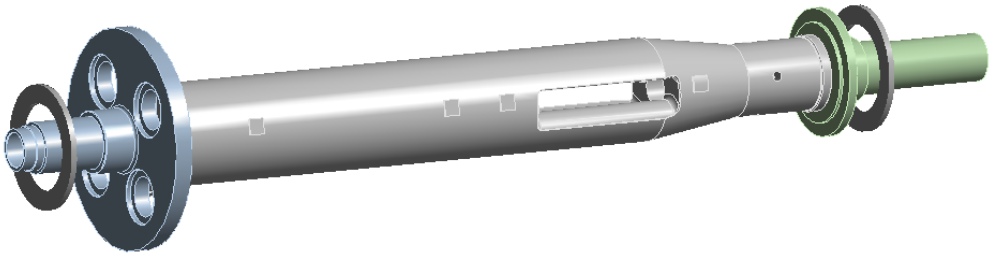

Figure E.6 Conveyor with flights removed and mounted on the liquid and solids end hubs

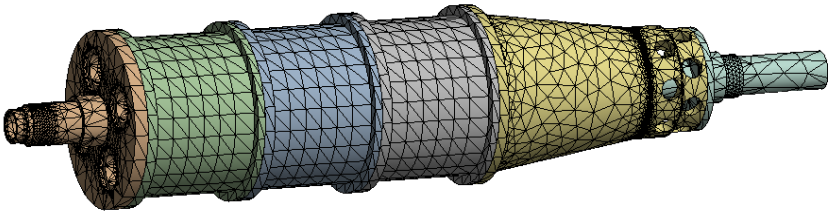

(a)

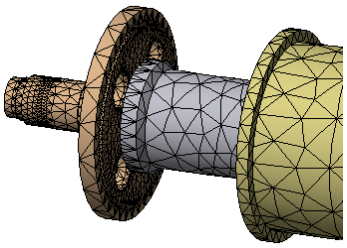

(b)

Figure E.7 Meshed model of the bowl assembly, (a) complete assembly (b) bowl section hidden to show part of meshed conveyor

ANSYS Work Bench automatically assigns element types according to the type of study and the geometry, but element type can still be specified by insertion of a command snippet if elements with particular characteristics are required. For example, not all element types can be used to model gyroscopic effects.

The insertion of bearings into the solution introduced some issues as the element type depends on whether the bearing is body to ground, as shown for the main bearings in Figures E.10 and E.11, or body to body, e.g. conveyor to bowl Figures E.12 and E1.3. In the latter case, the bearings are added as bushings under the joints tab see FigureE.12. Mention of this is made here as this is not covered in the ANSYS user manual or in the Rotor Dynamics Guide. The main rotor bearings (body to ground) are listed as bearings in the connections tab and ANSYS automatically assigns element type COMBIN214 to the selected face. This element is a 2D element of springs and dampers with inclusion of cross coupling. It is suggested that the bearing area has a *sized mesh* to allow ANSYS to select the mid nodes – i.e. the bearing surface mesh must be multiples of two elements wide.

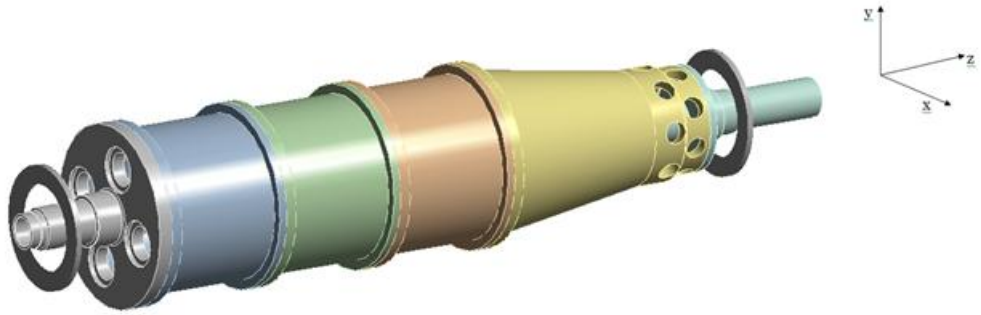

Figure E.8 The bowl assembly model with symbolic bearings

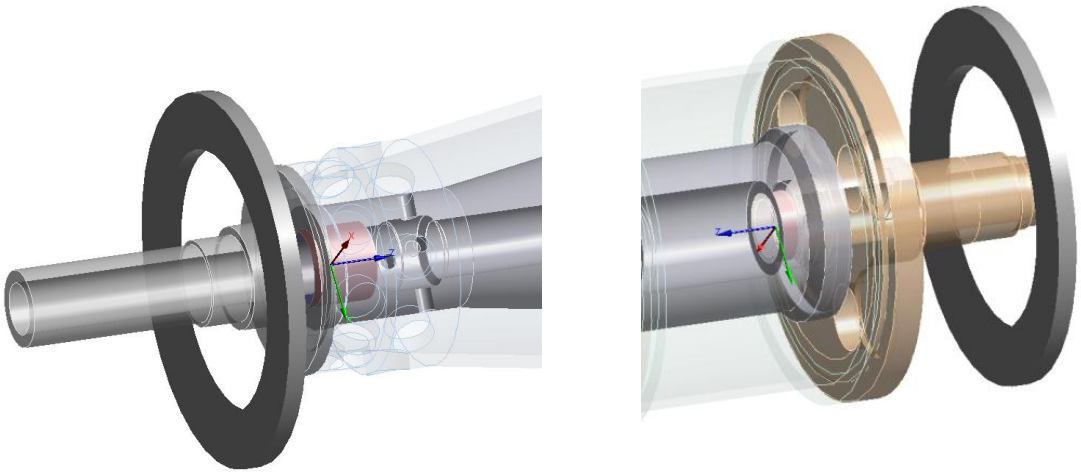

(a) (b)

Figure E.9 ANSYS symbolic representations for bearings (a) solids end, (b) liquid end. Note the difference between the representations of the internal MPC187 element and the external element COMBIN214

For the body to ground type bearing, the mains, the selection is made under the connections tab, insert/bearing, as shown in Figure E.10.

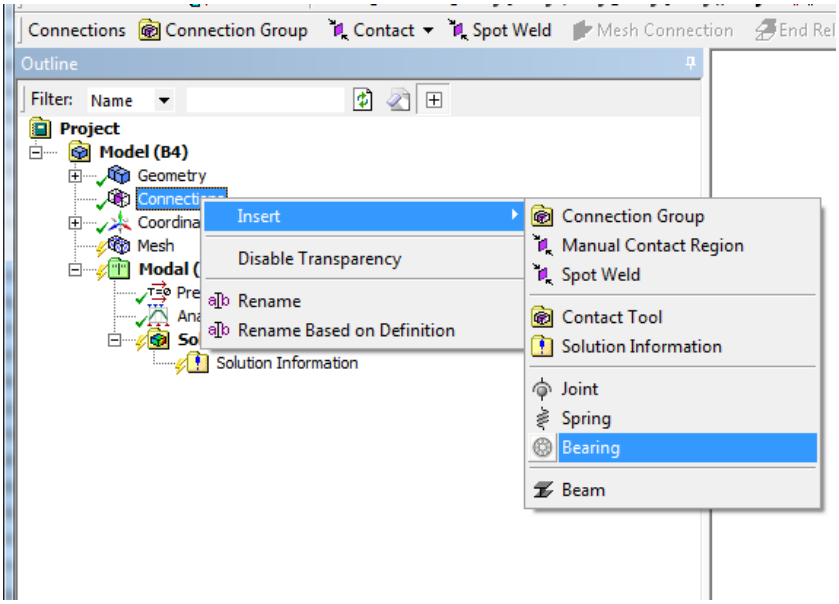

Figure E.10 Bearing selection

The Details tab drops down (Figure E.11) for entry of the face of the model where the bearing is located (Scope) and the stiffness and damping values. In APDL code the bearing is located at a node or pair of nodes – in Workbench a face is selected and the associated nodes are assigned by the program.

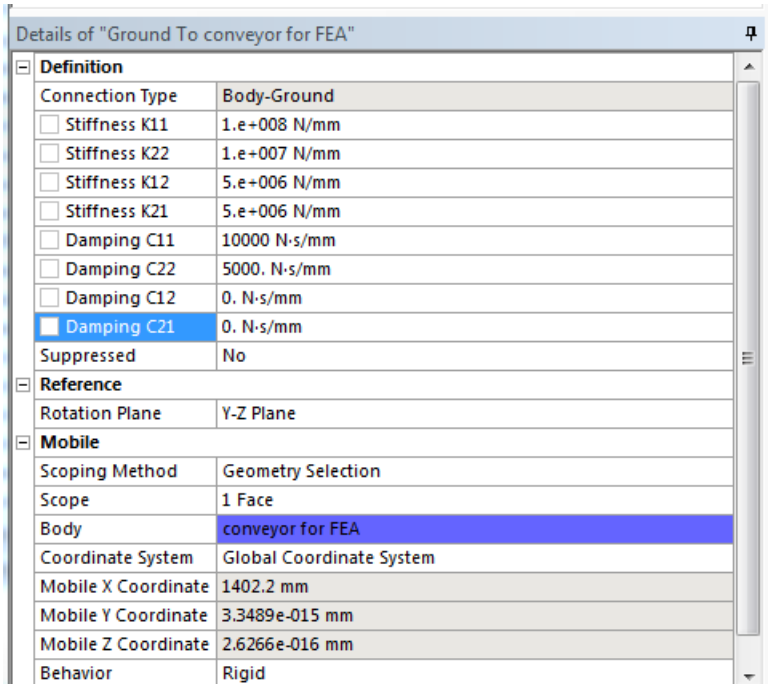

Figure E.11 Details tab for insertion of bearing parameters

For the body to body connection the bearing option is not available (it cannot be changed from “body to ground” and the joint option must be used – Figure E.12.

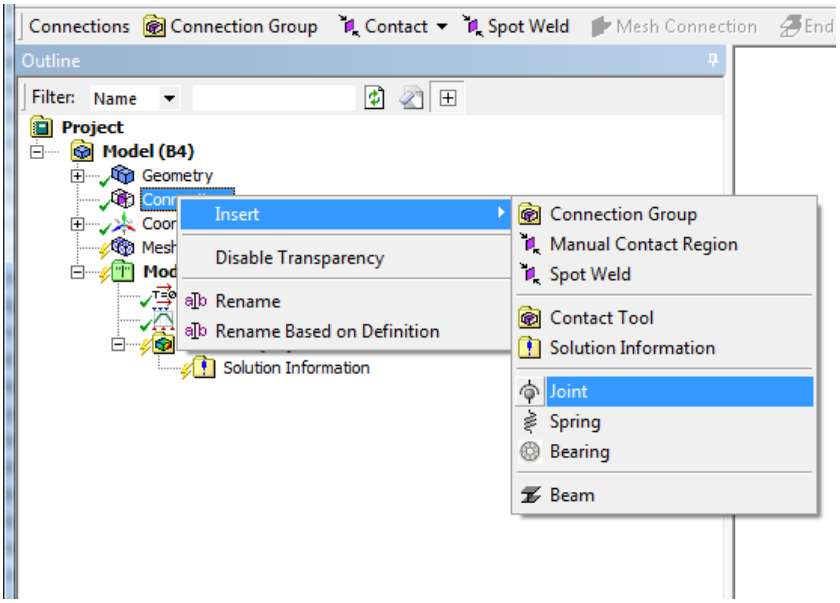

Figure E.12 Selection of the joint option for body to body connection

In the associated drop down Details tab the type of joint is selected as a “bushing” along with the entry of the face where the bearing is located. Once “bushing” is selected, a new Worksheet opens with a table where the bearing (joint) parameters are entered.

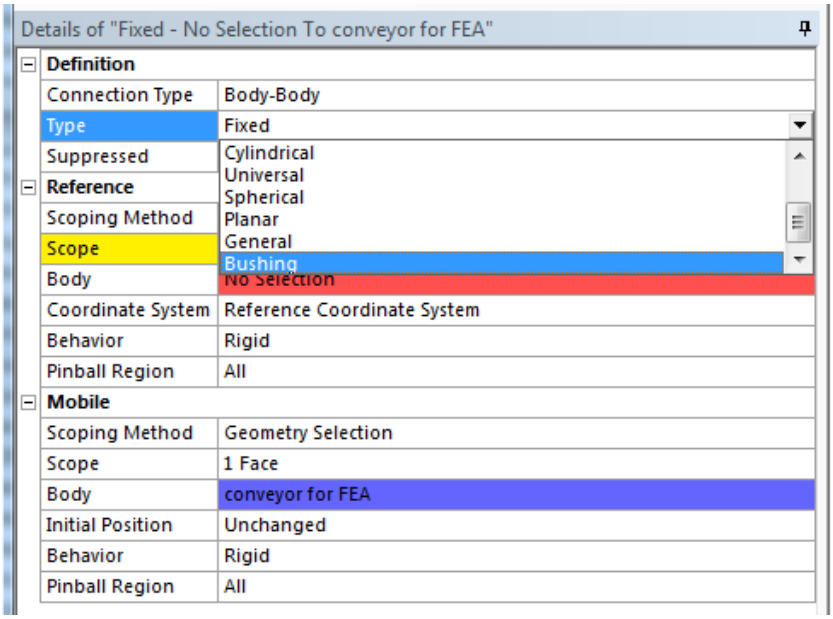

Figure E.13 Selection tab for joint type

The general approach in published works is to model the Jeffcott and offset Jeffcott rotors in order to demonstrate the effects of say, damping, speed, and

out of balance. ANSYS includes verification models to enable checking one's processing - such as meshing, in order to gain confidence in the procedure and the results of analyses before proceeding to more complex models. Figure E.14 shows a simple rotor used to gain an understanding of the function of the joint bushing.

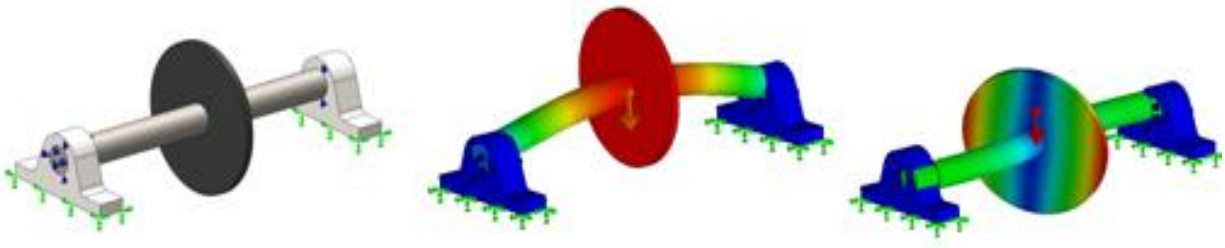

Figure E.14 Jeffcot rotor on bush type bearings, with first and second modes

Appendix F Drawings

The following drawings are pdf documents exported from Solid Works. The parts were all machined by Bellmor Engineering Ltd., Christchurch.

207-02 Wear ring – Solids End

208-02 Inner thrust ring

209-02 Bearing – Solids End

210-02 Seal cover

211-02 Bearing housing – Solids End

212-02 Mods to 17625 (main-drive spacer)

213-02 Modified solids end bearing

214-02 Bearing – Liquid End

215-02 Inner wear ring – Liquid End

216-02 Modified liquid end bearing

217-02 Dowel

218-02 Bearing housing – Liquid End

219-02 Modification to gearbox flange

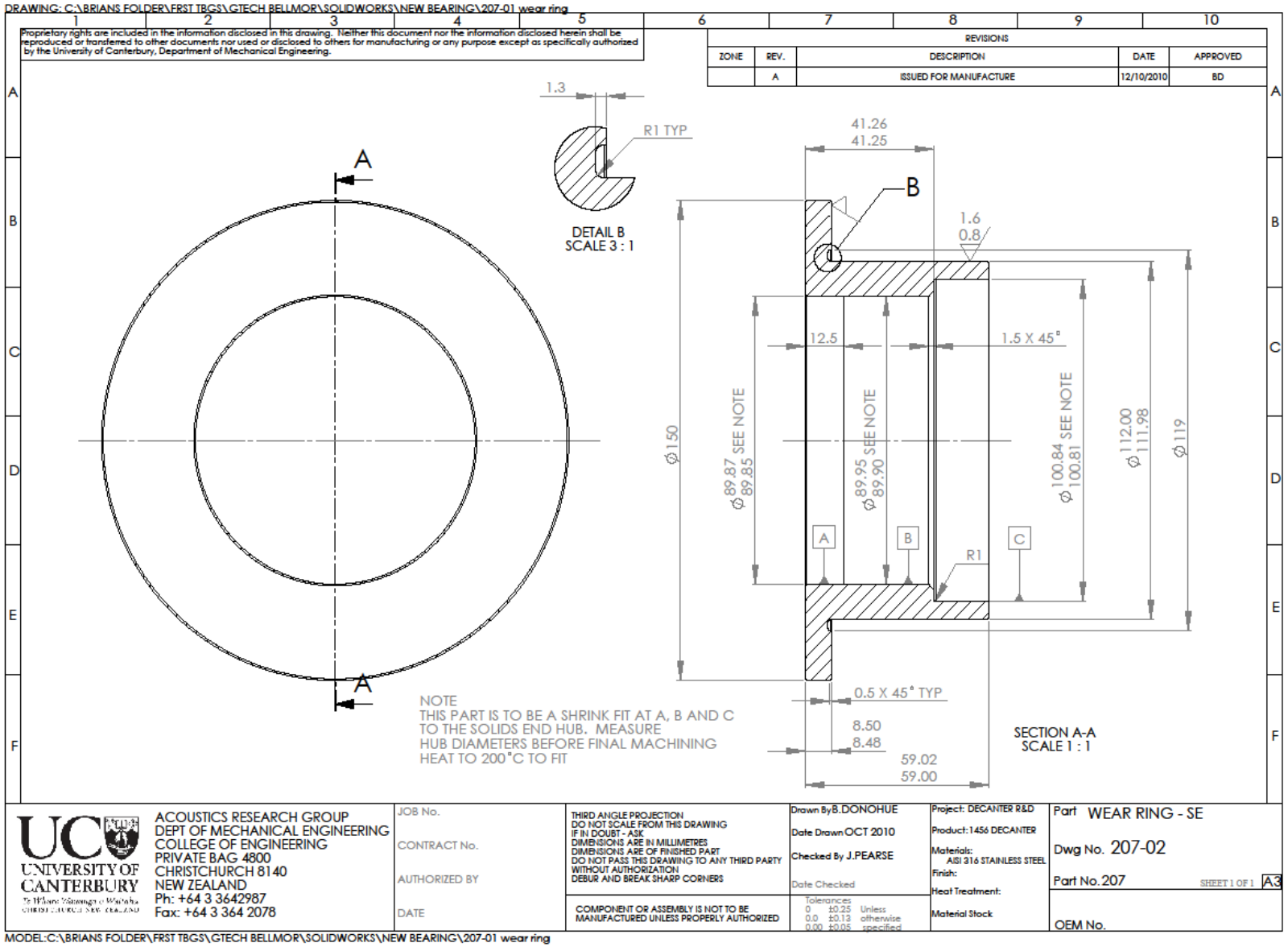
DRAWING: C:\BRIANS FOLDER\FRST TBGS\GTECH BELLMOR\SOLIDWORKS\NEW BEARING\207-01 wear ring
Proprietary rights are included in the information disclosed in this drawing. Neither this document nor the information disclosed herein shall be reproduced or transferred to other documents nor used or disclosed to others for manufacturing or any purpose except as specifically authorized by the University of Canterbury, Department of Mechanical Engineering.
REVISIONS
ZONE | REV. | DESCRIPTION | DATE | APPROVED
A | ISSUED FOR MANUFACTURE | 12/10/2010 | BD
1.3
R1 TYP
DETAIL B
SCALE 3 : 1
A
A
B
41.26
41.25
1.6
0.8
12.5
1.5 X 45°
Ø150
Ø89.87 SEE NOTE
Ø89.85
Ø89.95 SEE NOTE
Ø89.90
Ø100.84 SEE NOTE
Ø100.81
Ø112.00
Ø111.98
Ø119
A
B
C
R1
0.5 X 45° TYP
8.50
8.48
59.02
59.00
SECTION A-A
SCALE 1 : 1
NOTE
THIS PART IS TO BE A SHRINK FIT AT A, B AND C TO THE SOLIDS END HUB. MEASURE HUB DIAMETERS BEFORE FINAL MACHINING HEAT TO 200°C TO FIT
UNIVERSITY OF CANTERBURY
ACOUSTICS RESEARCH GROUP
DEPT OF MECHANICAL ENGINEERING
COLLEGE OF ENGINEERING
PRIVATE BAG 4800
CHRISTCHURCH 8140
NEW ZEALAND
Ph: +64 3 3642987
Fax: +64 3 364 2078
JOB No.
CONTRACT No.
AUTHORIZED BY
DATE
THIRD ANGLE PROJECTION
DO NOT SCALE FROM THIS DRAWING
IF IN DOUBT - ASK
DIMENSIONS ARE IN MILLIMETRES
DIMENSIONS ARE OF FINISHED PART
DO NOT PASS THIS DRAWING TO ANY THIRD PARTY WITHOUT AUTHORIZATION
DEBUR AND BREAK SHARP CORNERS
COMPONENT OR ASSEMBLY IS NOT TO BE MANUFACTURED UNLESS PROPERLY AUTHORIZED
Drawn By B.DONOHUE
Date Drawn OCT 2010
Checked By J.PEARSE
Date Checked
Tolerances
0 ±0.25 Unless
0.0 ±0.13 otherwise
0.00 ±0.05 specified
Project: DECANTER R&D
Product: 1456 DECANTER
Materials: AISI 316 STAINLESS STEEL
Finish:
Heat Treatment:
Material Stock
Part WEAR RING - SE
Dwg No. 207-02
Part No. 207
SHEET 1 OF 1 A3
OEM No.
MODEL:C:\BRIANS FOLDER\FRST TBGS\GTECH BELLMOR\SOLIDWORKS\NEW BEARING\207-01 wear ring

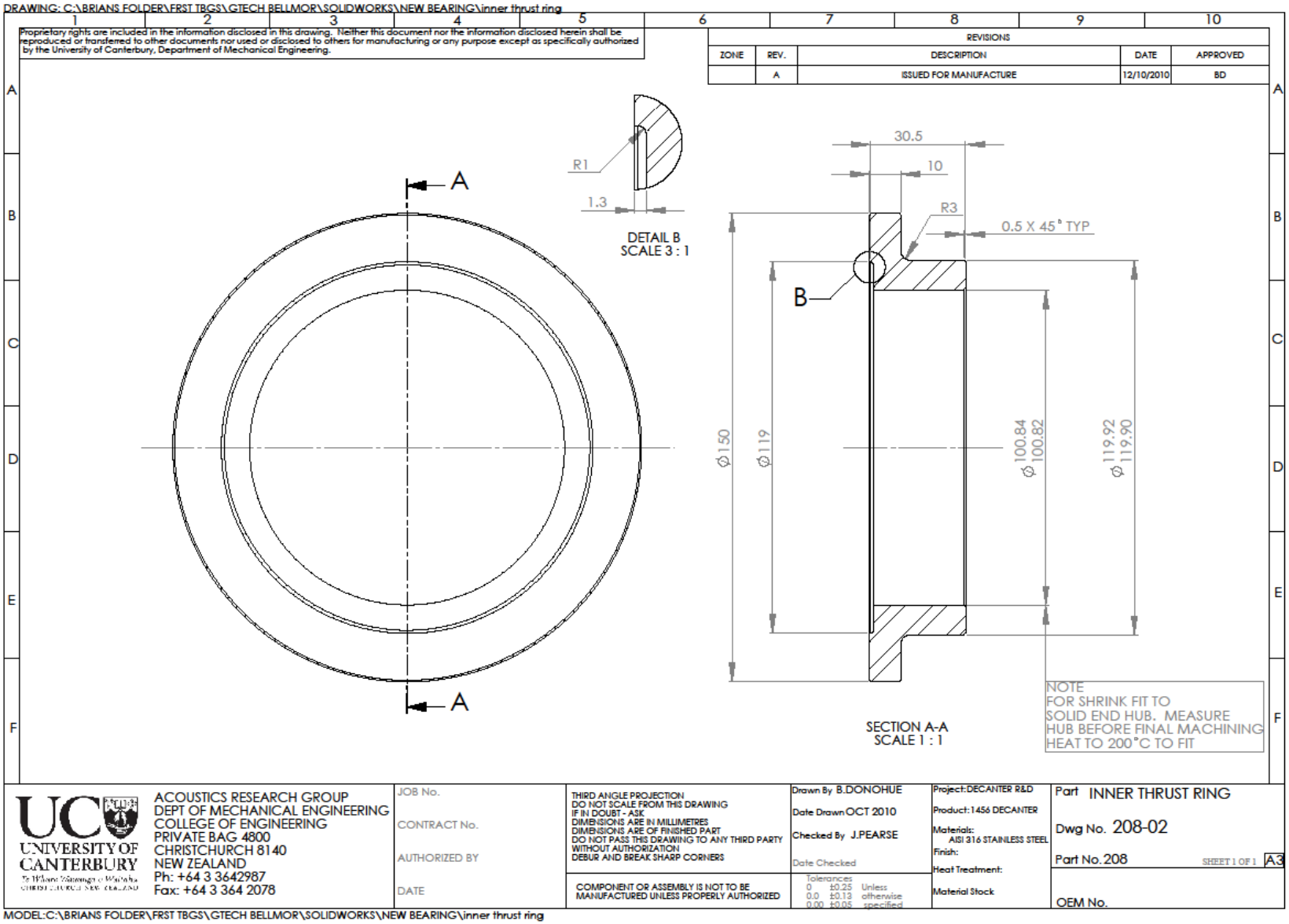
DRAWING: C:\BRIANS FOLDER\FRST TBGS\GTECH BELLMOR\SOLIDWORKS\NEW BEARING\inner thrust ring
Proprietary rights are included in the information disclosed in this drawing. Neither this document nor the information disclosed herein shall be reproduced or transferred to other documents nor used or disclosed to others for manufacturing or any purpose except as specifically authorized by the University of Canterbury, Department of Mechanical Engineering.
REVISIONS
ZONE | REV. | DESCRIPTION | DATE | APPROVED
A | ISSUED FOR MANUFACTURE | 12/10/2010 | BD
A
R1
1.3
DETAIL B
SCALE 3 : 1
30.5
10
R3
0.5 X 45° TYP
B
Ø150
Ø119
Ø100.84
100.82
Ø119.92
119.90
SECTION A-A
SCALE 1 : 1
NOTE
FOR SHRINK FIT TO
SOLID END HUB. MEASURE
HUB BEFORE FINAL MACHINING
HEAT TO 200°C TO FIT
UNIVERSITY OF CANTERBURY
ACOUSTICS RESEARCH GROUP
DEPT OF MECHANICAL ENGINEERING
COLLEGE OF ENGINEERING
PRIVATE BAG 4800
CHRISTCHURCH 8140
NEW ZEALAND
Ph: +64 3 3642987
Fax: +64 3 364 2078
JOB No.
CONTRACT No.
AUTHORIZED BY
DATE
THIRD ANGLE PROJECTION
DO NOT SCALE FROM THIS DRAWING
IF IN DOUBT - ASK
DIMENSIONS ARE IN MILLIMETRES
DIMENSIONS ARE OF FINISHED PART
DO NOT PASS THIS DRAWING TO ANY THIRD PARTY WITHOUT AUTHORIZATION
DEBUR AND BREAK SHARP CORNERS
COMPONENT OR ASSEMBLY IS NOT TO BE MANUFACTURED UNLESS PROPERLY AUTHORIZED
Drawn By B.DONOHUE
Date Drawn OCT 2010
Checked By J.PEARSE
Date Checked
Tolerances
0 ±0.25 Unless
0.0 ±0.13 otherwise
0.00 ±0.05 specified
Project: DECANTER R&D
Product: 1456 DECANTER
Materials: AISI 316 STAINLESS STEEL
Finish:
Heat Treatment:
Material Stock
Part INNER THRUST RING
Dwg No. 208-02
Part No. 208
SHEET 1 OF 1
A3
OEM No.
MODEL:C:\BRIANS FOLDER\FRST TBGS\GTECH BELLMOR\SOLIDWORKS\NEW BEARING\inner thrust ring

DRAWING: C:\BRIANS FOLDER\FRST TBGS\GTECH BELLMOR\SOLIDWORKS\NEW BEARING\SE_bearing

REVISIONS				
ZONE	REV.	DESCRIPTION	DATE	APPROVED
	A	ISSUED FOR MANUFACTURE	12/10/2010	BD
F8	B	ANTI-ROTATION DOWEL HOLE ADDED	18/10/2010	BD
B3/C1	C	SLOT ADDED	1/02/2011	BD
	D	5MM HOLE ADDED	27/02/2012	BD

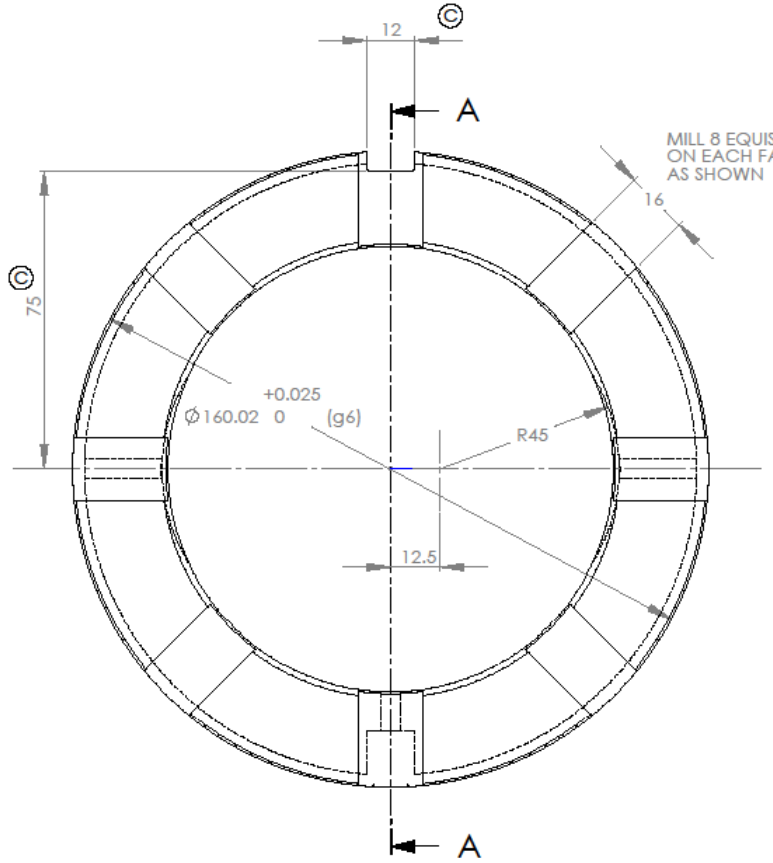

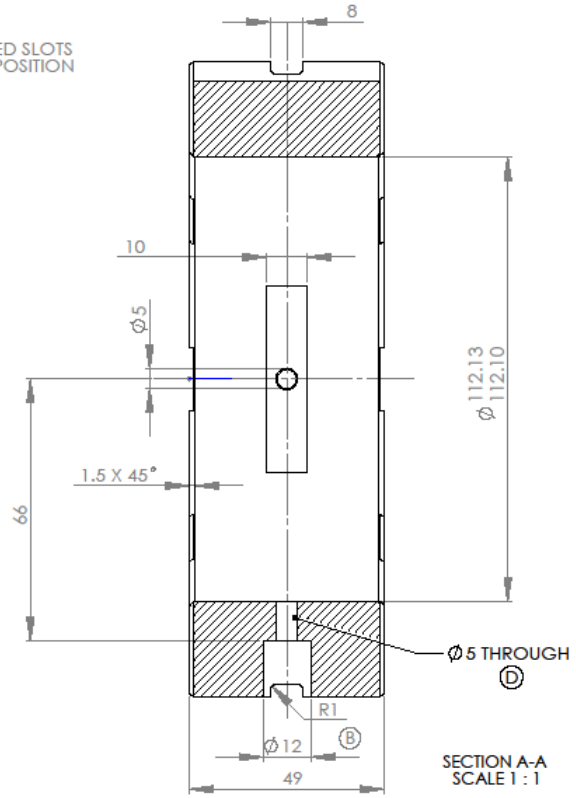

SECTION A-A
SCALE 1 : 1

UNIVERSITY OF CANTERBURY
Te Whare Wānanga o Waitaha
CHRISTCHURCH NEW ZEALAND

ACOUSTICS RESEARCH GROUP
DEPT OF MECHANICAL ENGINEERING
COLLEGE OF ENGINEERING
PRIVATE BAG 4800
CHRISTCHURCH 8140
NEW ZEALAND
Ph: +64 3 3642987
Fax: +64 3 364 2078

JOB No.
CONTRACT No.
AUTHORIZED BY
DATE

THIRD ANGLE PROJECTION
DO NOT SCALE FROM THIS DRAWING
IF IN DOUBT - ASK
DIMENSIONS ARE IN MILLIMETRES
DIMENSIONS ARE OF FINISHED PART
DO NOT PASS THIS DRAWING TO ANY THIRD PARTY WITHOUT AUTHORIZATION
DEBUR AND BREAK SHARP CORNERS

COMPONENT OR ASSEMBLY IS NOT TO BE MANUFACTURED UNLESS PROPERLY AUTHORIZED

Drawn By B.DONOHUE
Date Drawn 28AUG2009
Checked By JPEARSE
Date Checked 31AUG2009

Tolerances
0 ±0.25 Unless
0.0 ±0.13 otherwise
0.00 ±0.05 specified

Project: DECANTER R&D
Product: TRIAL BEARINGS
Materials: LG1-BRONZE
Finish:
Heat Treatment:
Material Stock

Part BEARING - SE
Dwg No. 209-02
Part No. 209
SHEET 1 OF 1 A3
OEM No.

MODEL:C:\BRIANS FOLDER\FRST TBGS\GTECH BELLMOR\SOLIDWORKS\NEW BEARING\SE_bearing

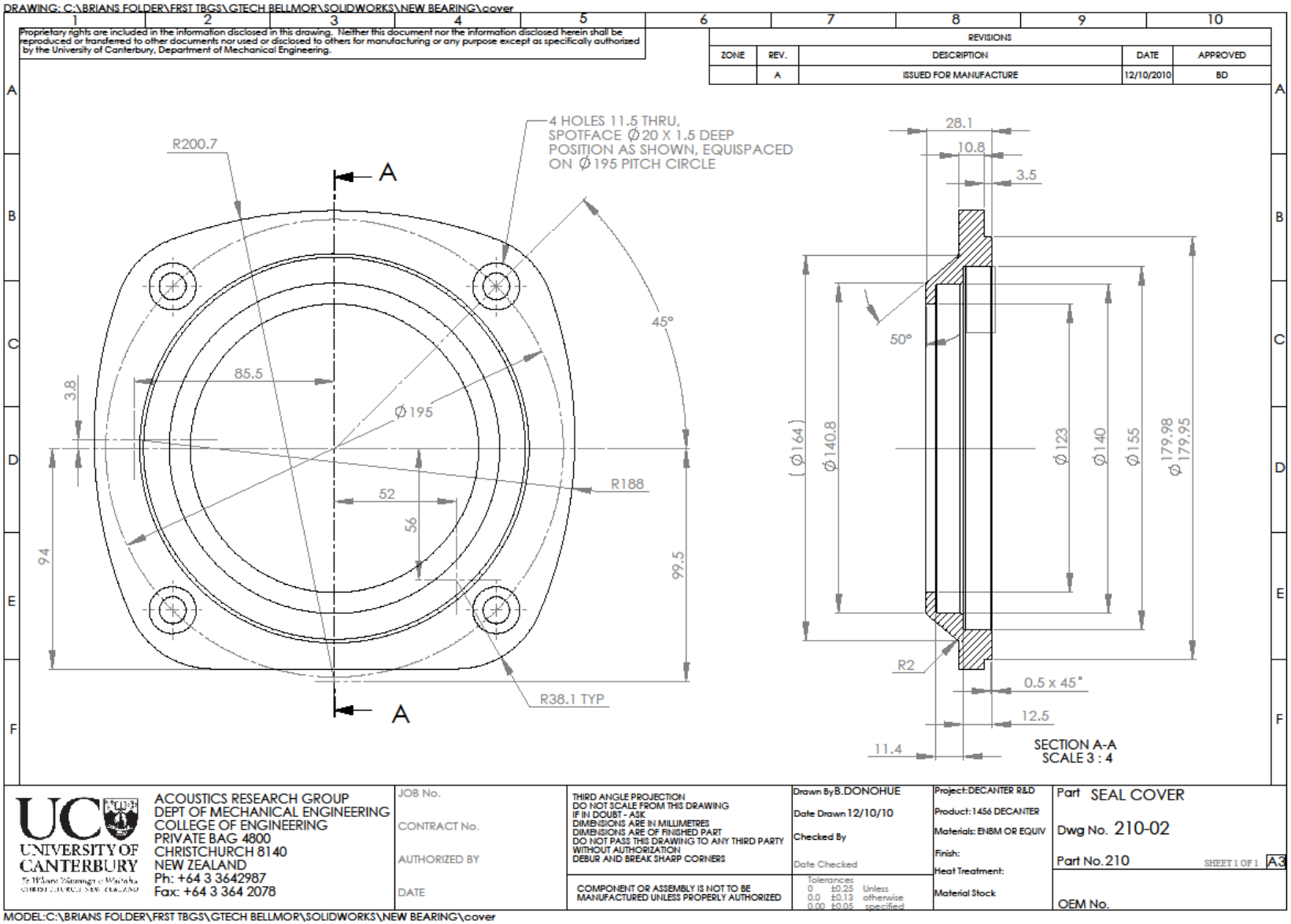
DRAWING: C:\BRIANS FOLDER\FRST TBGS\GTECH BELLMOR\SOLIDWORKS\NEW BEARING\cover
Proprietary rights are included in the information disclosed in this drawing. Neither this document nor the information disclosed herein shall be reproduced or transferred to other documents nor used or disclosed to others for manufacturing or any purpose except as specifically authorized by the University of Canterbury, Department of Mechanical Engineering.
REVISIONS
ZONE | REV. | DESCRIPTION | DATE | APPROVED
A | ISSUED FOR MANUFACTURE | 12/10/2010 | BD
R200.7
4 HOLES 11.5 THRU, SPOTFACE Ø20 X 1.5 DEEP POSITION AS SHOWN, EQUISPACED ON Ø195 PITCH CIRCLE
A
45°
85.5
3.8
Ø195
52
56
94
99.5
R188
R38.1 TYP
28.1
10.8
3.5
50°
(Ø164)
Ø140.8
Ø123
Ø140
Ø155
Ø179.98
Ø179.95
R2
0.5 x 45°
12.5
11.4
SECTION A-A
SCALE 3 : 4
UNIVERSITY OF CANTERBURY
ACOUSTICS RESEARCH GROUP
DEPT OF MECHANICAL ENGINEERING
COLLEGE OF ENGINEERING
PRIVATE BAG 4800
CHRISTCHURCH 8140
NEW ZEALAND
Ph: +64 3 3642987
Fax: +64 3 364 2078
JOB No.
CONTRACT No.
AUTHORIZED BY
DATE
THIRD ANGLE PROJECTION
DO NOT SCALE FROM THIS DRAWING
IF IN DOUBT - ASK
DIMENSIONS ARE IN MILLIMETRES
DIMENSIONS ARE OF FINISHED PART
DO NOT PASS THIS DRAWING TO ANY THIRD PARTY WITHOUT AUTHORIZATION
DEBUR AND BREAK SHARP CORNERS
COMPONENT OR ASSEMBLY IS NOT TO BE MANUFACTURED UNLESS PROPERLY AUTHORIZED
Drawn By B.DONOHUE
Date Drawn 12/10/10
Checked By
Date Checked
Tolerances
0 ±0.25 Unless
0.0 ±0.13 otherwise
0.00 ±0.05 specified
Project: DECANTER R&D
Product: 1456 DECANTER
Materials: EN8M OR EQUIV
Finish:
Heat Treatment:
Material Stock
Part SEAL COVER
Dwg No. 210-02
Part No. 210
SHEET 1 OF 1 A3
OEM No.
MODEL:C:\BRIANS FOLDER\FRST TBGS\GTECH BELLMOR\SOLIDWORKS\NEW BEARING\cover

DRAWING: C:\BRIANS FOLDER\FRST TBGS\GTECH BELLMOR\SOLIDWORKS\NEW BEARING\brg housing

REVISIONS				
ZONE	REV.	DESCRIPTION	DATE	APPROVED
	A	ISSUED FOR MANUFACTURE	12/10/2010	BD
B7/D9	B	TOP TAPPING CHANGED, LABYRINTH DIMENSIONS AMENDED	9/11/2010	BD
D6	C	BORE TOL CHANGED	1/02/2011	BD

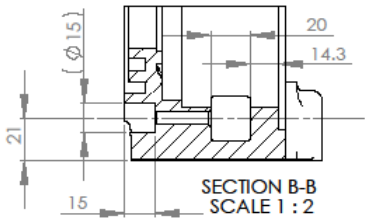

SECTION B-B
SCALE 1 : 2

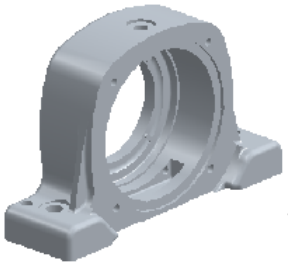

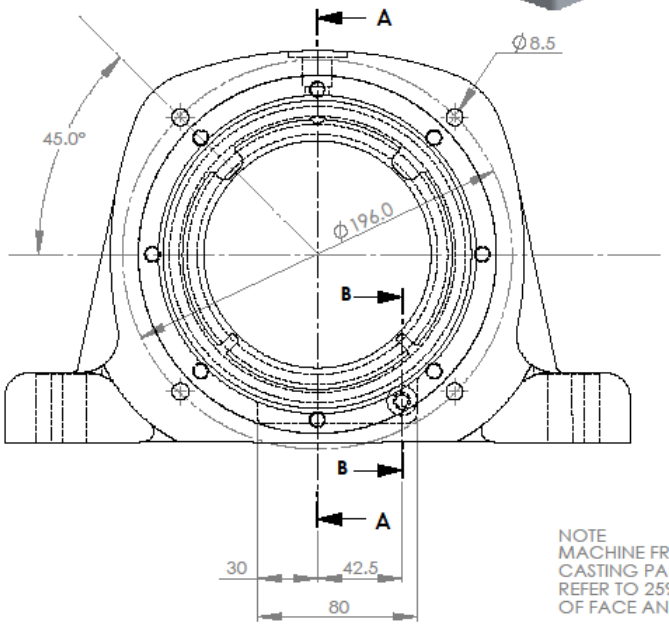

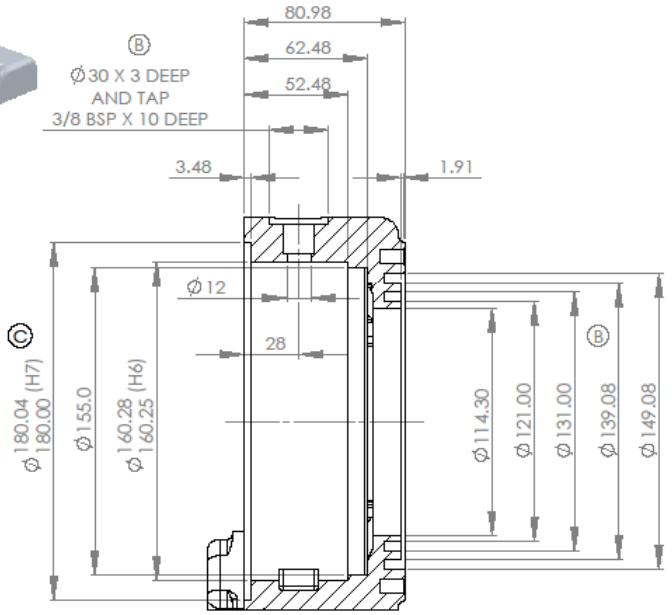

SECTION A-A
SCALE 1 : 2

NOTE
MACHINE FROM STANDARD
CASTING PART 25971-02
REFER TO 25971-01 FOR DETAIL
OF FACE AND FOOT DRILLINGS

UNIVERSITY OF CANTERBURY
Te Whare Wānanga o Waitaha
CHRISTCHURCH NEW ZEALAND

ACOUSTICS RESEARCH GROUP
DEPT OF MECHANICAL ENGINEERING
COLLEGE OF ENGINEERING
PRIVATE BAG 4800
CHRISTCHURCH 8140
NEW ZEALAND
Ph: +64 3 3642987
Fax: +64 3 364 2078

JOB No.
CONTRACT No.
AUTHORIZED BY
DATE

THIRD ANGLE PROJECTION
DO NOT SCALE FROM THIS DRAWING
IF IN DOUBT - ASK
DIMENSIONS ARE IN MILLIMETRES
DIMENSIONS ARE OF FINISHED PART
DO NOT PASS THIS DRAWING TO ANY THIRD PARTY WITHOUT AUTHORIZATION
DEBUR AND BREAK SHARP CORNERS

COMPONENT OR ASSEMBLY IS NOT TO BE MANUFACTURED UNLESS PROPERLY AUTHORIZED

Drawn By B.DONOHUE
Date Drawn 11OCT2010
Checked By
Date Checked

Tolerances
0 ±0.25 Unless
0.0 ±0.13 otherwise
0.00 ±0.05 specified

Project: DECANTER R&D
Product: 1456 DECANTER
Materials: SG IRON 500/7
Finish:
Heat Treatment:
Material Stock

Part BEARING HOUSING - SE
Dwg No. 211-02
Part No. 211 SHEET 1 OF 1 A3
OEM No.

MODEL:C:\BRIANS FOLDER\FRST TBGS\GTECH BELLMOR\SOLIDWORKS\NEW BEARING\brg housing

DRAWING: C:\BRIANS FOLDER\FRST TBGS\GTECH BELLMOR\SOLIDWORKS\NEW BEARING\17625mod

REVISIONS				
ZONE	REV.	DESCRIPTION	DATE	APPROVED
	A	ISSUED FOR MANUFACTURE	13/10/2010	BD

NOTE
PART IS STANDARD PART 17625
REDUCED IN LENGTH AS SHOWN

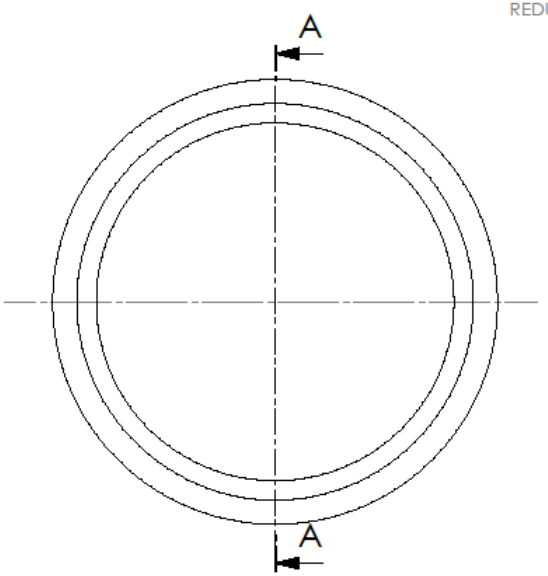

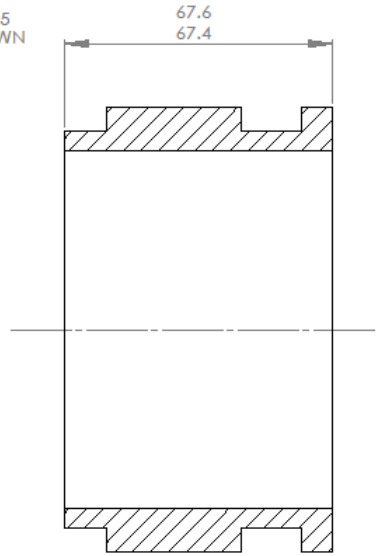

SECTION A-A
SCALE 1 : 1

UNIVERSITY OF CANTERBURY
Te Whare Wānanga o Waitaha
CHRISTCHURCH NEW ZEALAND

ACOUSTICS RESEARCH GROUP
DEPT OF MECHANICAL ENGINEERING
COLLEGE OF ENGINEERING
PRIVATE BAG 4800
CHRISTCHURCH 8140
NEW ZEALAND
Ph: +64 3 3642987
Fax: +64 3 364 2078

JOB No.
CONTRACT No.
AUTHORIZED BY
DATE

THIRD ANGLE PROJECTION
DO NOT SCALE FROM THIS DRAWING
IF IN DOUBT - ASK
DIMENSIONS ARE IN MILLIMETRES
DIMENSIONS ARE OF FINISHED PART
DO NOT PASS THIS DRAWING TO ANY THIRD PARTY WITHOUT AUTHORIZATION
DEBUR AND BREAK SHARP CORNERS

COMPONENT OR ASSEMBLY IS NOT TO BE MANUFACTURED UNLESS PROPERLY AUTHORIZED

Drawn By B.DONOHUE
Date Drawn 13/10/10
Checked By
Date Checked

Tolerances
0 ±0.25 Unless
0.0 ±0.13 otherwise
0.00 ±0.05 specified

Project: DECANTER R&D
Product: 1456 DECANTER
Materials: STAINLESS STEEL
Finish:
Heat Treatment:
Material Stock

Part MOD TO 17625
Dwg No. 212-01
Part No. 212
SHEET 1 OF 1 A3
OEM No.

MODEL:C:\BRIANS FOLDER\FRST TBGS\GTECH BELLMOR\SOLIDWORKS\NEW BEARING\17625mod

DRAWING: C:\BRIANS FOLDER\FRST TBGS\GTECH BELLMOR\SOLIDWORKS\NEW BEARING\new SEhub assembly2

REVISIONS				
ZONE	REV.	DESCRIPTION	DATE	APPROVED
	A	ISSUED FOR MANUFACTURE	14/10/2010	BD

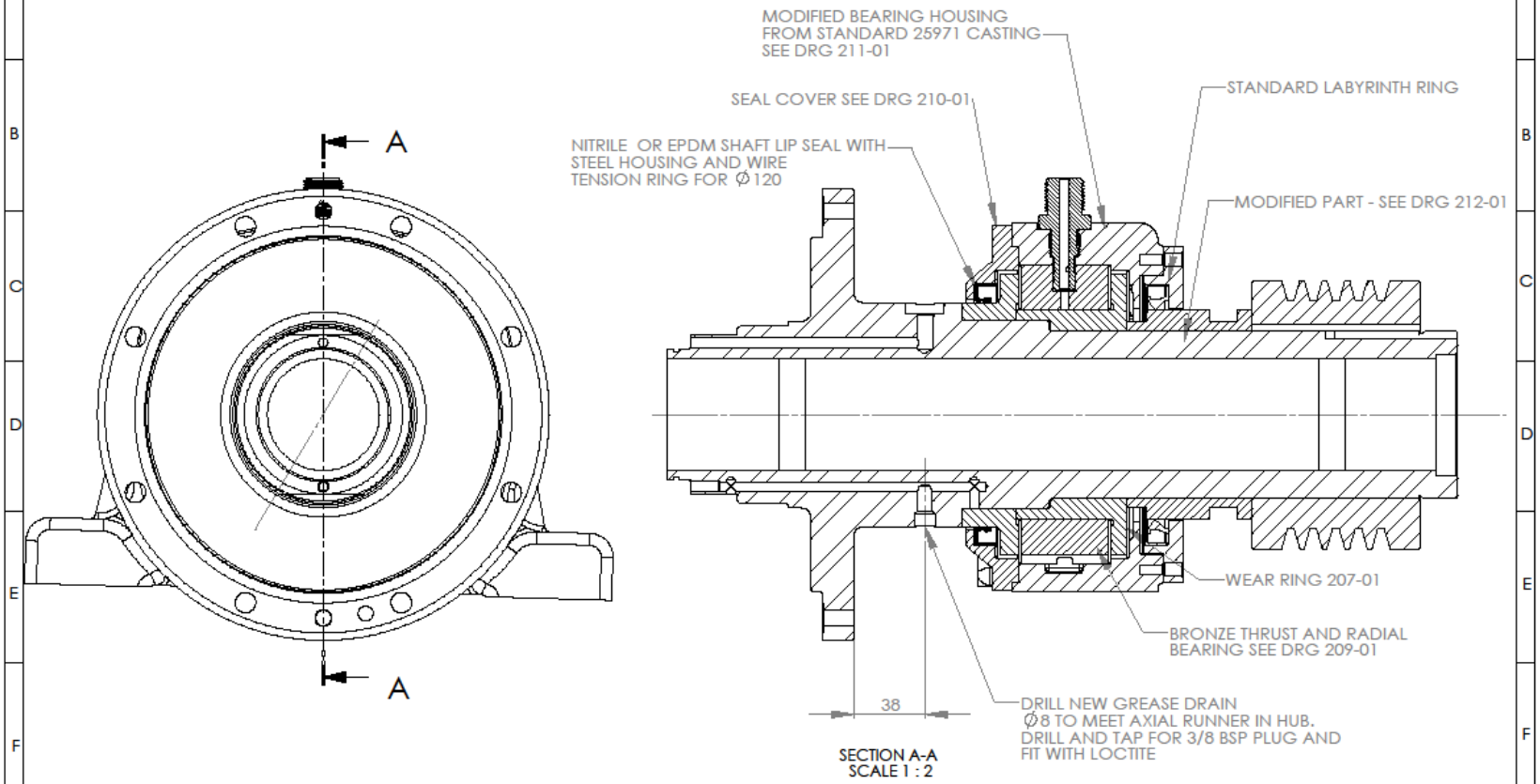

SECTION A-A
SCALE 1 : 2

UNIVERSITY OF CANTERBURY
Te Whare Wānanga o Waitaha
CHRISTCHURCH NEW ZEALAND

ACOUSTICS RESEARCH GROUP
DEPT OF MECHANICAL ENGINEERING
COLLEGE OF ENGINEERING
PRIVATE BAG 4800
CHRISTCHURCH 8140
NEW ZEALAND
Ph: +64 3 3642987
Fax: +64 3 364 2078

JOB No.
CONTRACT No.
AUTHORIZED BY
DATE

THIRD ANGLE PROJECTION
DO NOT SCALE FROM THIS DRAWING
IF IN DOUBT - ASK
DIMENSIONS ARE IN MILLIMETRES
DIMENSIONS ARE OF FINISHED PART
DO NOT PASS THIS DRAWING TO ANY THIRD PARTY WITHOUT AUTHORIZATION
DEBUR AND BREAK SHARP CORNERS

COMPONENT OR ASSEMBLY IS NOT TO BE MANUFACTURED UNLESS PROPERLY AUTHORIZED

Drawn By B.DONOHUE
Date Drawn 13/10/10
Checked By
Date Checked

Tolerances
0 ±0.25 Unless
0.0 ±0.13 otherwise
0.00 ±0.05 specified

Project: DECANTER R&D
Product: 1456 DECANTER
Materials:
Finish:
Heat Treatment:
Material Stock

Part
MODIFIED SOLIDS END BEARING
Dwg No. 213-01
Part No.
SHEET 1 OF 1 A3
OEM No.

MODEL:C:\BRIANS FOLDER\FRST TBGS\GTECH BELLMOR\SOLIDWORKS\NEW BEARING\new SEhub assembly2

DRAWING: C:\BRIANS FOLDER\FRST TBGS\GTECH BELLMOR\SOLIDWORKS\NEW BEARING\LE_bearing

REVISIONS				
ZONE	REV.	DESCRIPTION	DATE	APPROVED
	A	ISSUED FOR MANUFACTURE	12/10/2010	BD
B3	B	ANTI-ROTATION DOWEL HOLE ADDED	18/10/2010	BD
F5-8	C	THRU SLOT ADDED	1/02/2011	BD
	D	5mm HOLE ADDED	27/02/2012	BD

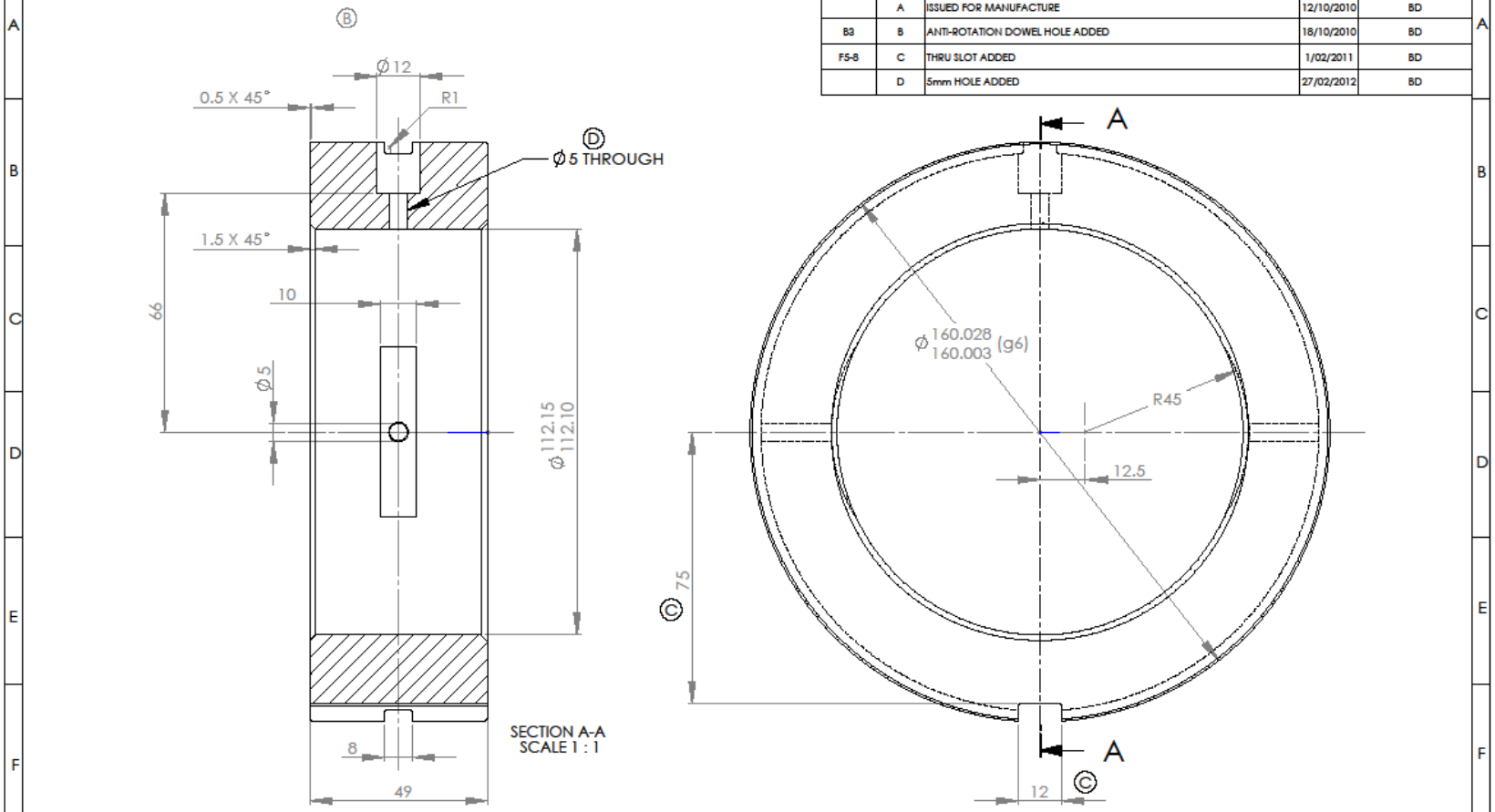

UNIVERSITY OF CANTERBURY
Te Whare Wānanga o Waitaha
CHRISTCHURCH NEW ZEALAND

ACOUSTICS RESEARCH GROUP
DEPT OF MECHANICAL ENGINEERING
COLLEGE OF ENGINEERING
PRIVATE BAG 4800
CHRISTCHURCH 8140
NEW ZEALAND
Ph: +64 3 3642987
Fax: +64 3 364 2078

JOB No.
CONTRACT No.
AUTHORIZED BY
DATE

THIRD ANGLE PROJECTION
DO NOT SCALE FROM THIS DRAWING
IF IN DOUBT - ASK
DIMENSIONS ARE IN MILLIMETRES
DIMENSIONS ARE OF FINISHED PART
DO NOT PASS THIS DRAWING TO ANY THIRD PARTY WITHOUT AUTHORIZATION
DEBUR AND BREAK SHARP CORNERS

COMPONENT OR ASSEMBLY IS NOT TO BE MANUFACTURED UNLESS PROPERLY AUTHORIZED

Drawn By B.DONOHUE
Date Drawn 28AUG2009
Checked By JPEARSE
Date Checked 31AUG2009

Tolerances
0 ±0.25 Unless
0.0 ±0.13 otherwise
0.00 ±0.05 specified

Project: DECANTER R&D
Product: TRIAL BEARINGS
Material: LG1-BRONZE
Finish:
Heat Treatment:
Material Stock

Part BEARING - LE
Dwg No. 214-02
Part No. 214
SHEET 1 OF 1 A3
OEM No.

MODEL:C:\BRIANS FOLDER\FRST TBGS\GTECH BELLMOR\SOLIDWORKS\NEW BEARING\LE_bearing

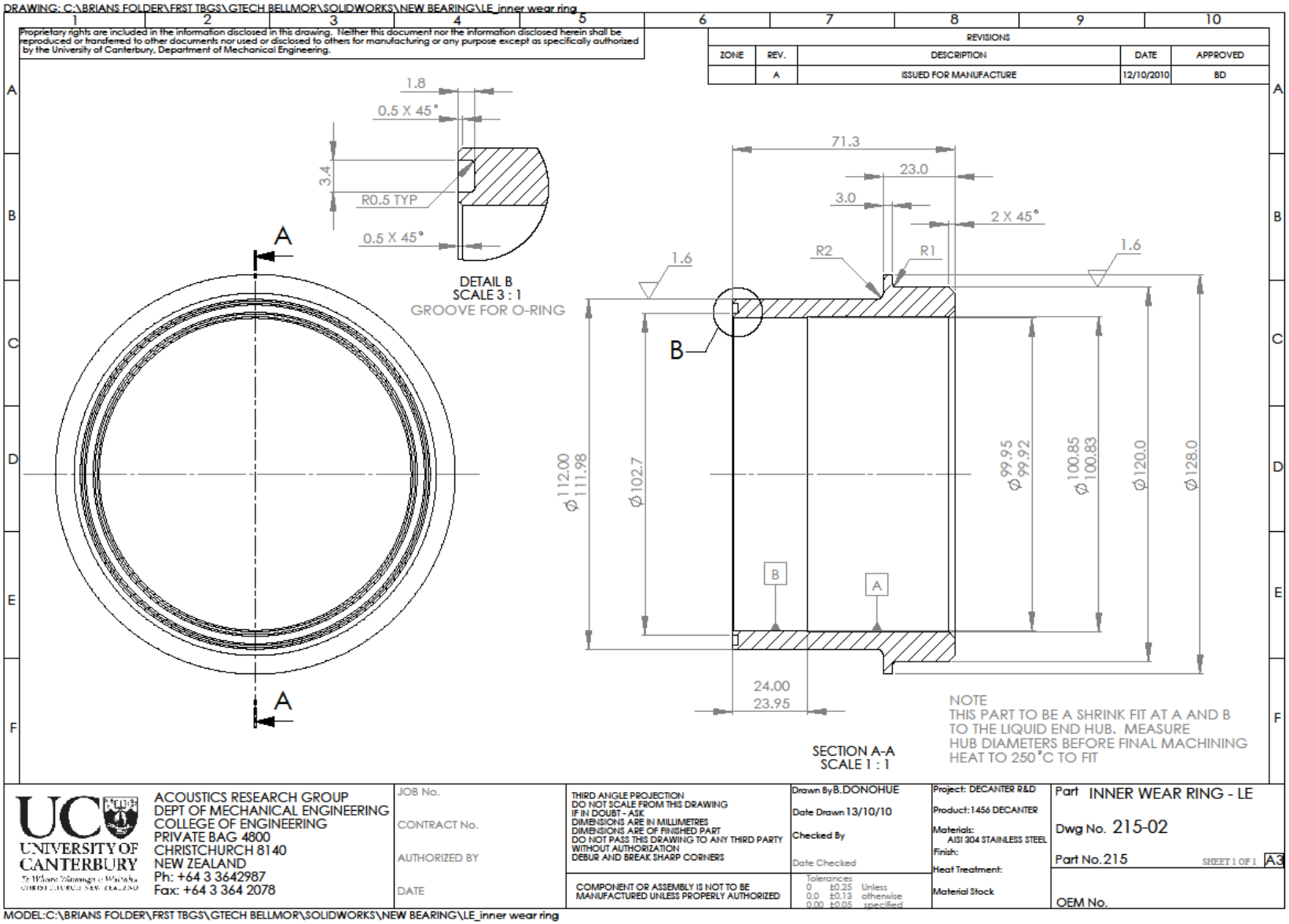
DRAWING: C:\BRIANS FOLDER\FRST TBGS\GTECH BELLMOR\SOLIDWORKS\NEW BEARING\LE_inner wear ring
Proprietary rights are included in the information disclosed in this drawing. Neither this document nor the information disclosed herein shall be reproduced or transferred to other documents nor used or disclosed to others for manufacturing or any purpose except as specifically authorized by the University of Canterbury, Department of Mechanical Engineering.
REVISIONS
ZONE | REV. | DESCRIPTION | DATE | APPROVED
A | ISSUED FOR MANUFACTURE | 12/10/2010 | BD
1.8
0.5 X 45°
3.4
R0.5 TYP
0.5 X 45°
DETAIL B
SCALE 3 : 1
GROOVE FOR O-RING
71.3
23.0
3.0
2 X 45°
R2
R1
1.6
1.6
B
Ø112.00
Ø111.98
Ø102.7
Ø99.95
Ø99.92
Ø100.85
Ø100.83
Ø120.0
Ø128.0
24.00
23.95
SECTION A-A
SCALE 1 : 1
NOTE
THIS PART TO BE A SHRINK FIT AT A AND B
TO THE LIQUID END HUB. MEASURE
HUB DIAMETERS BEFORE FINAL MACHINING
HEAT TO 250°C TO FIT
UNIVERSITY OF CANTERBURY
ACOUSTICS RESEARCH GROUP
DEPT OF MECHANICAL ENGINEERING
COLLEGE OF ENGINEERING
PRIVATE BAG 4800
CHRISTCHURCH 8140
NEW ZEALAND
Ph: +64 3 3642987
Fax: +64 3 364 2078
JOB No.
CONTRACT No.
AUTHORIZED BY
DATE
THIRD ANGLE PROJECTION
DO NOT SCALE FROM THIS DRAWING
IF IN DOUBT - ASK
DIMENSIONS ARE IN MILLIMETRES
DIMENSIONS ARE OF FINISHED PART
DO NOT PASS THIS DRAWING TO ANY THIRD PARTY WITHOUT AUTHORIZATION
DEBUR AND BREAK SHARP CORNERS
COMPONENT OR ASSEMBLY IS NOT TO BE MANUFACTURED UNLESS PROPERLY AUTHORIZED
Drawn By B.DONOHUE
Date Drawn 13/10/10
Checked By
Date Checked
Tolerances
0 ±0.25 Unless
0.0 ±0.13 otherwise
0.00 ±0.05 specified
Project: DECANTER R&D
Product: 1456 DECANTER
Materials: AISI 304 STAINLESS STEEL
Finish:
Heat Treatment:
Material Stock
Part INNER WEAR RING - LE
Dwg No. 215-02
Part No. 215
SHEET 1 OF 1
A3
OEM No.
MODEL:C:\BRIANS FOLDER\FRST TBGS\GTECH BELLMOR\SOLIDWORKS\NEW BEARING\LE_inner wear ring

DRAWING: C:\BRIANS FOLDER\FRST TBGS\GTECH BELLMOR\SOLIDWORKS\NEW BEARING\LE_new assembly

REVISIONS				
ZONE	REV.	DESCRIPTION	DATE	APPROVED
	A	ISSUED FOR MANUFACTURE	14/10/2010	BD

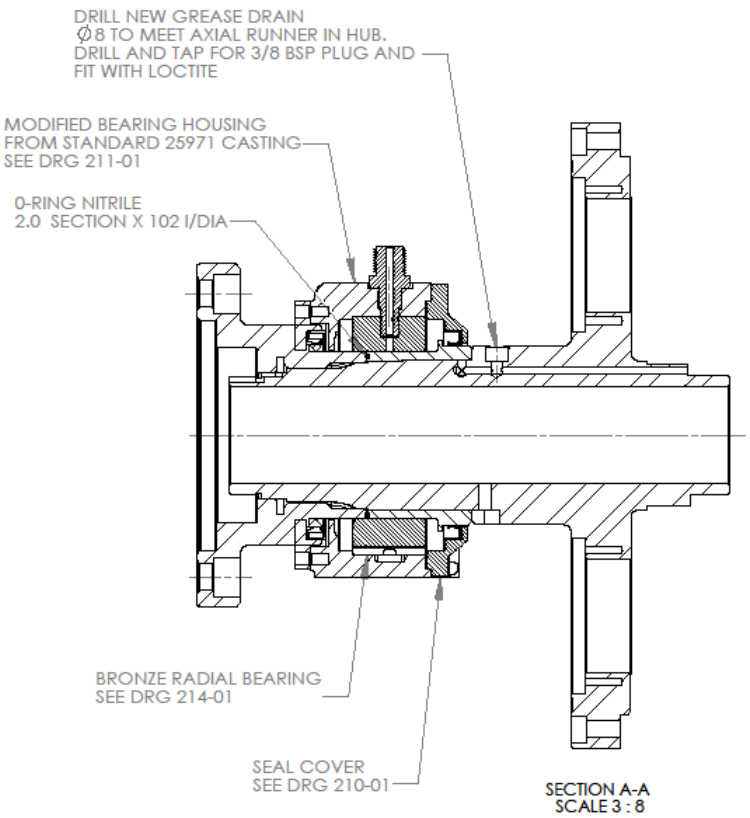

SECTION A-A
SCALE 3 : 8

UNIVERSITY OF CANTERBURY
Te Whare Wānanga o Waitaha
CHRISTCHURCH NEW ZEALAND

ACOUSTICS RESEARCH GROUP
DEPT OF MECHANICAL ENGINEERING
COLLEGE OF ENGINEERING
PRIVATE BAG 4800
CHRISTCHURCH 8140
NEW ZEALAND
Ph: +64 3 3642987
Fax: +64 3 364 2078

JOB No.
CONTRACT No.
AUTHORIZED BY
DATE

THIRD ANGLE PROJECTION
DO NOT SCALE FROM THIS DRAWING
IF IN DOUBT - ASK
DIMENSIONS ARE IN MILLIMETRES
DIMENSIONS ARE OF FINISHED PART
DO NOT PASS THIS DRAWING TO ANY THIRD PARTY WITHOUT AUTHORIZATION
DEBUR AND BREAK SHARP CORNERS

COMPONENT OR ASSEMBLY IS NOT TO BE MANUFACTURED UNLESS PROPERLY AUTHORIZED

Drawn By B.DONOHUE
Date Drawn 13/10/10
Checked By
Date Checked

Tolerances
0 ±0.25 Unless
0.0 ±0.13 otherwise
0.00 ±0.05 specified

Project: DECANTER R&D
Product: 1456 DECANTER
Materials:
Finish:
Heat Treatment:
Material Stock

Part
MODIFIED LIQUID END BEARING
Dwg No. 216-01
Part No.
SHEET 1 OF 1 A3
OEM No.

MODEL:C:\BRIANS FOLDER\FRST TBGS\GTECH BELLMOR\SOLIDWORKS\NEW BEARING\LE_new assembly

DRAWING: C:\BRIANS FOLDER\FRST TBGS\GTECH BELLMOR\SOLIDWORKS\NEW BEARING\dowel

REVISIONS				
ZONE	REV.	DESCRIPTION	DATE	APPROVED
	A	ISSUED FOR MANUFACTURE	9/11/2010	BD
	B	CENTRE HOLE DRILLED THROUGH PART	27/02/2012	BD

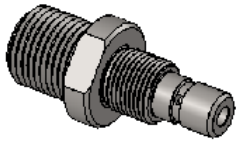

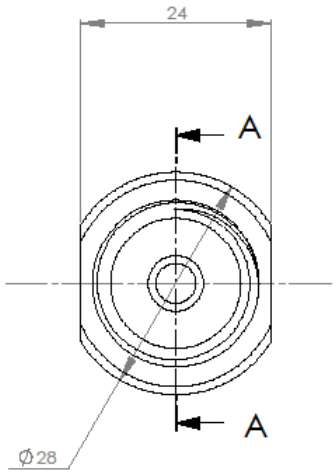

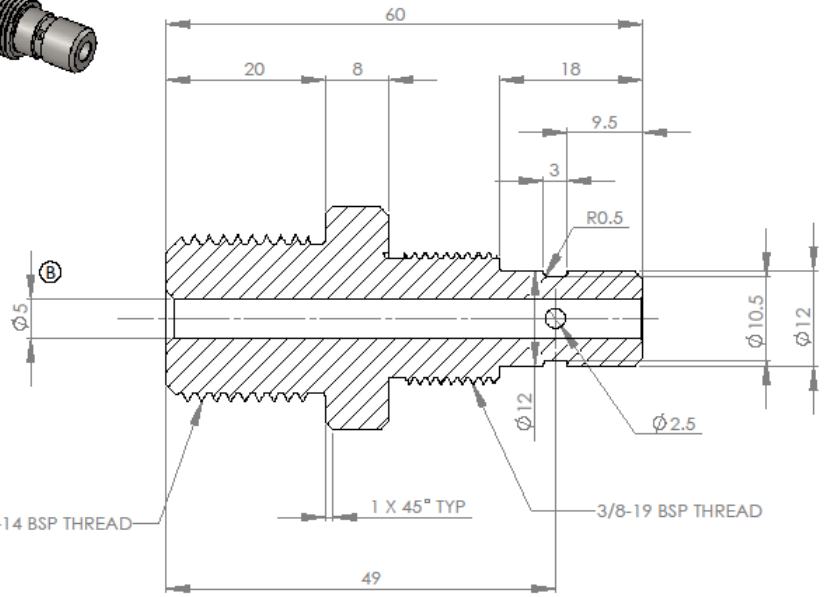

SECTION A-A

UNIVERSITY OF CANTERBURY Te Whare Wānanga o Waitaha CHRISTCHURCH NEW ZEALAND	ACOUSTICS RESEARCH GROUP DEPT OF MECHANICAL ENGINEERING COLLEGE OF ENGINEERING PRIVATE BAG 4800 CHRISTCHURCH 8140 NEW ZEALAND Ph: +64 3 3642987 Fax: +64 3 364 2078	JOB No. CONTRACT No. AUTHORIZED BY DATE	THIRD ANGLE PROJECTION DO NOT SCALE FROM THIS DRAWING IF IN DOUBT - ASK DIMENSIONS ARE IN MILLIMETRES DIMENSIONS ARE OF FINISHED PART DO NOT PASS THIS DRAWING TO ANY THIRD PARTY WITHOUT AUTHORIZATION DEBUR AND BREAK SHARP CORNERS COMPONENT OR ASSEMBLY IS NOT TO BE MANUFACTURED UNLESS PROPERLY AUTHORIZED	Drawn By B.DONOHUE Date Drawn 3 NOV 2010 Checked By Date Checked Tolerances 0 ±0.25 Unless 0.0 ±0.13 otherwise 0.00 ±0.05 specified	Project: DECANTER R&D Product: 1456 DECANTER Materials: AISI 316 STAINLESS STEEL Finish: Heat Treatment: Material Stock	Part DOWEL Dwg No. 217-01 Part No. 217 SHEET 1 OF 1 A3 OEM No.

MODEL:C:\BRIANS FOLDER\FRST TBGS\GTECH BELLMOR\SOLIDWORKS\NEW BEARING\dowel

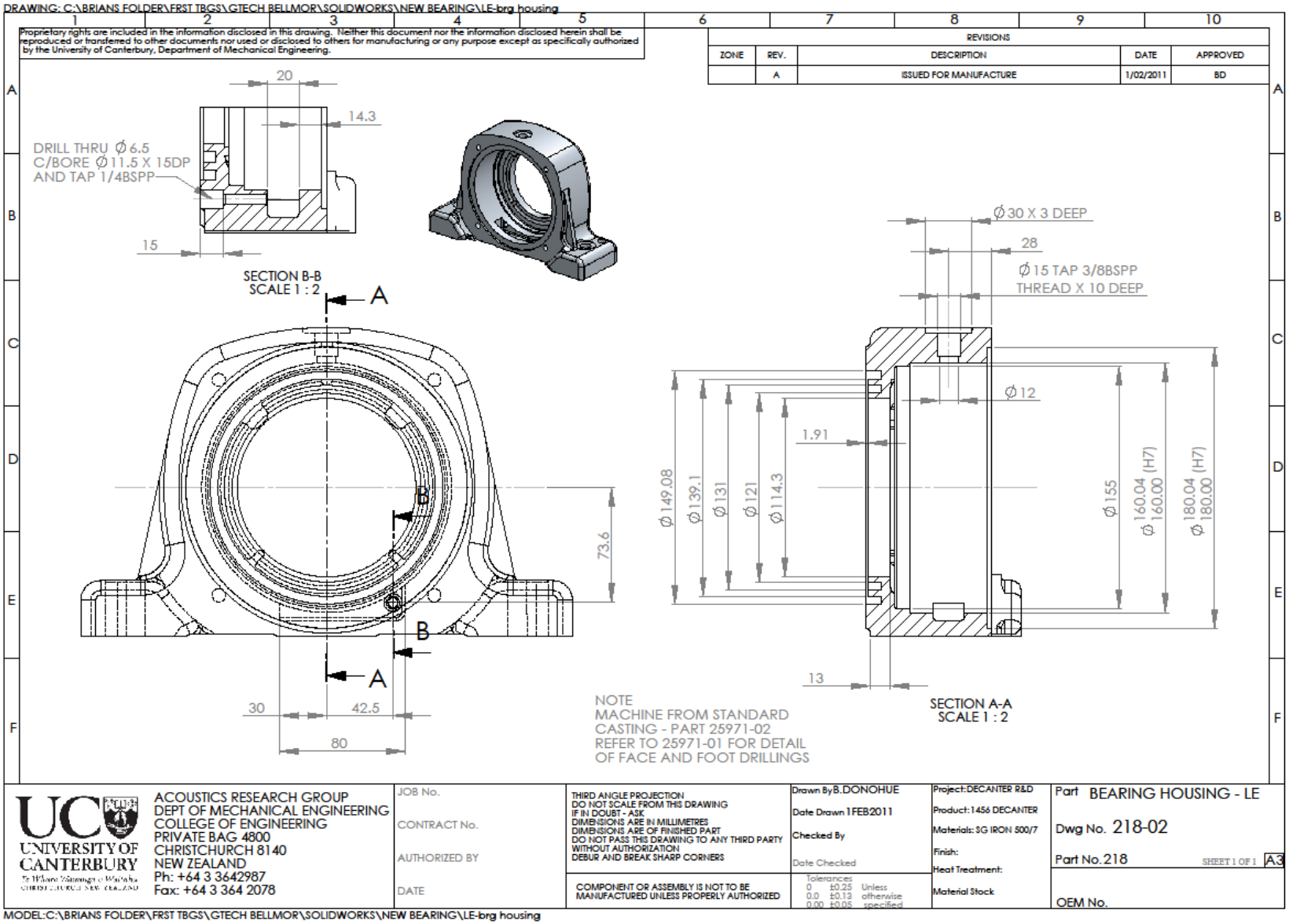
DRAWING: C:\BRIANS FOLDER\FRST TBGS\GTECH BELLMOR\SOLIDWORKS\NEW BEARING\LE-brg housing
Proprietary rights are included in the information disclosed in this drawing. Neither this document nor the information disclosed herein shall be reproduced or transferred to other documents nor used or disclosed to others for manufacturing or any purpose except as specifically authorized by the University of Canterbury, Department of Mechanical Engineering.
REVISIONS
ZONE | REV. | DESCRIPTION | DATE | APPROVED
A | ISSUED FOR MANUFACTURE | 1/02/2011 | BD
20
14.3
DRILL THRU Ø6.5
C/BORE Ø11.5 X 15DP
AND TAP 1/4BSPP
15
SECTION B-B
SCALE 1 : 2
A
B
73.6
30
42.5
80
Ø30 X 3 DEEP
28
Ø15 TAP 3/8BSPP
THREAD X 10 DEEP
Ø12
1.91
Ø149.08
Ø139.1
Ø131
Ø121
Ø114.3
Ø155
Ø160.04 (H7)
Ø160.00
Ø180.04 (H7)
Ø180.00
13
SECTION A-A
SCALE 1 : 2
NOTE
MACHINE FROM STANDARD
CASTING - PART 25971-02
REFER TO 25971-01 FOR DETAIL
OF FACE AND FOOT DRILLINGS
UNIVERSITY OF CANTERBURY
ACOUSTICS RESEARCH GROUP
DEPT OF MECHANICAL ENGINEERING
COLLEGE OF ENGINEERING
PRIVATE BAG 4800
CHRISTCHURCH 8140
NEW ZEALAND
Ph: +64 3 3642987
Fax: +64 3 364 2078
JOB No.
CONTRACT No.
AUTHORIZED BY
DATE
THIRD ANGLE PROJECTION
DO NOT SCALE FROM THIS DRAWING
IF IN DOUBT - ASK
DIMENSIONS ARE IN MILLIMETRES
DIMENSIONS ARE OF FINISHED PART
DO NOT PASS THIS DRAWING TO ANY THIRD PARTY WITHOUT AUTHORIZATION
DEBUR AND BREAK SHARP CORNERS
COMPONENT OR ASSEMBLY IS NOT TO BE MANUFACTURED UNLESS PROPERLY AUTHORIZED
Drawn By B.DONOHUE
Date Drawn 1FEB2011
Checked By
Date Checked
Tolerances
0 ±0.25 Unless
0.0 ±0.13 otherwise
0.00 ±0.05 specified
Project: DECANTER R&D
Product: 1456 DECANTER
Materials: SG IRON 500/7
Finish:
Heat Treatment:
Material Stock
Part BEARING HOUSING - LE
Dwg No. 218-02
Part No. 218
SHEET 1 OF 1
A3
OEM No.
MODEL:C:\BRIANS FOLDER\FRST TBGS\GTECH BELLMOR\SOLIDWORKS\NEW BEARING\LE-brg housing

DRAWING: C:\BRIANS FOLDER\FRST TBGS\GTECH BELLMOR\SOLIDWORKS\NEW BEARING\25965

REVISIONS				
ZONE	REV.	DESCRIPTION	DATE	APPROVED
	A	ISSUED FOR MANUFACTURE	19/06/2012	BD

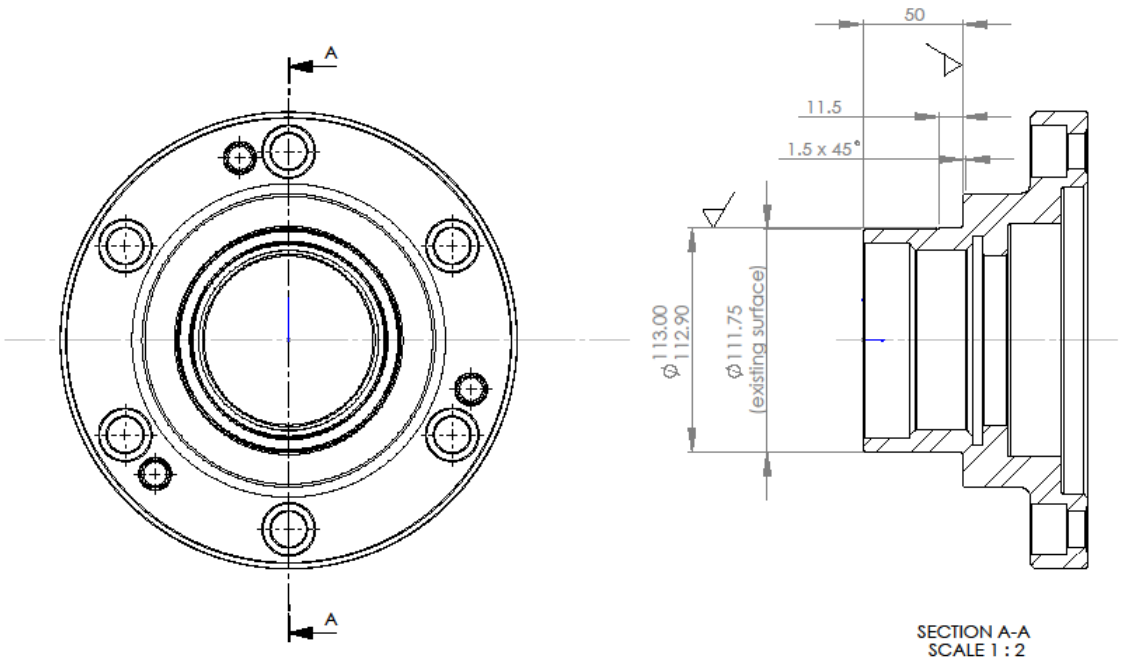

SECTION A-A
SCALE 1 : 2

UNIVERSITY OF CANTERBURY
Te Whare Wānanga o Waitaha
CHRISTCHURCH NEW ZEALAND

ACOUSTICS RESEARCH GROUP
DEPT OF MECHANICAL ENGINEERING
COLLEGE OF ENGINEERING
PRIVATE BAG 4800
CHRISTCHURCH 8140
NEW ZEALAND
Ph: +64 3 3642987
Fax: +64 3 364 2078

JOB No.
CONTRACT No.
AUTHORIZED BY
DATE

THIRD ANGLE PROJECTION
DO NOT SCALE FROM THIS DRAWING
IF IN DOUBT - ASK
DIMENSIONS ARE IN MILLIMETRES
DIMENSIONS ARE OF FINISHED PART
DO NOT PASS THIS DRAWING TO ANY THIRD PARTY WITHOUT AUTHORIZATION
DEBUR AND BREAK SHARP CORNERS

COMPONENT OR ASSEMBLY IS NOT TO BE MANUFACTURED UNLESS PROPERLY AUTHORIZED

Drawn By B.DONOHUE
Date Drawn 19 JUNE 2012
Checked By
Date Checked

Tolerances
0 ±0.25 Unless
0.0 ±0.13 otherwise
0.00 ±0.05 specified

Project: TBG
Product:
Materials:
Finish:
Heat Treatment:
Material Stock

Part MODIFICATION TO GEARBOX FLANGE
Dwg No. 219-02
Part No.
SHEET 1 OF 1 A3
OEM No.

MODEL:C:\BRIANS FOLDER\FRST TBGS\GTECH BELLMOR\SOLIDWORKS\NEW BEARING\25965